Theoretical Notes
Note 240

UNCLASSIFIED

SECURITY CLASSIFICATION OF THIS PAGE (When Data Entered)

REPORT DOCUMENTATION PAGE	READ INSTRUCTIONS BEFORE COMPLETING FORM
1. REPORT NUMBER: HDL-TR-1727	2. GOVT ACCESSION NO. / 3. RECIPIENT'S CATALOG NUMBER
4. TITLE (and Subtitle): Transient Ionization Effects from Neutron-Secondary Gamma Radiation in the Upper Atmosphere	5. TYPE OF REPORT & PERIOD COVERED: Technical Report 6. PERFORMING ORG. REPORT NUMBER
7. AUTHOR(s): John P. Roberts John S. Wicklund	8. CONTRACT OR GRANT NUMBER(s): DA: 1W162118AH75
9. PERFORMING ORGANIZATION NAME AND ADDRESS: Harry Diamond Laboratories 2800 Powder Mill Road Adelphi, MD 20783	10. PROGRAM ELEMENT, PROJECT, TASK AREA & WORK UNIT NUMBERS: Program Element: 6.21.18.A
11. CONTROLLING OFFICE NAME AND ADDRESS: Commander, US Army Materiel Command 5001 Eisenhower Avenue Alexandria, VA 22333	12. REPORT DATE: October 1975 13. NUMBER OF PAGES: 111
14. MONITORING AGENCY NAME & ADDRESS(if different from Controlling Office)	15. SECURITY CLASS. (of this report): Unclassified 15a. DECLASSIFICATION/DOWNGRADING SCHEDULE

16. DISTRIBUTION STATEMENT (of this Report)

Approved for public release; distribution unlimited.

17. DISTRIBUTION STATEMENT (of the abstract entered in Block 20, if different from Report)

18. SUPPLEMENTARY NOTES

HDL Project No: X75523
AMCMS Code: 612118.11H7500

19. KEY WORDS (Continue on reverse side if necessary and identify by block number)

Neutron transport
Neutron-gamma transport
Monte Carlo
FASTER III code
Transient ionization effects
EMP driving functions

20. ABSTRACT (Continue on reverse side if necessary and identify by block number)

The transport of neutrons and secondary gamma radiation produced by the interactions of these neutrons with the atmosphere has been studied to determine transient ionization effects for two source energy spectra (a 14-MeV band and fission) as a function of time for unit impulse sources at 45-km altitude. These Monte Carlo calculations using the FASTER III code included altitude-dependent density, curvature of the earth,

DD FORM 1 JAN 73 1473 EDITION OF 1 NOV 65 IS OBSOLETE

UNCLASSIFIED

 SECURITY CLASSIFICATION OF THIS PAGE (When Data Entered)

ENDF/B III neutron point-cross-section data, and Rayleigh scattering and polarization of the photons. Data were obtained on energy, angle, and time distributions for 20 detector positions for each source spectrum.

One important result is observed. A large contribution to ionization production rates occurs at late (~1 to 10 ms) local times, primarily due to the arrival of the neutrons with their attendant secondary gamma production in a volume near the detectors. This contribution exceeds that of earlier times by as much as an order of magnitude or more.

CONTENTS

APPENDICES

FIGURES

TABLES

1. INTRODUCTION

The authors have performed a series of radiation transport calculations for primary gamma and neutron sources to determine electromagnetic pulse (EMP) source drivers-ionization production rates due to primary and secondary gamma photons and Compton source currents. The code used was the FASTER III Monte Carlo code[1] modified considerably to provide the data required. Data for neutron cross sections were obtained from the Oak Ridge National Laboratory Radiation Shielding Information Center (RSIC). The ENDF/B-III point cross-section data for nitrogen (DNA MAT 4133 Mod 3) and oxygen (DNA MAT 4134 Mod 1) were used from the Defense Nuclear Agency (DNA) Working Cross Section Library maintained by RSIC.[2] Photon cross-section data were also obtained from RSIC data tape DLC-17. Incoherent and coherent scattering form factor values were obtained from studies by Veigele and coworkers.[3]

The values determined in these calculations will be used by the Electromagnetic Effects Laboratory of the Harry Diamond Laboratories in future EMP code calculations as source data.

The results presented here are for a 14-MeV neutron source (actually a 12.2 to 15 MeV band spectrum) and for a neutron fission spectrum source[4] (table I) 45 km above the earth. (Results for a primary gamma source, a fission gamma spectrum, have been published.[5]) These point sources are delta functions in time. Point detectors are located along radials from the source at distances corresponding to 1, 5, 10, 15, and 20 mean free path (mfp) lengths for a 14-MeV neutron (fig. 1). The

---

[1] *T. M. Jordan, FASTER III, A Generalized Monte Carlo Computer Program for the Transport of Neutrons and Gamma Rays, Vol. II, Users Manual, ART Research Corporation, ART-45 (November 1970).*

[2] *R. W. Roussin and J. B. Wright, Defense Nuclear Agency Working Cross Section Library, ORNL-RSIC-34, Vol. 1, Oak Ridge National Laboratory (June 1974).*

[3] *W. J. Veigele et al, X-ray Cross Section Compilation from 0.1 keV to 1 MeV, Input Data and Supplemental Results, Vol. II, Revision 1, DNA2433FO (31 July 1971).*

[4] *E. A. Straker and M. L. Gritzner, Neutron and Secondary-Gamma Transport in Infinite Homogeneous Air, ORNL-4464, Oak Ridge National Laboratory (December 1969).*

[5] *J. P. Roberts and J. S. Wicklund, Transient Ionization Effects from Primary Gamma Fission Radiation in the Upper Atmosphere, Harry Diamond Laboratories TR-1725 (October 1975).*

TABLE I. ENERGY DISTRIBUTION FOR FISSION SOURCE

Energy (MeV)	Fraction in group
12.2 - 15.0	1.568(-4)[1]
10.0 - 12.2	8.932(-4)
8.19 - 10.0	3.480(-3)
6.36 - 8.19	1.392(-2)
4.97 - 6.36	3.457(-2)
4.07 - 4.97	3.507(-2)
3.01 - 4.07	1.072(-1)
2.46 - 3.01	8.898(-2)
2.35 - 2.46	2.323(-2)
1.83 - 2.35	1.203(-1)
1.11 - 1.83	2.181(-1)
0.55 - 1.11	1.983(-1)
0.11 - 0.55	1.403(-1)
0.0335 - 0.110	1.550(-2)

[1]*Read as 1.568 x 10^{-4}*

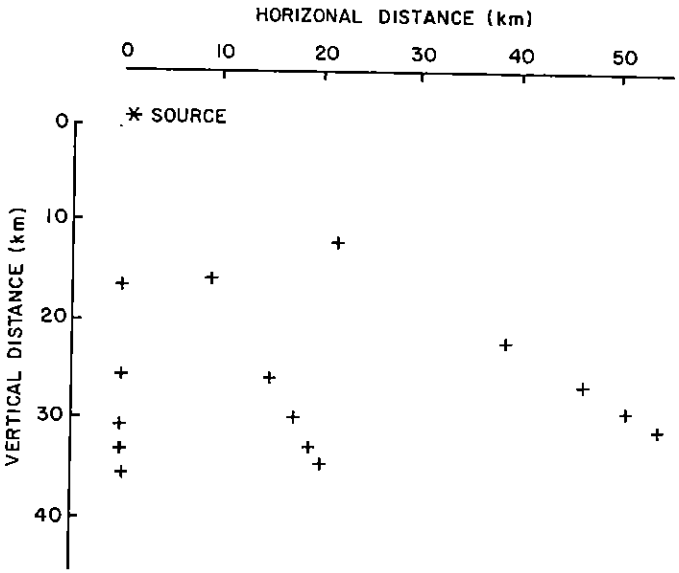

Figure 1. Source detector geometries.

position of the lowest detector directly below the source (at 20 mfp lengths) is 9.75 km aboveground, close to that range in the atmosphere in which mass equivalent (ρR) scaling is feasible for calculated results.[6] The radials along which the detectors are positioned are at 5, 30, 60, and 90 deg below the horizontal. Detectors 1 to 5 along the 5-deg radial lie off the horizontal scale of the plot and are not shown. In order of mass distance from the source, detectors 6 to 10 lie along the 30-deg radial, detectors 11 to 15 along the 60-deg radial, and detectors 16 to 20 along the 90-deg radial.

2. RESULTS

In the results of the 20 detector positions for the two source spectra (fig. 2 to 41), ionization production rate in megaelectronvolts per square meter-second is shown as a function of local time (in seconds). Local time begins with the arrival at a detector of the first unscattered secondary gamma photon. Results are fitted with an eighth-order polynomial,

$$Y = \sum_{i=0}^{8} a_i X^i$$

weighted by the inverse square of the probable error (the parameters are explained in appendix A, and the method is explained elsewhere[5]). Polynomial coefficients, a_i, for all detectors are given in table II for the 14-MeV neutron source and in table III for the neutron fission spectrum source.

---

[5] *J. P. Roberts and J. S. Wicklund, Transient Ionization Effects from Primary Gamma Fission Radiation in the Upper Atmosphere, Harry Diamond Laboratories TR-1725 (October 1975).*

[6] *E. A. Straker, Status of Neutron Transport in the Atmosphere, ORNL-TM-3065, Oak Ridge National Laboratory (29 July 1970).*

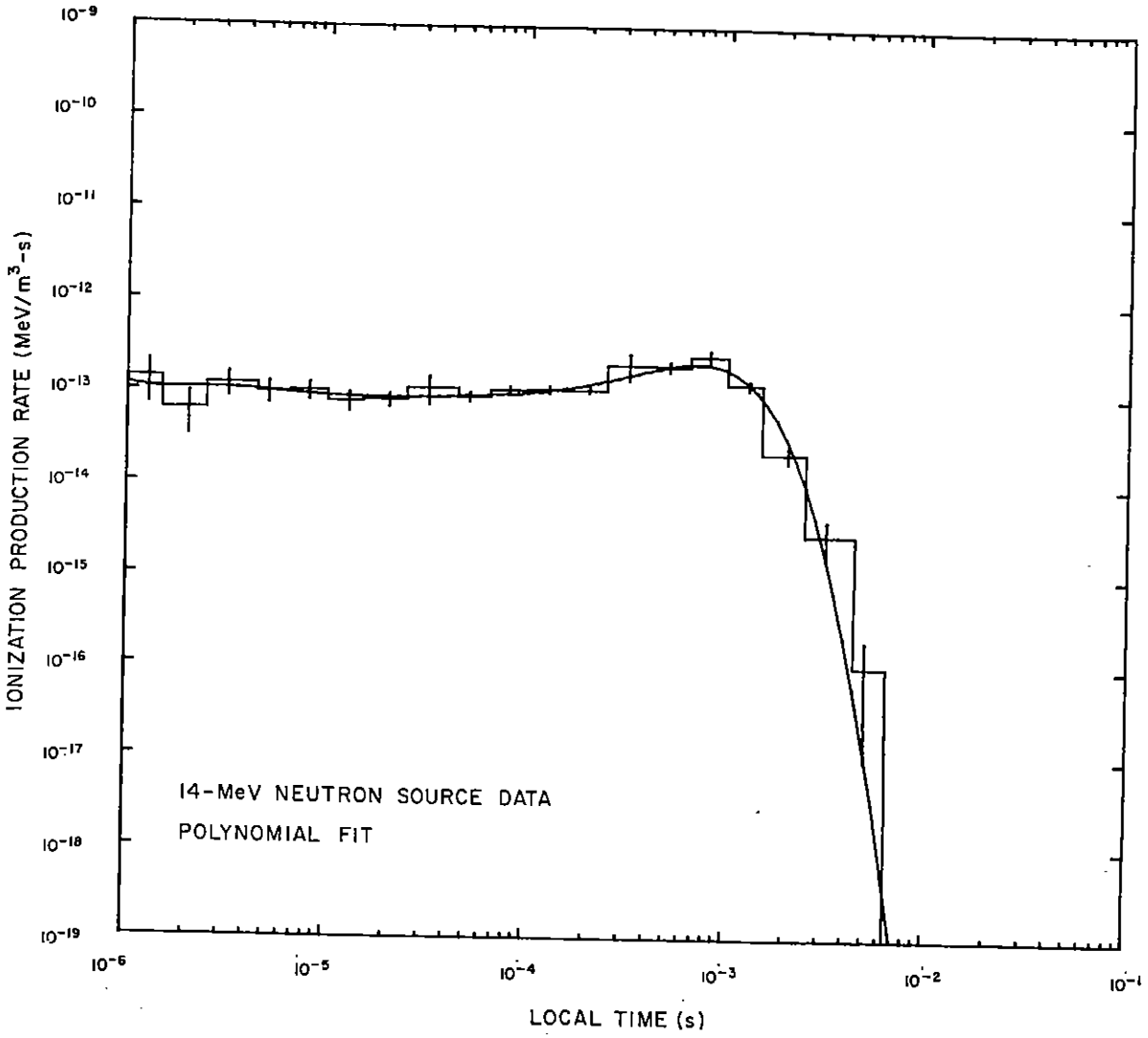

Figure 2. Ionization rate versus time for detector 1.

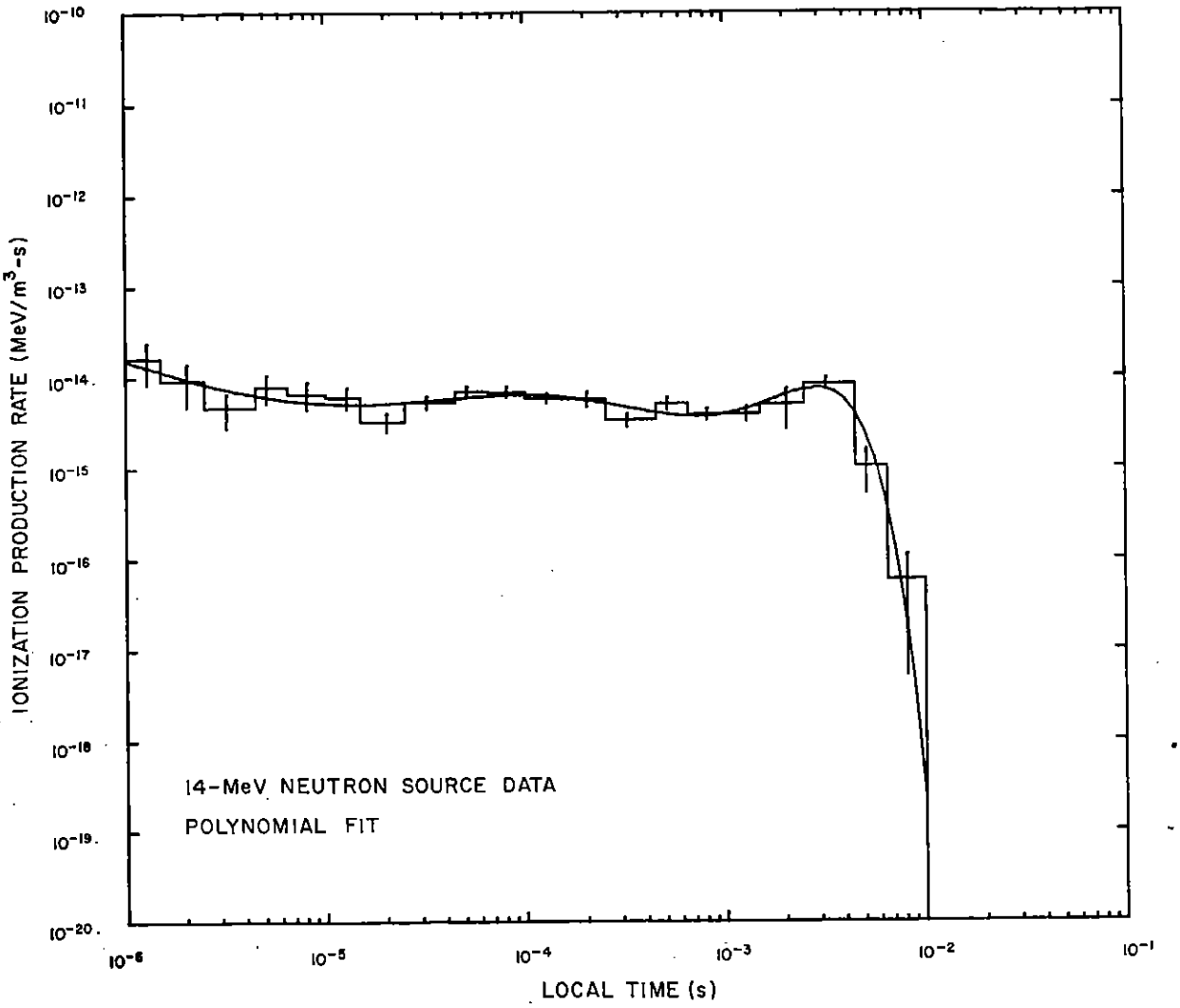

Figure 3. Ionization rate versus time for detector 2.

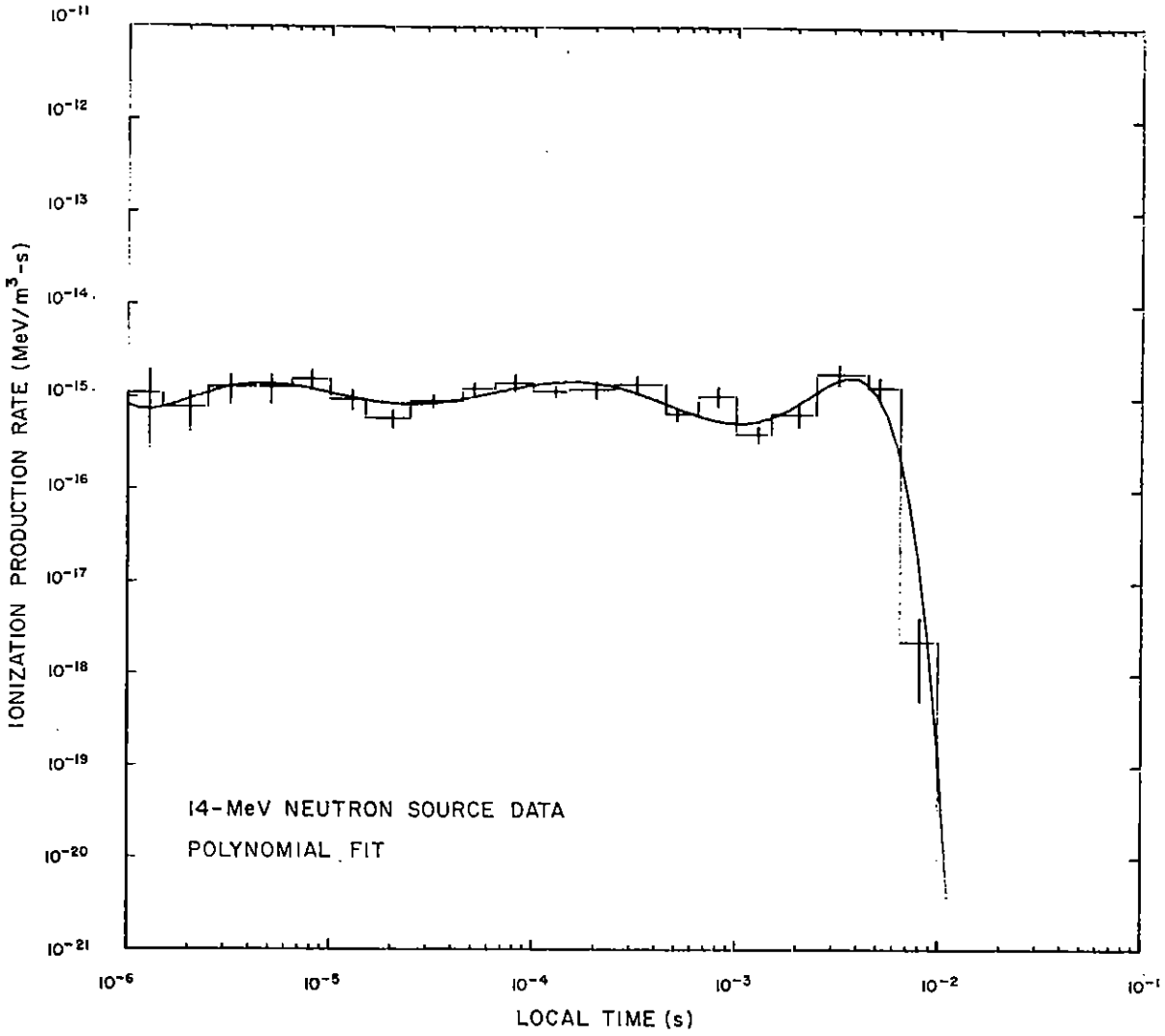

Figure 4. Ionization rate versus time for detector 3.

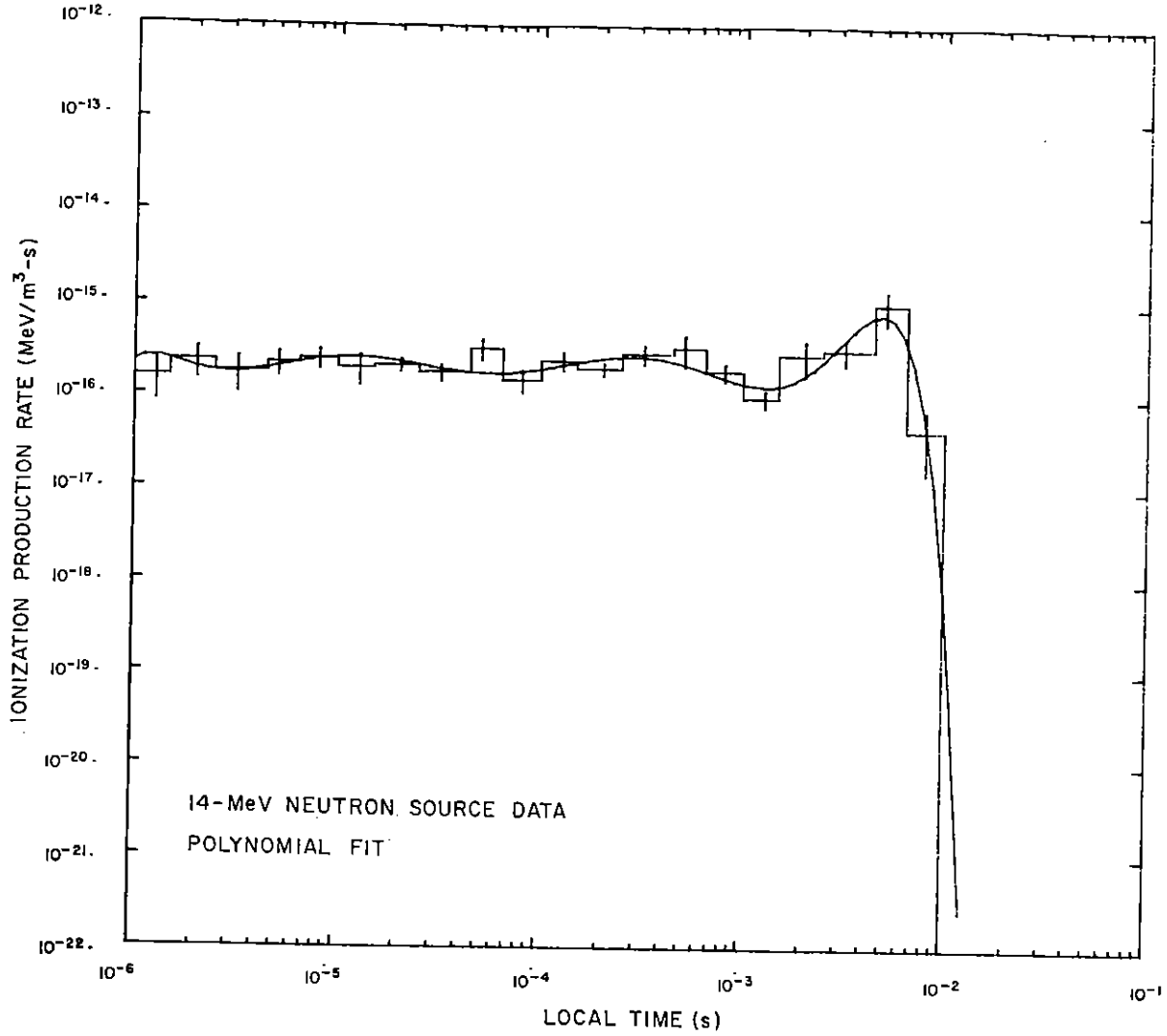

Figure 5. Ionization rate versus time for detector 4.

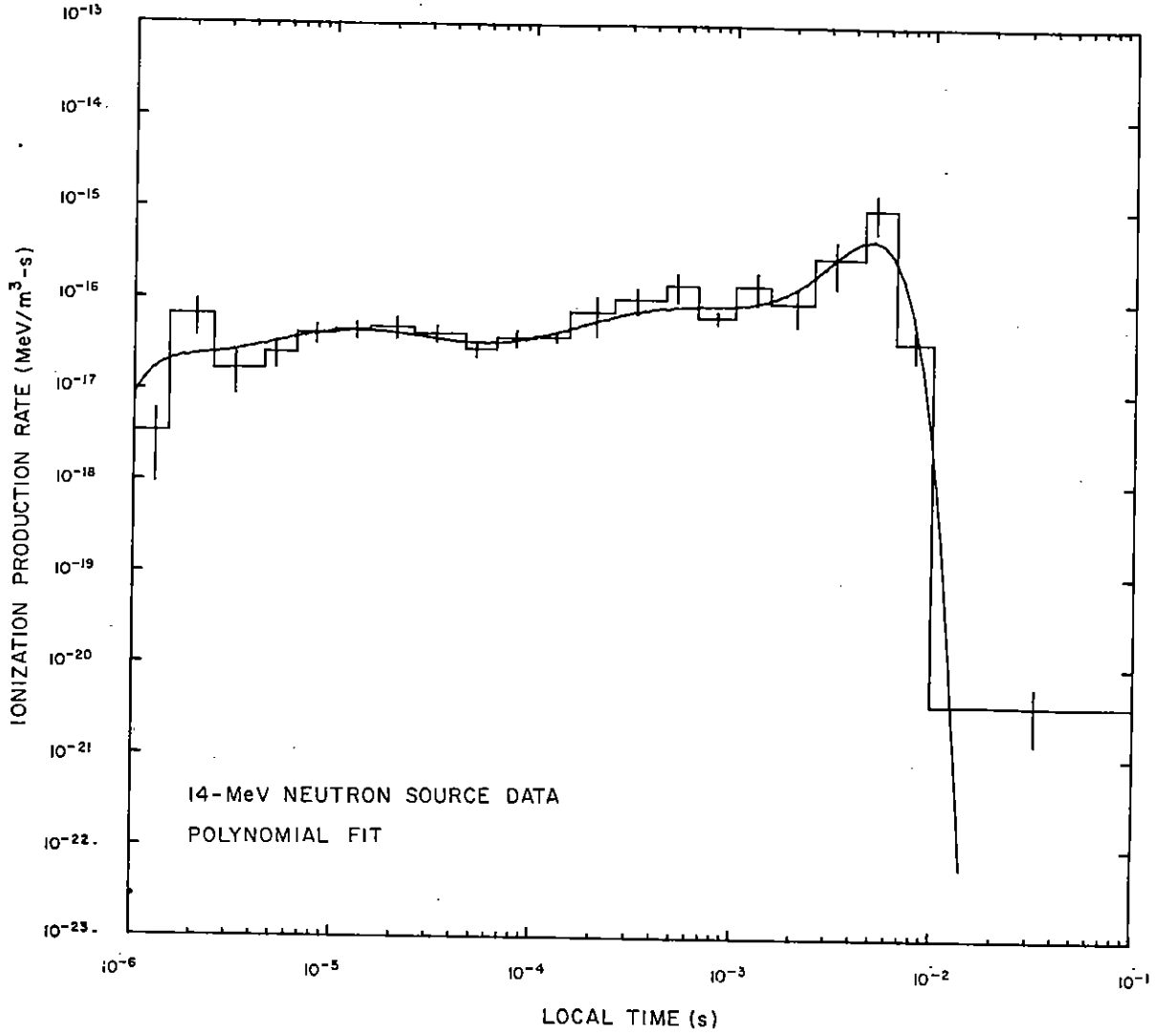

Figure 6. Ionization rate versus time for detector 5.

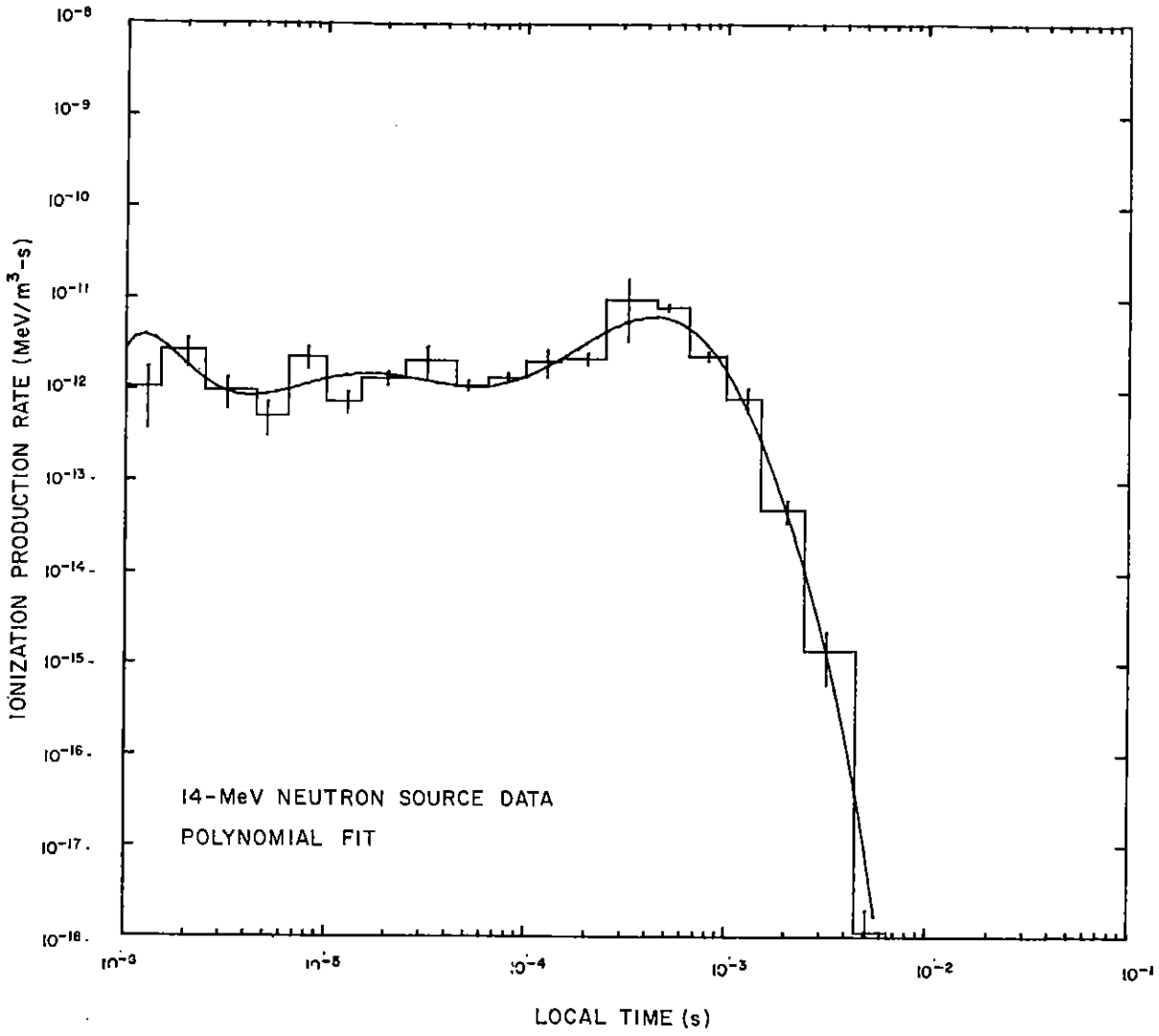

Figure 7. Ionization rate versus time for detector 6.

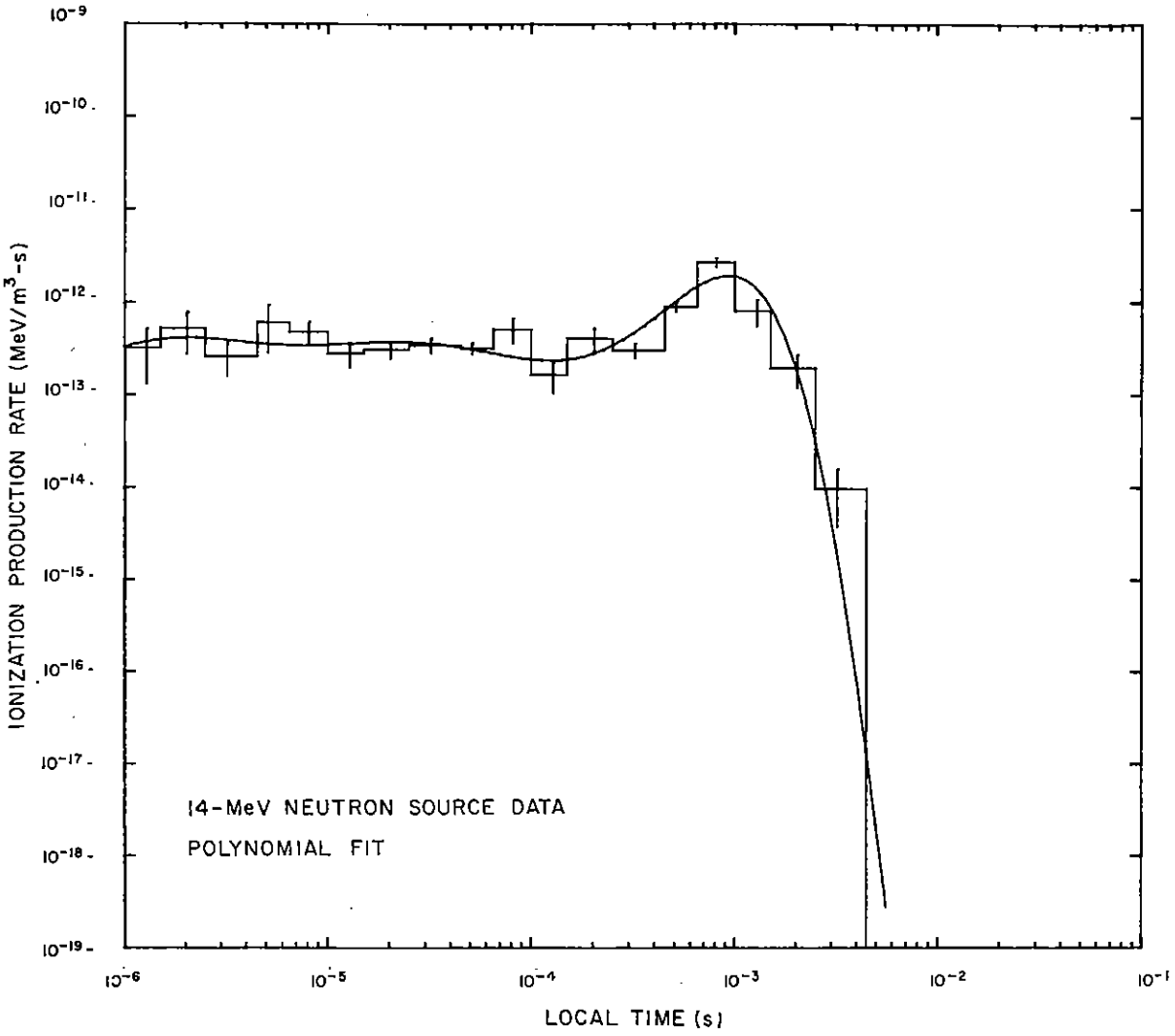

Figure 8. Ionization rate versus time for detector 7.

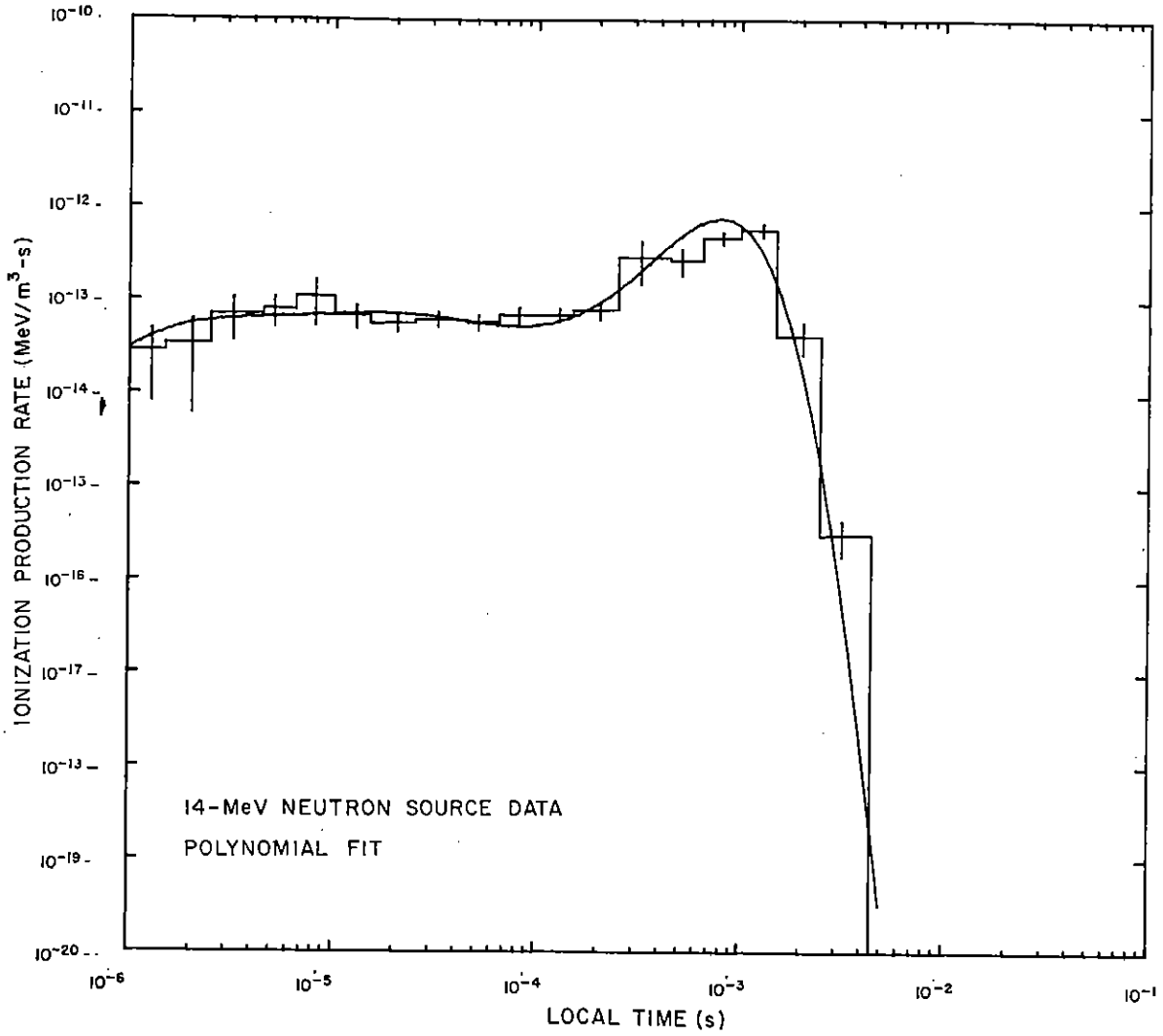

Figure 9. Ionization rate versus time for detector 8.

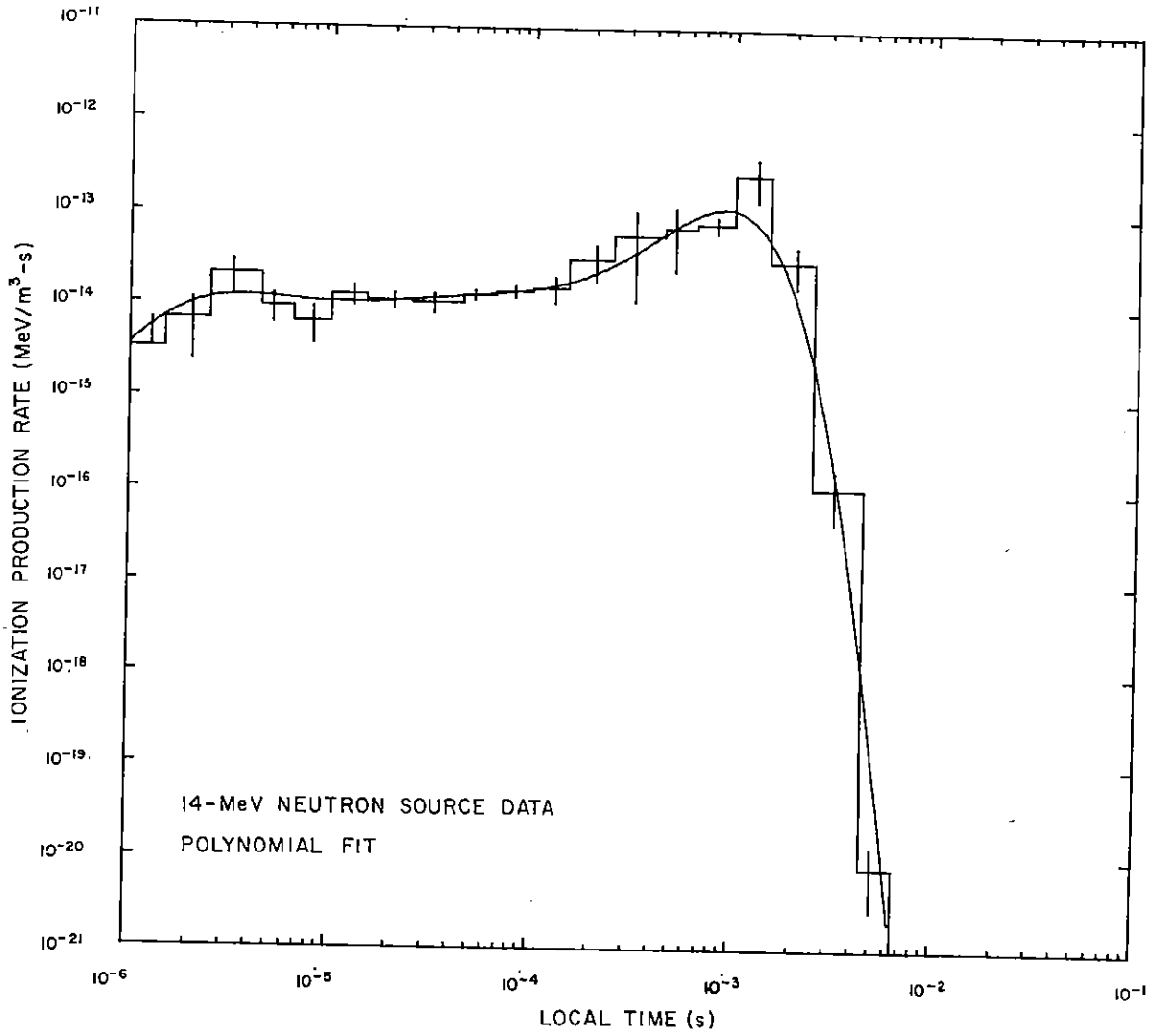

Figure 10. Ionization rate versus time for detector 9.

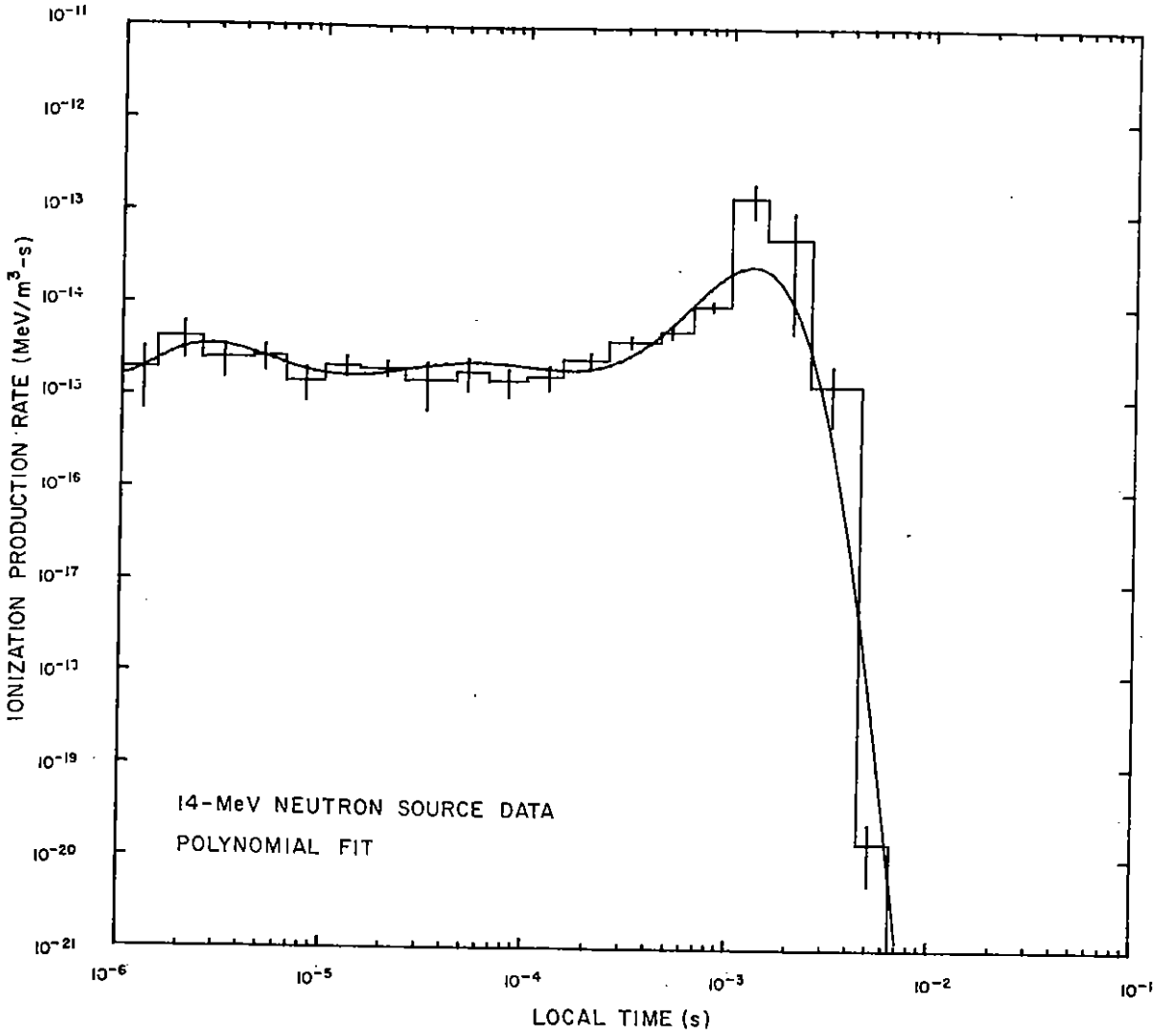

Figure 11. Ionization rate versus time for detector 10.

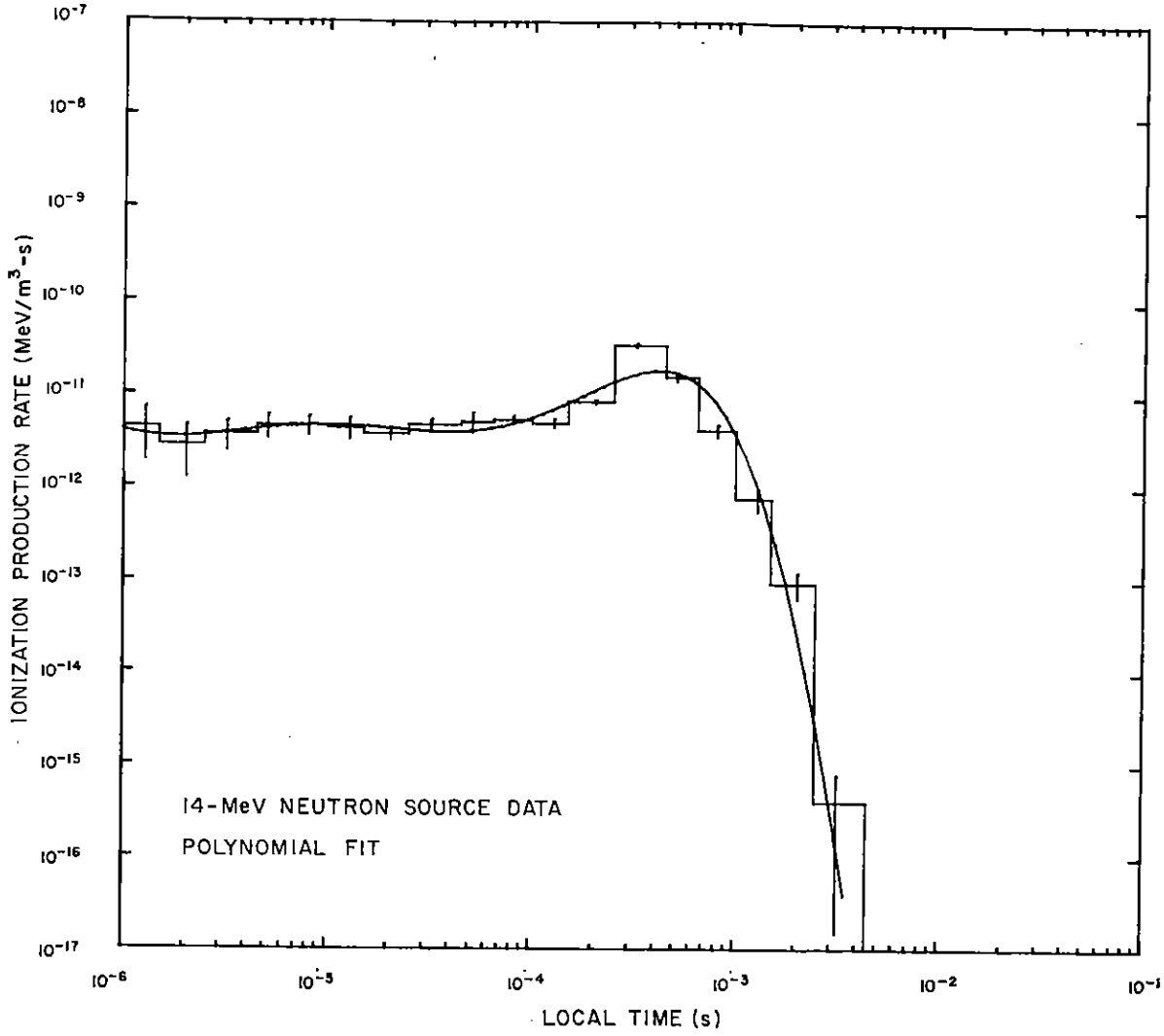

Figure 12. Ionization rate versus time for detector 11.

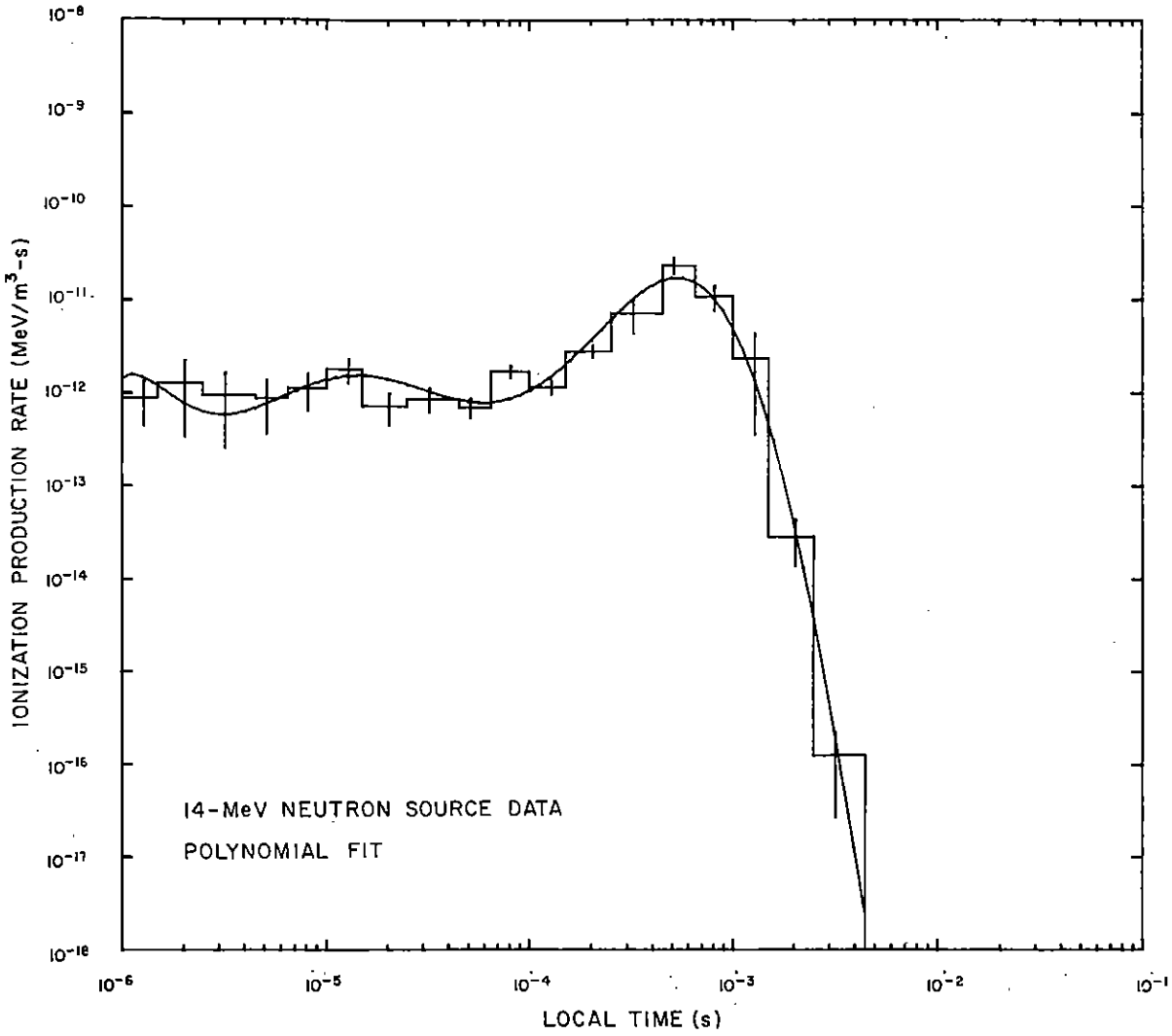

Figure 13. Ionization rate versus time for detector 12.

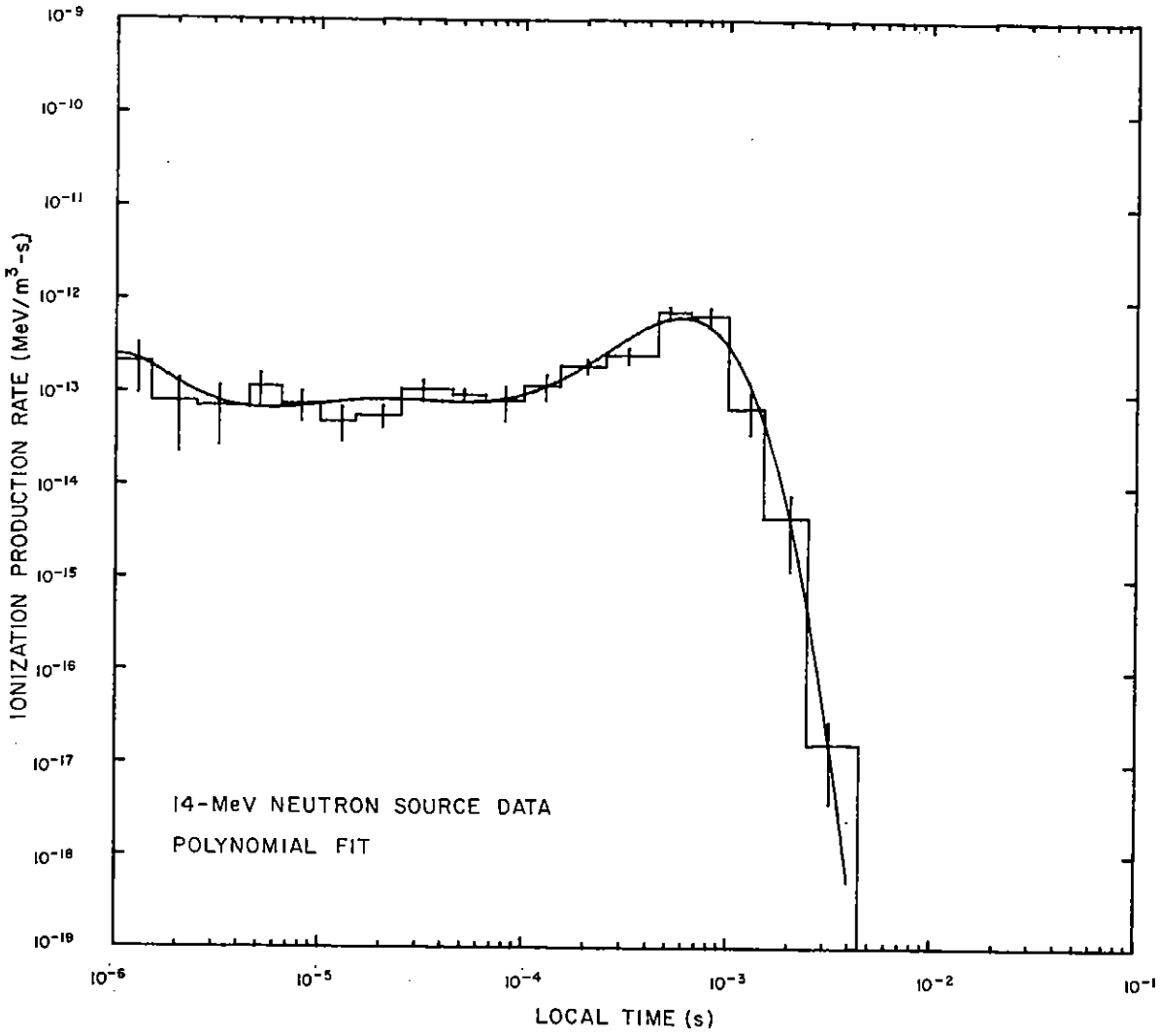

Figure 14. Ionization rate versus time for detector 13.

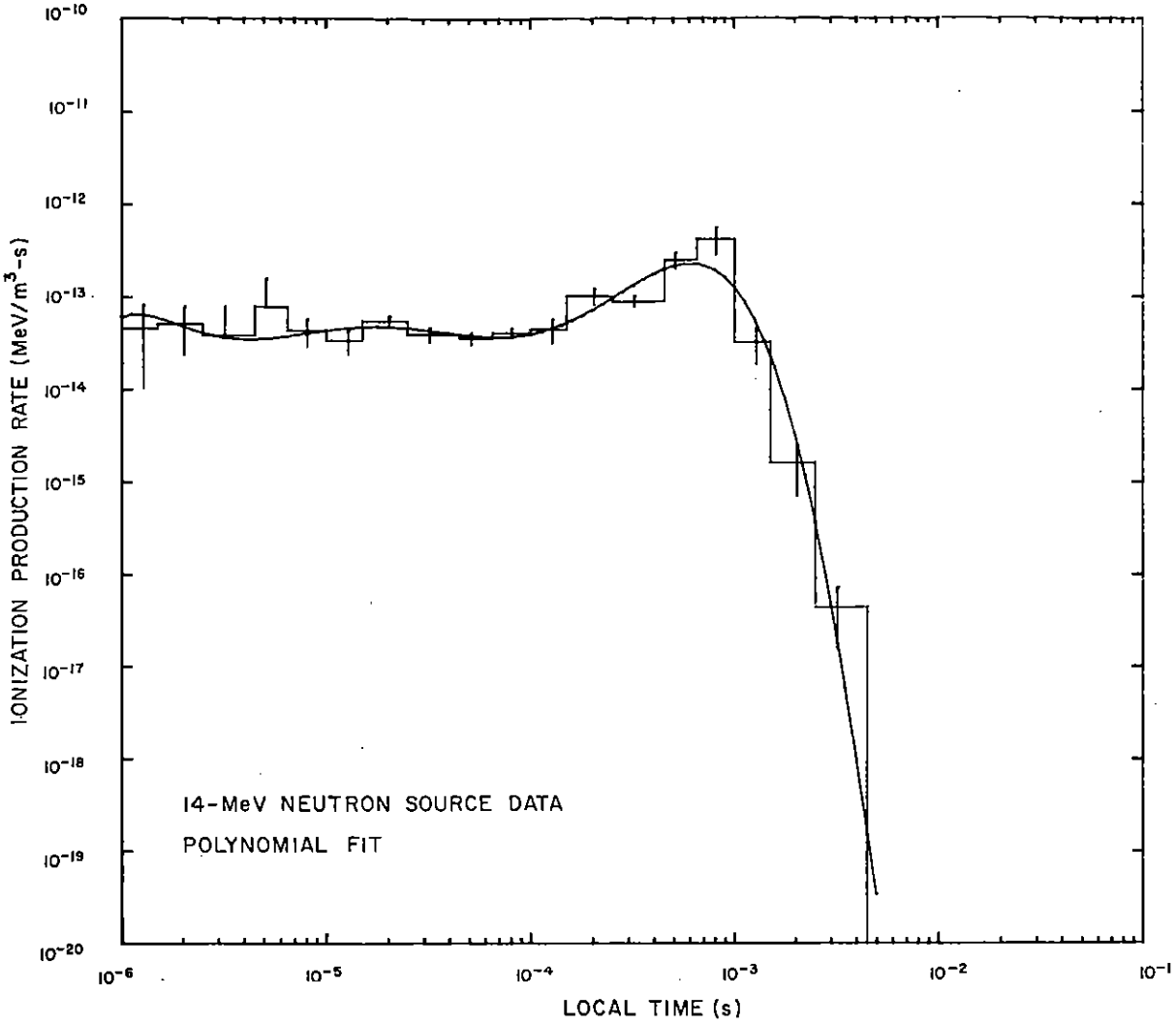

Figure 15. Ionization rate versus time for detector 14.

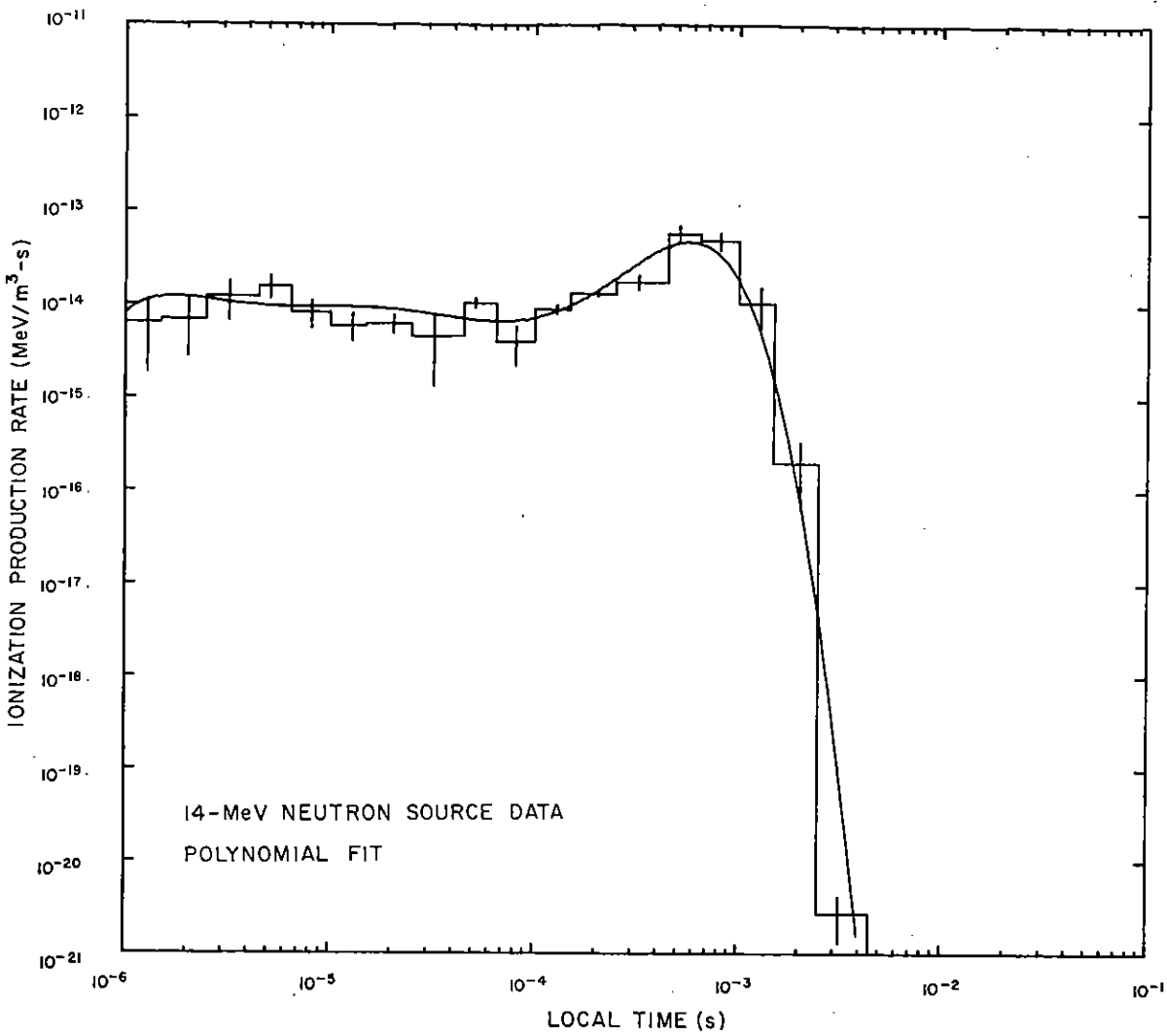

Figure 16. Ionization rate versus time for detector 15.

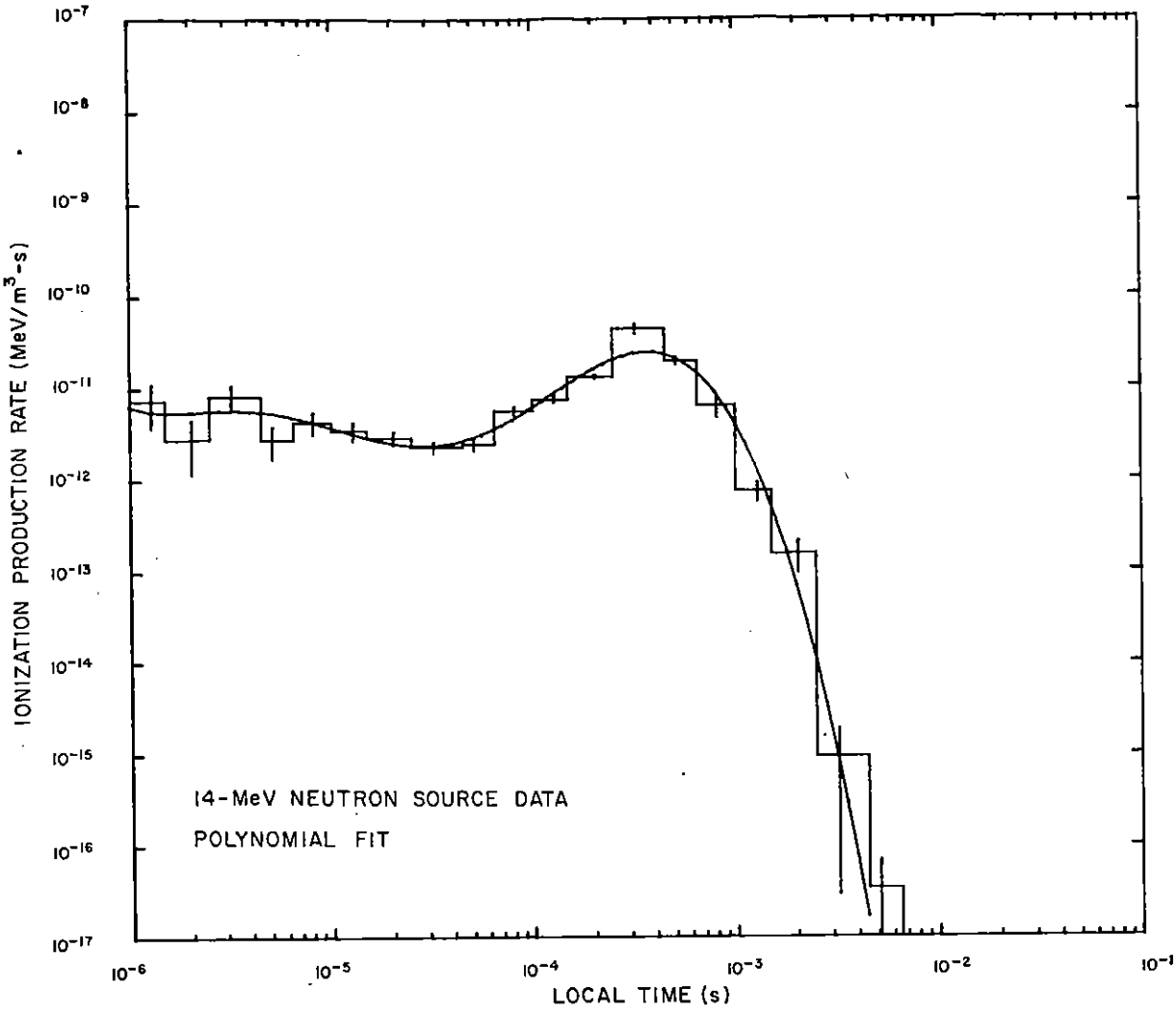

Figure 17. Ionization rate versus time for detector 16.

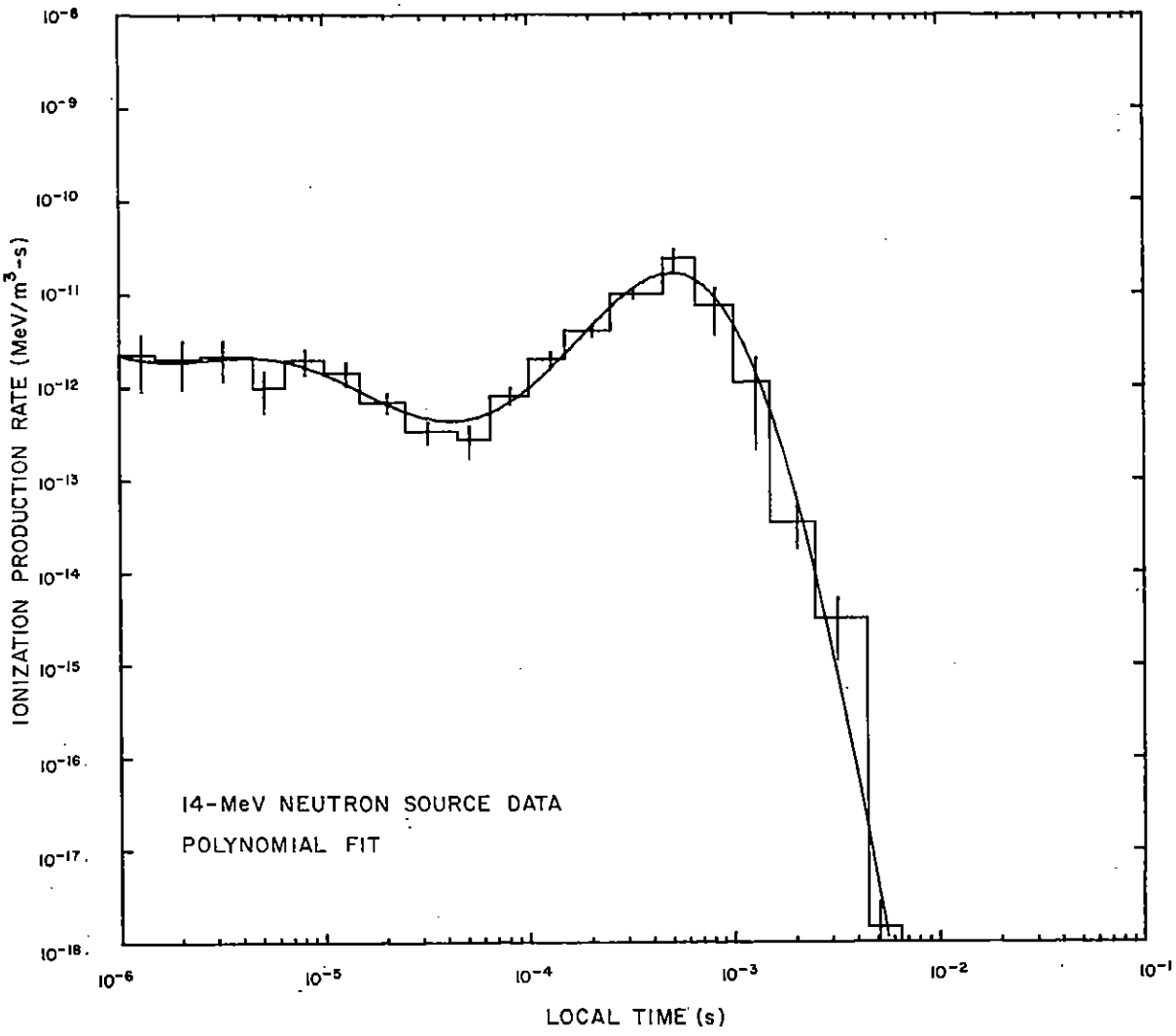

Figure 18. Ionization rate versus time for detector 17.

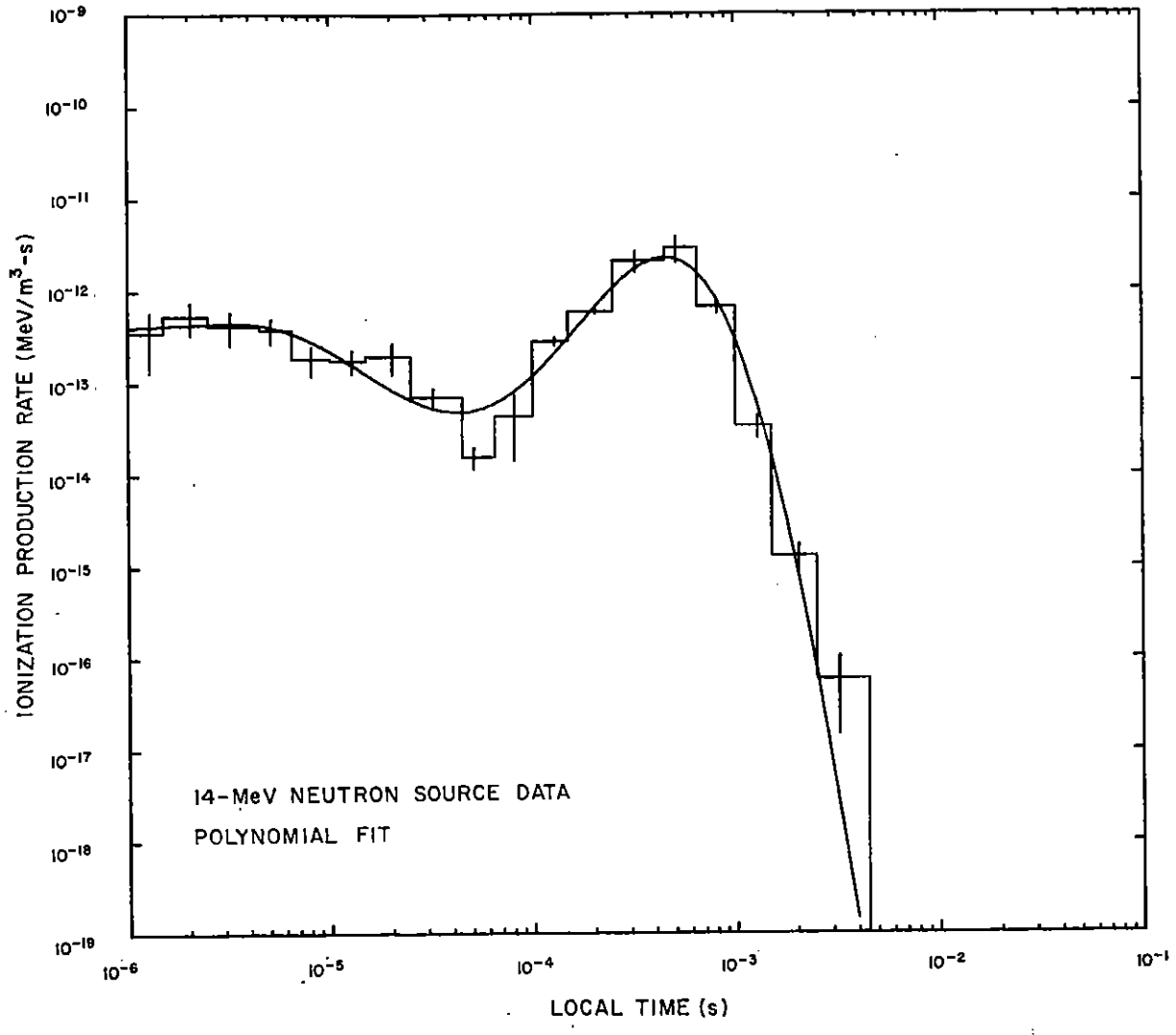

Figure 19. Ionization rate versus time for detector 18.

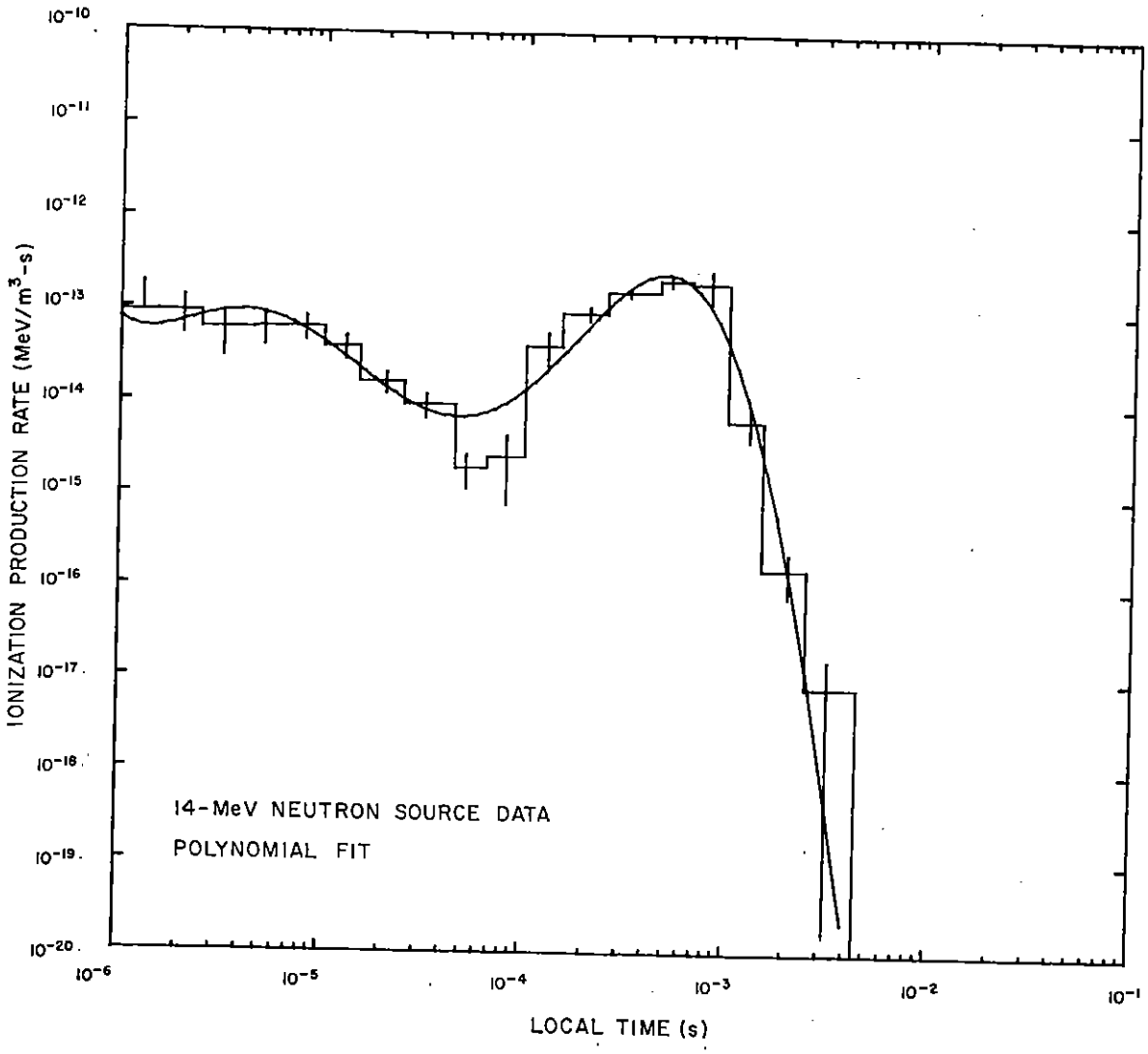

Figure 20. Ionization rate versus time for detector 19.

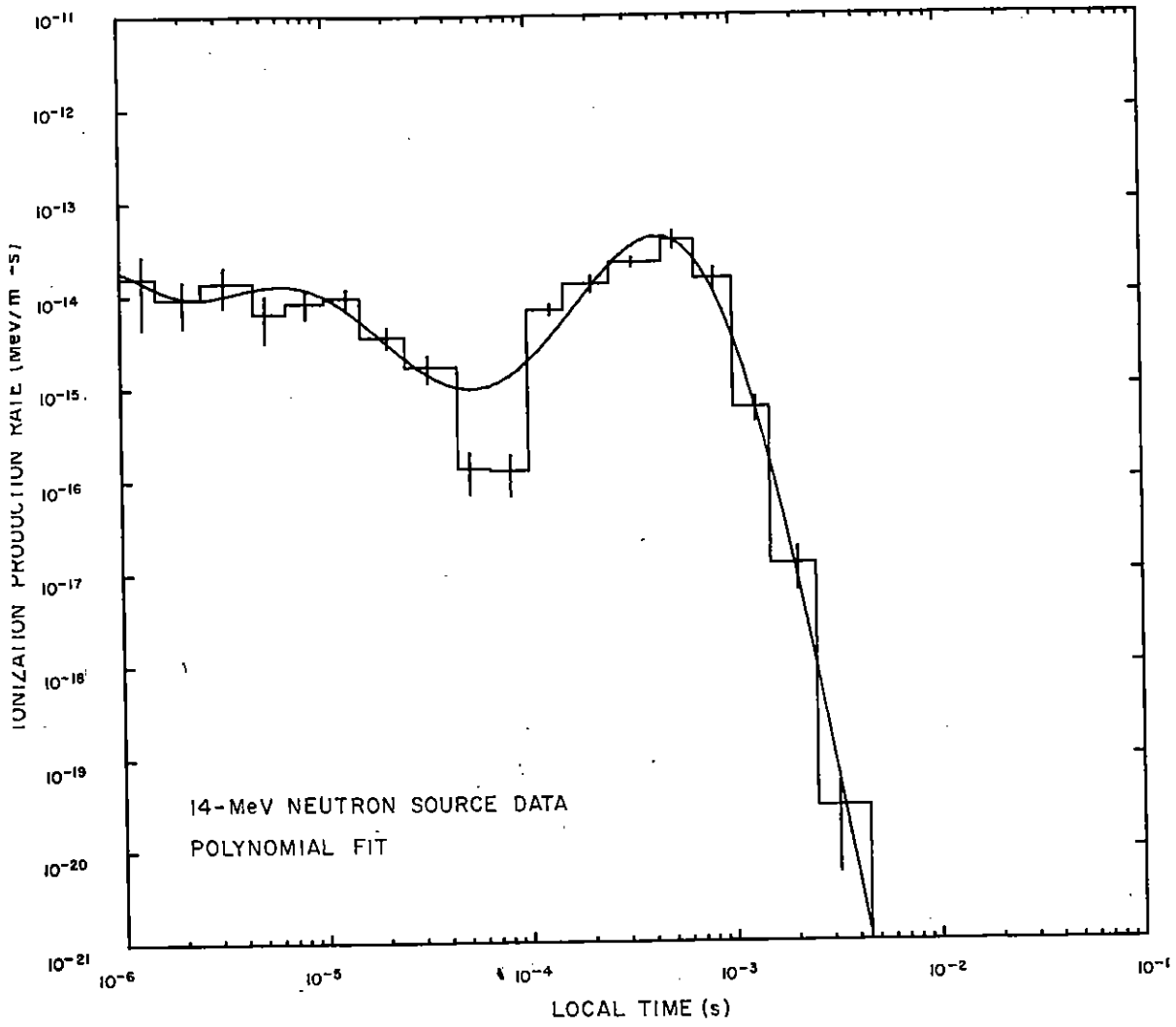

Figure 21. Ionization rate versus time for detector 20.

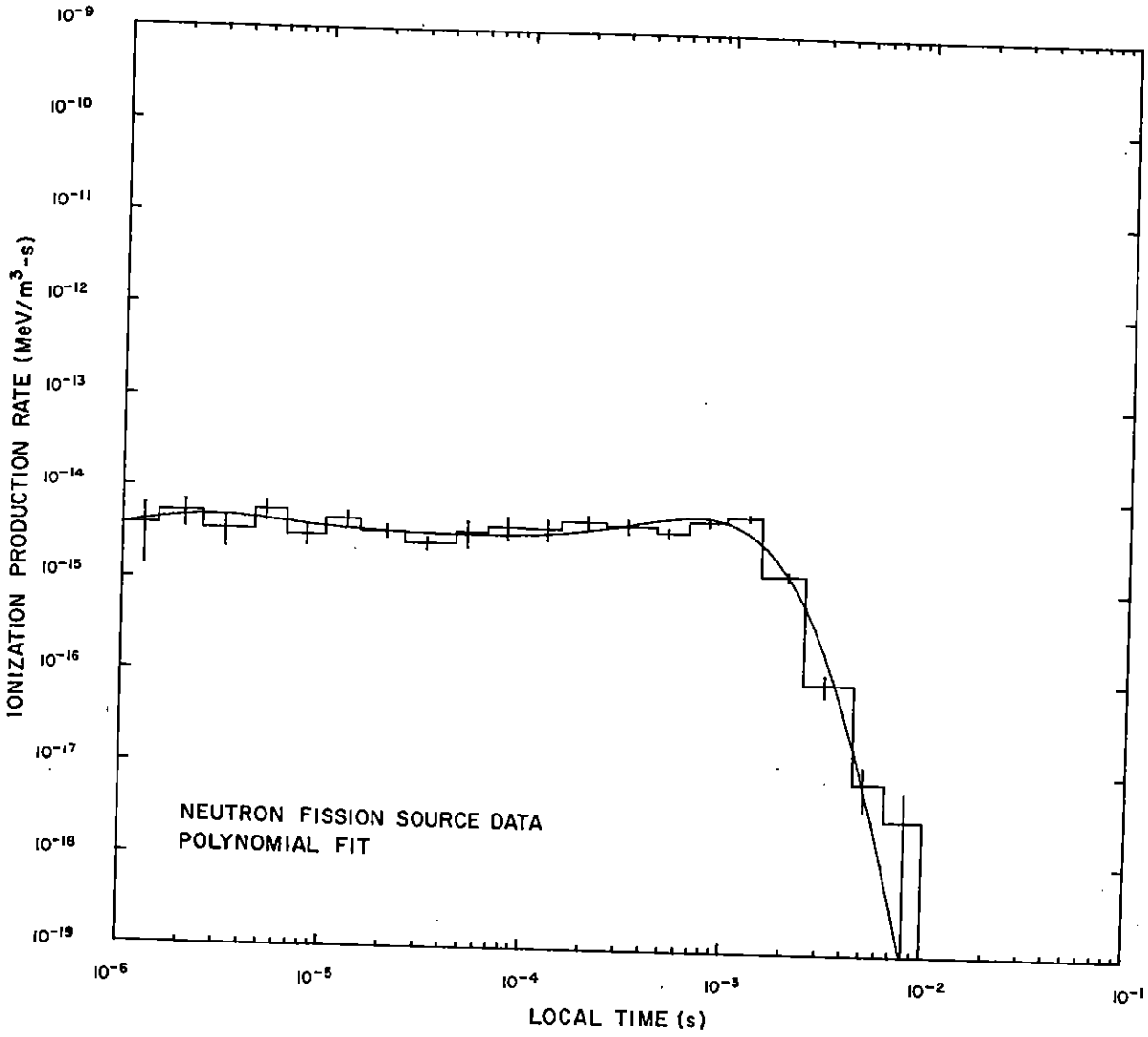

Figure 22. Ionization rate versus time for detector 1.

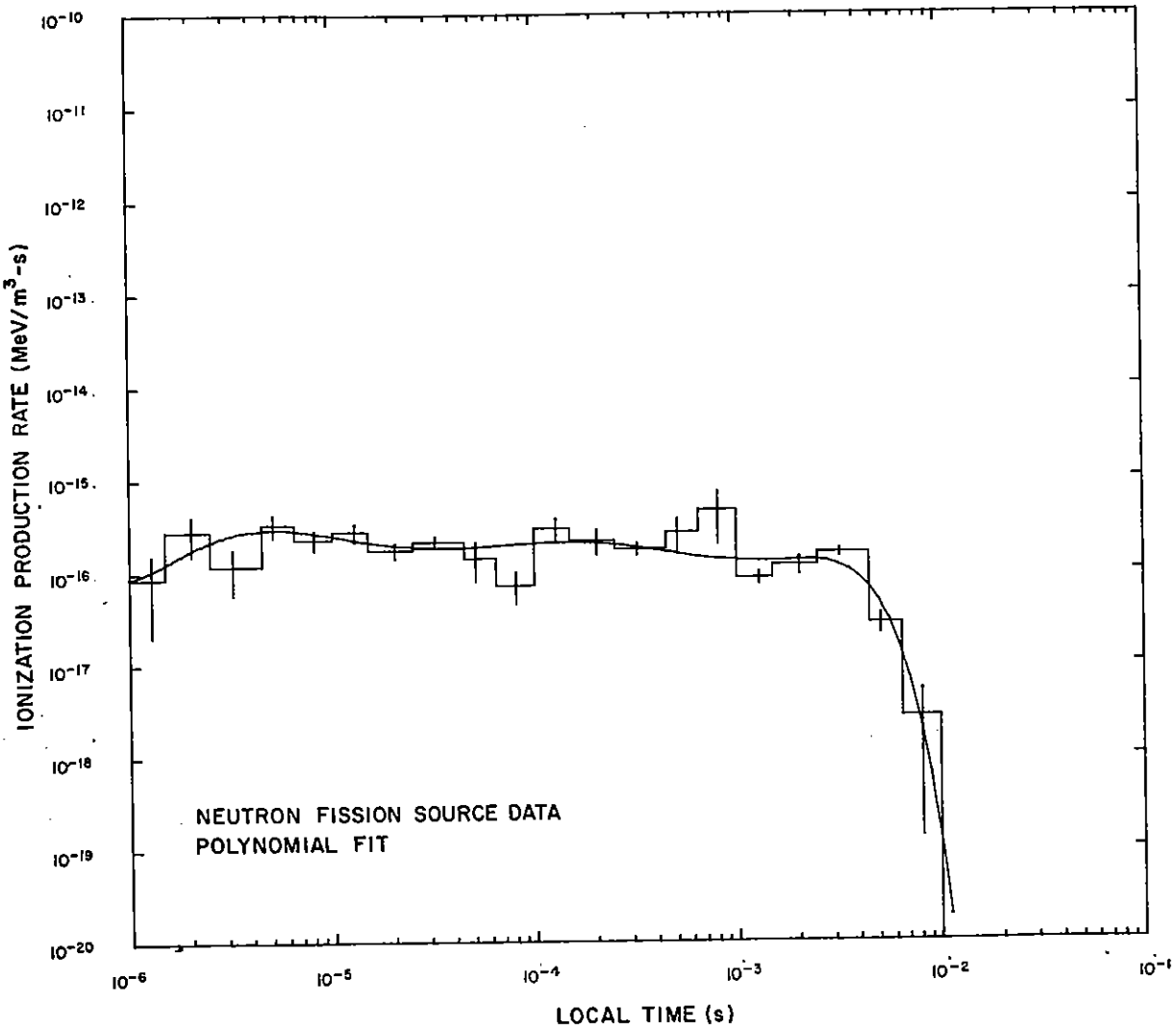

Figure 23. Ionization rate versus time for detector 2.

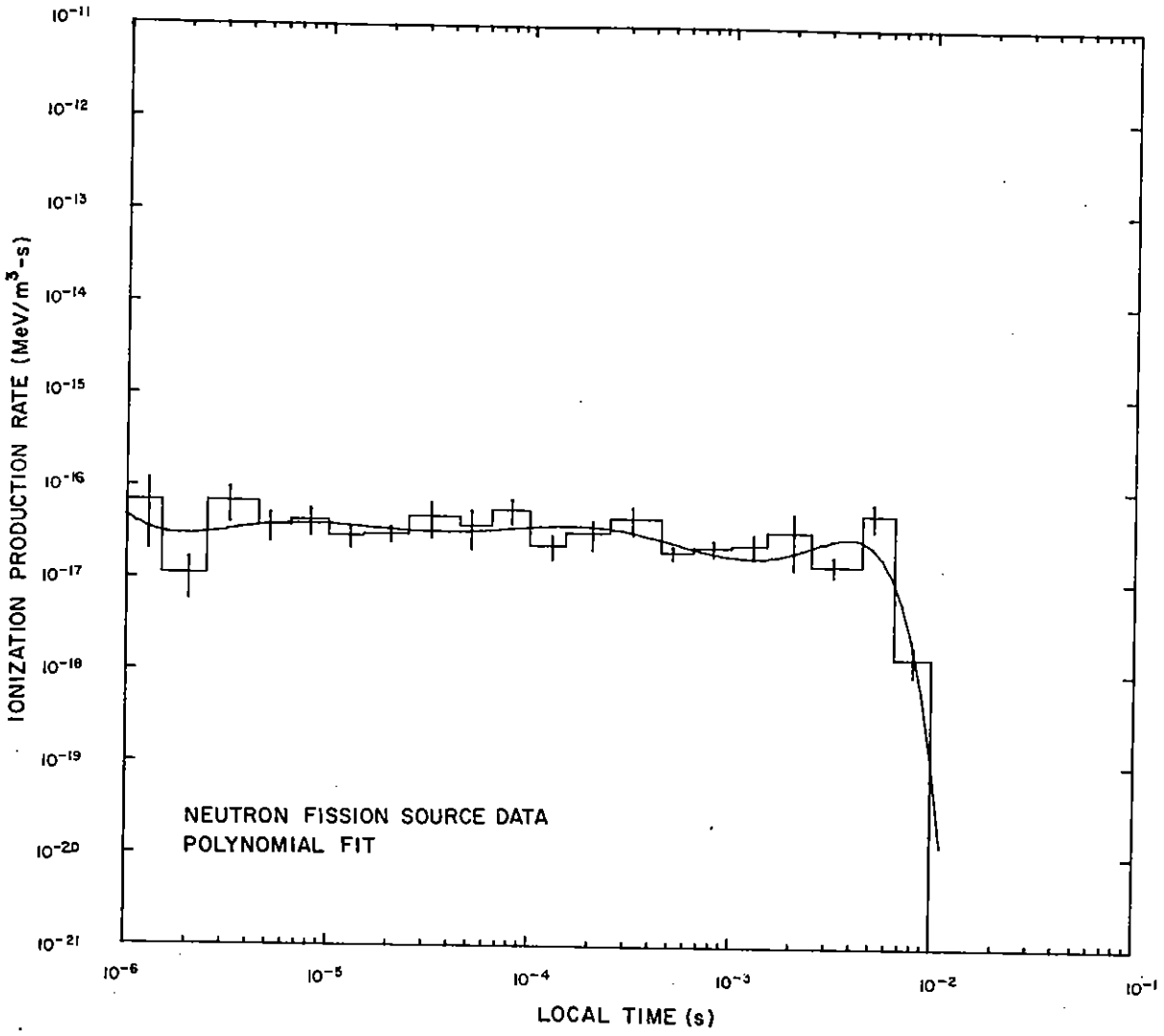

Figure 24. Ionization rate versus time for detector 3.

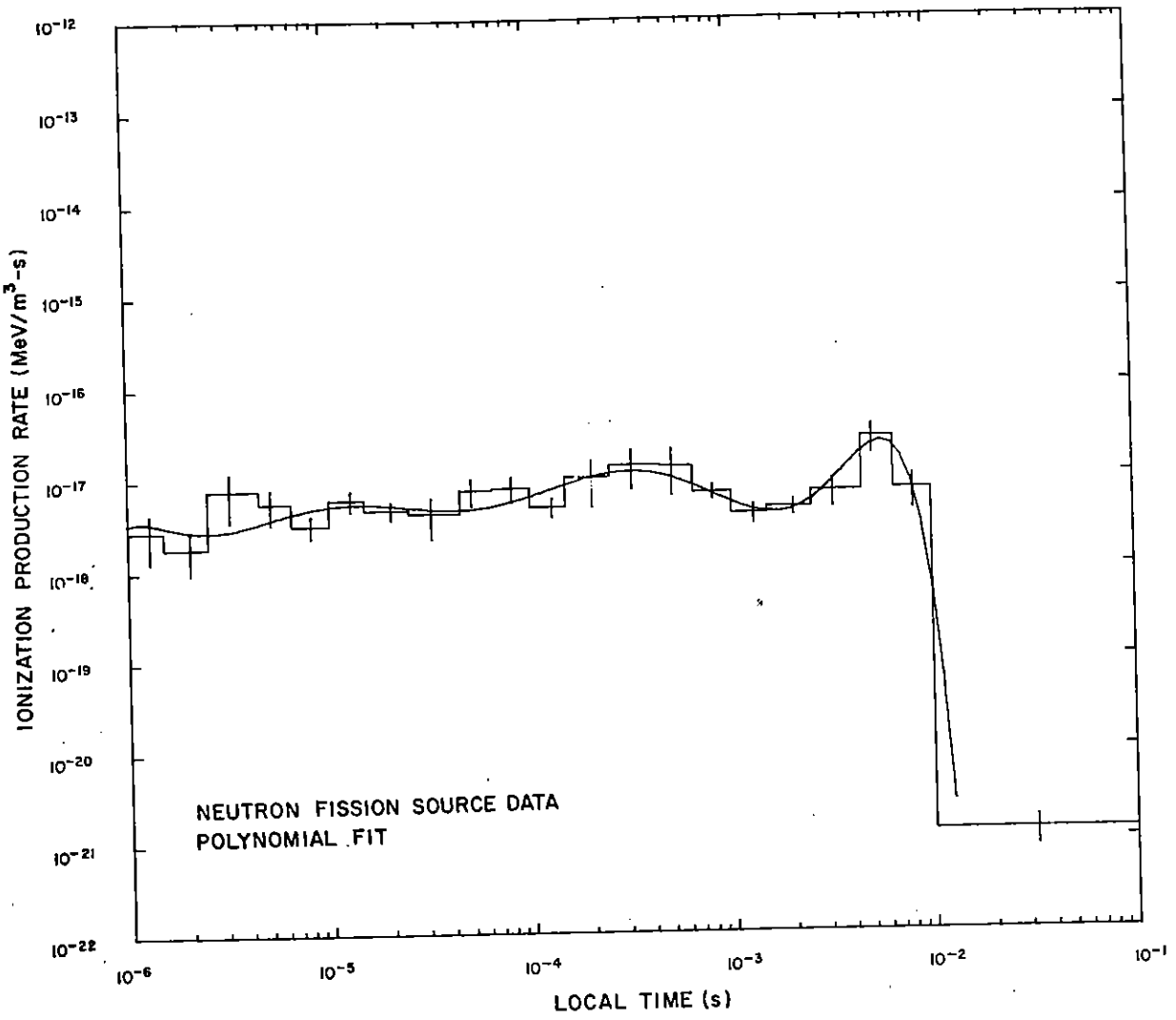

Figure 25. Ionization rate versus time for detector 4.

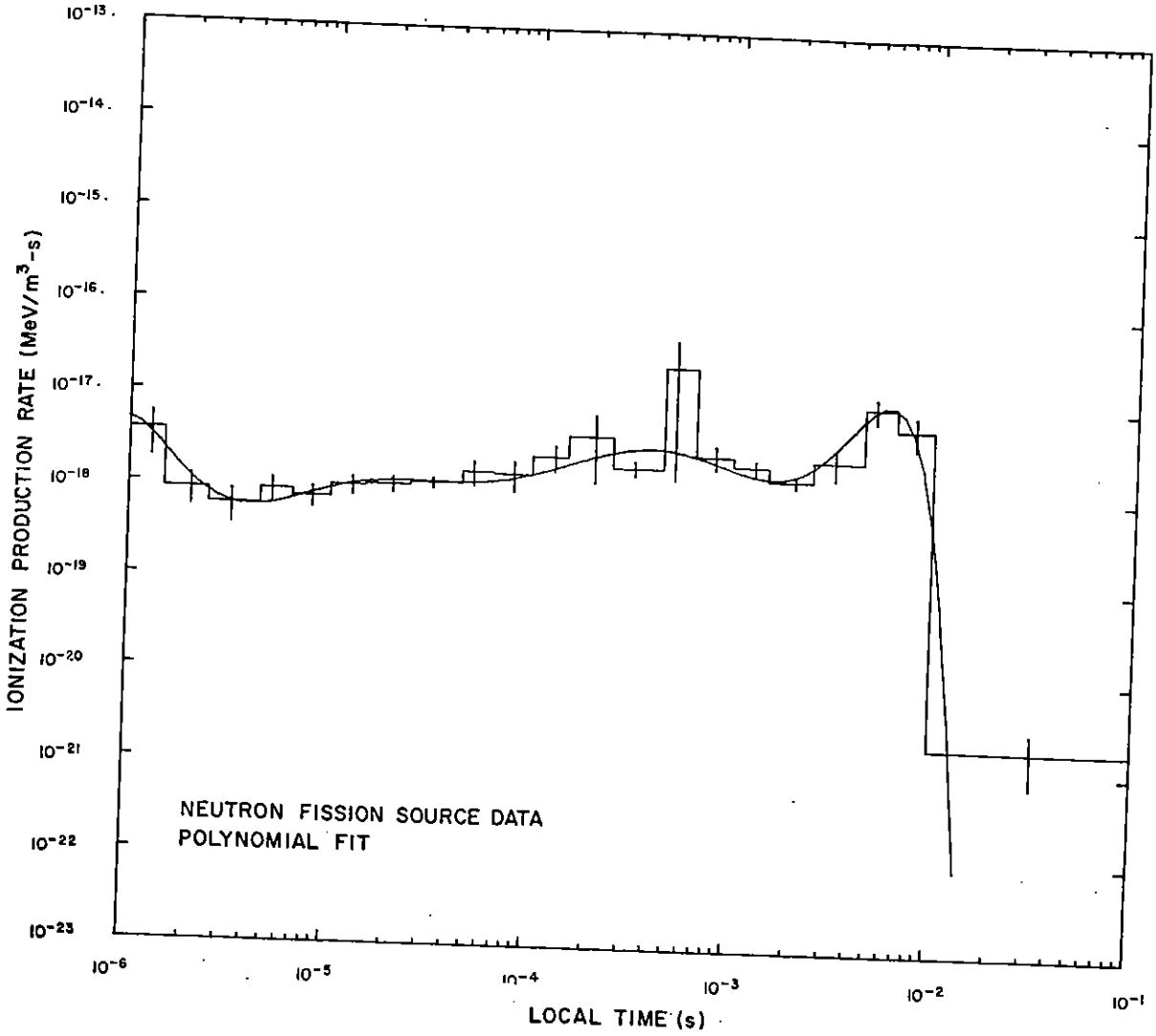

Figure 26. Ionization rate versus time for detector 5.

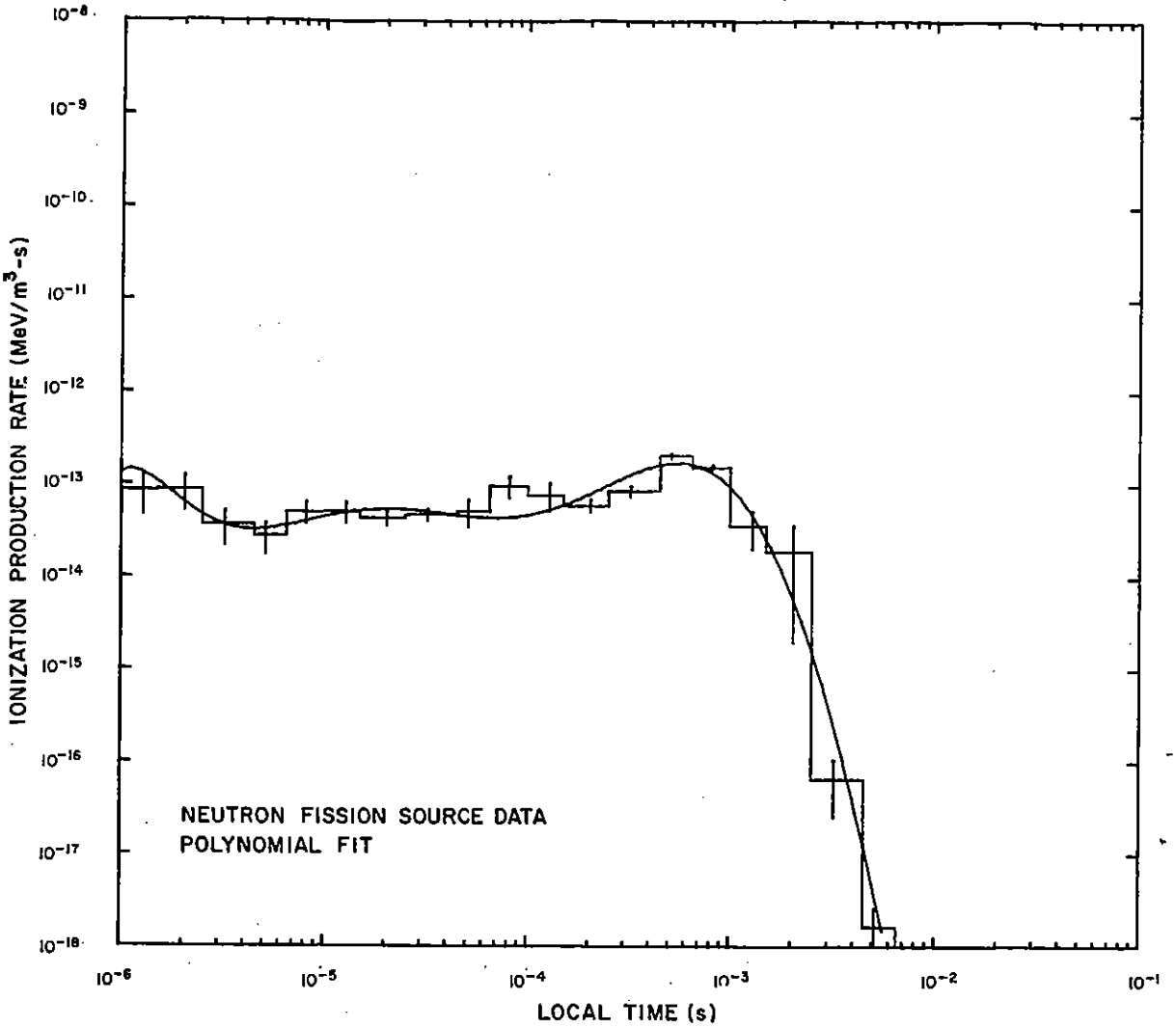

Figure 27. Ionization rate versus time for detector 6.

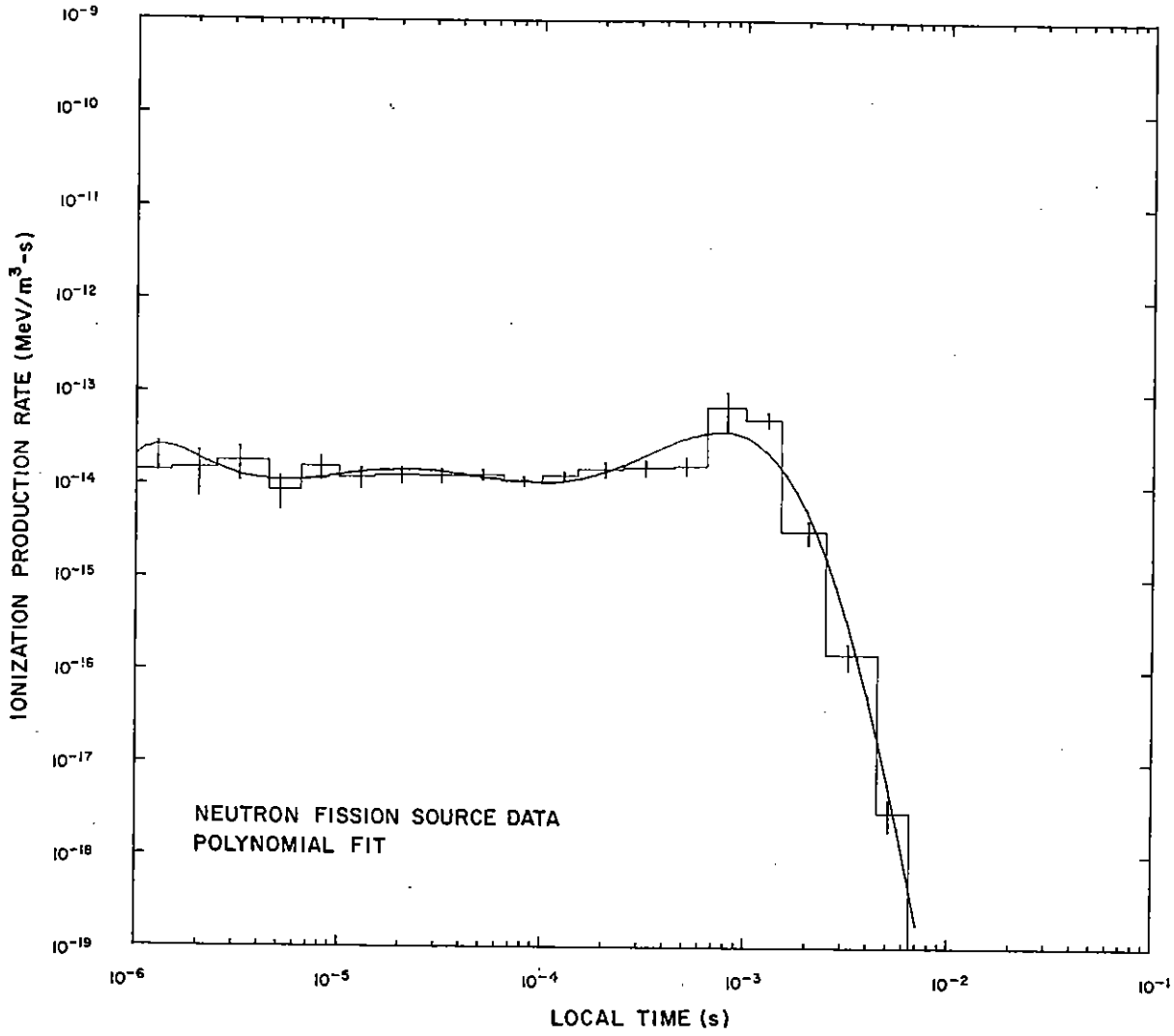

Figure 28. Ionization rate versus time for detector 7.

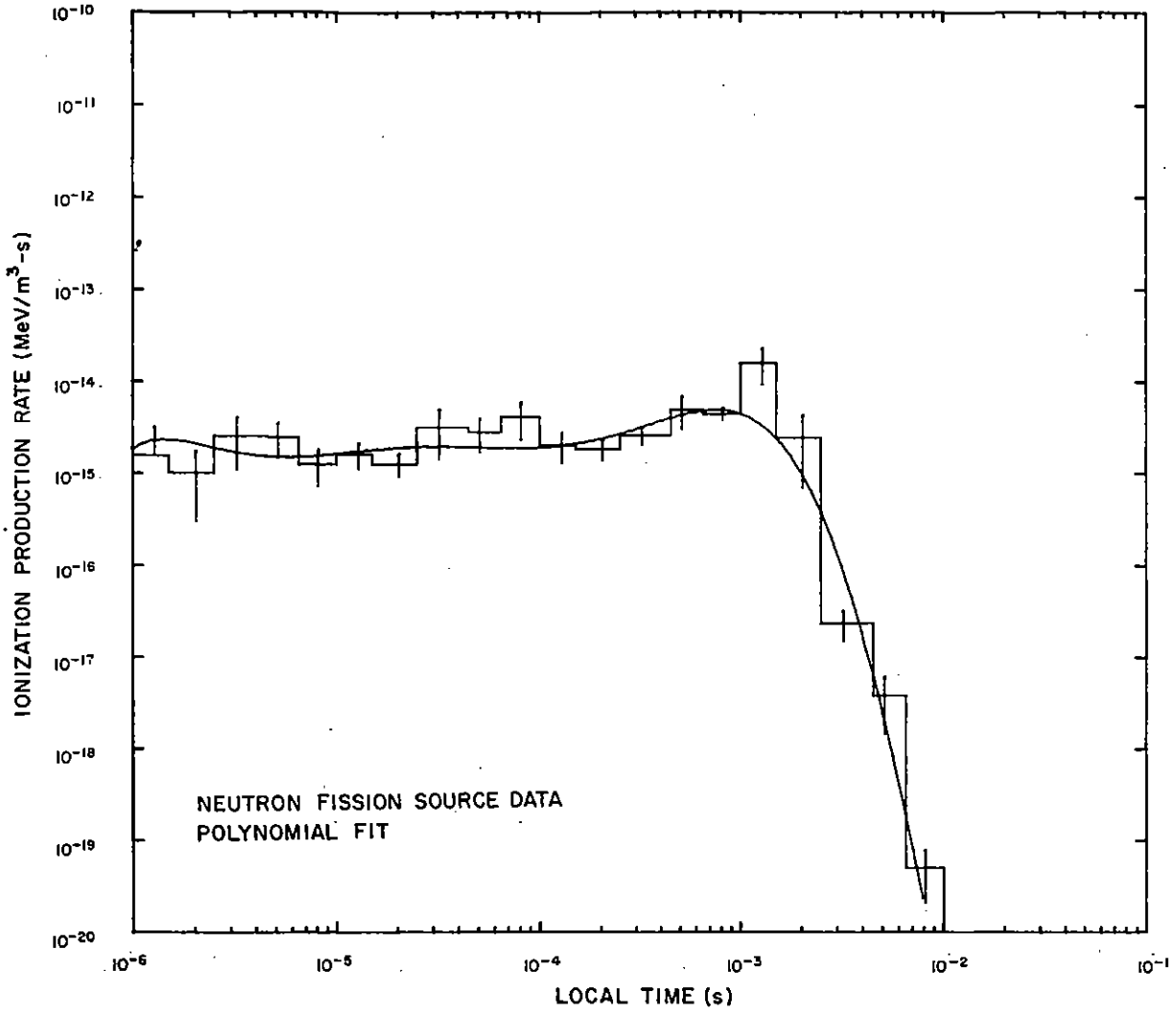

Figure 29. Ionization rate versus time for detector 8.

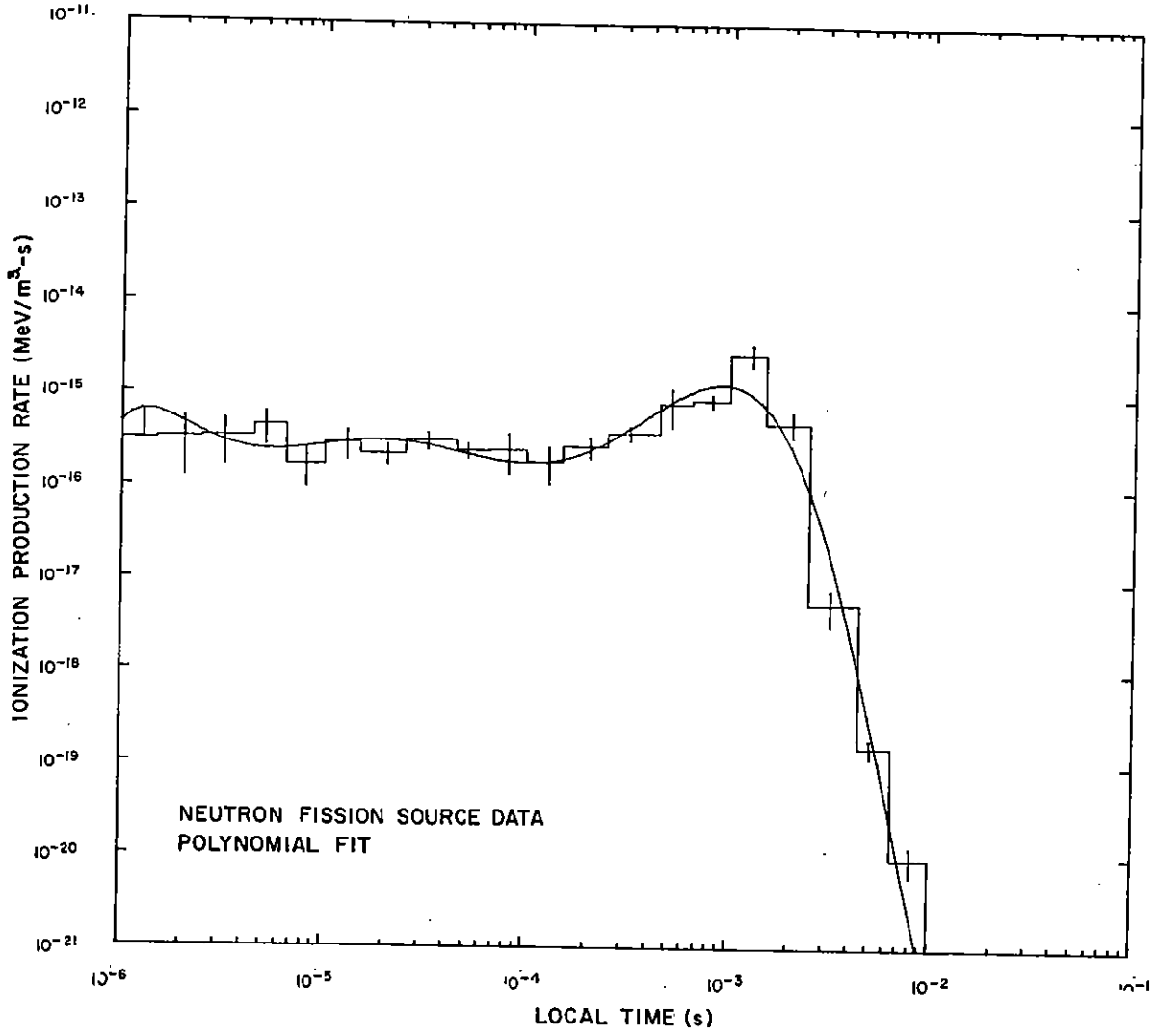

Figure 30. Ionization rate versus time for detector 9.

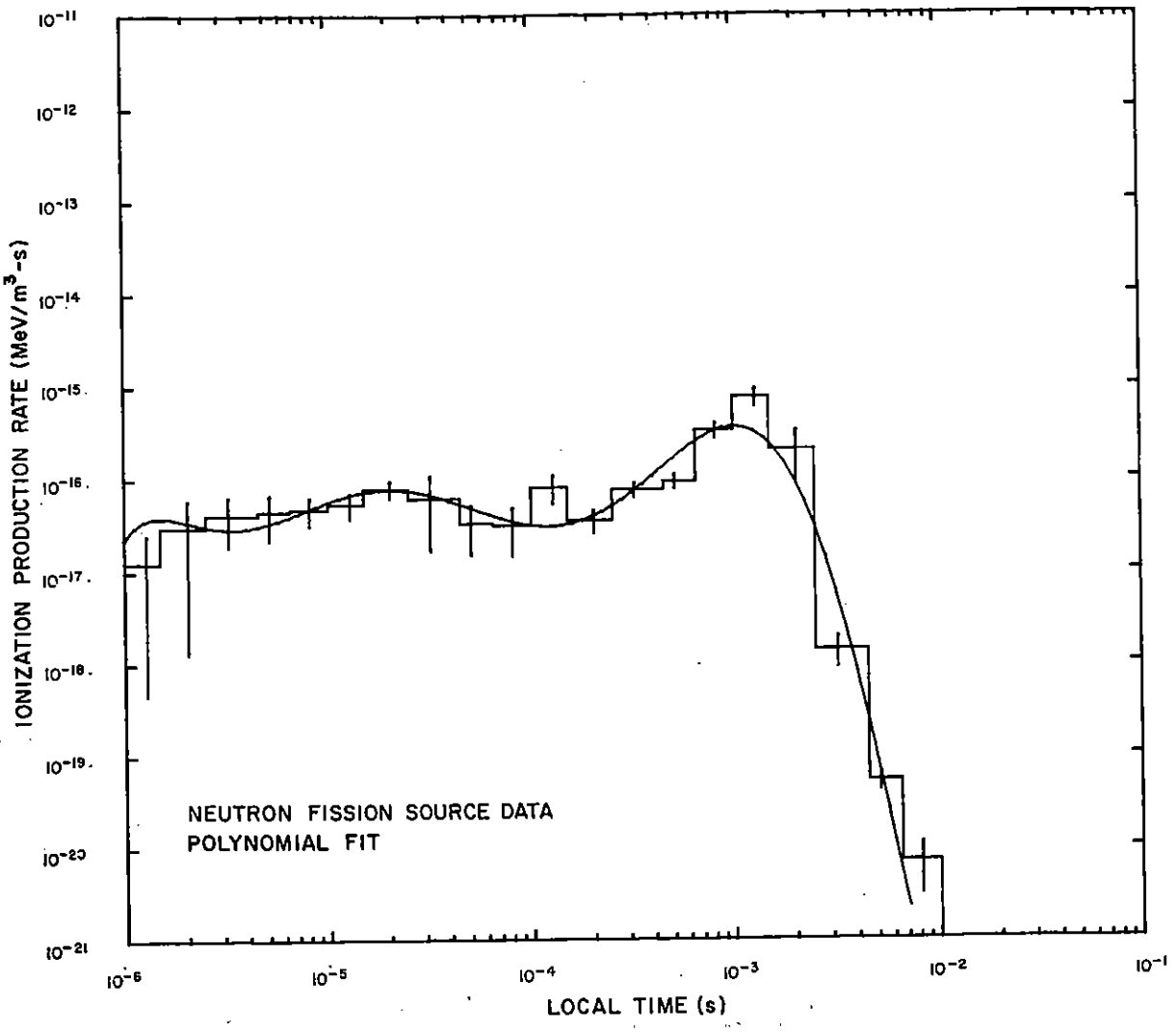

Figure 31. Ionization rate versus time for detector 10.

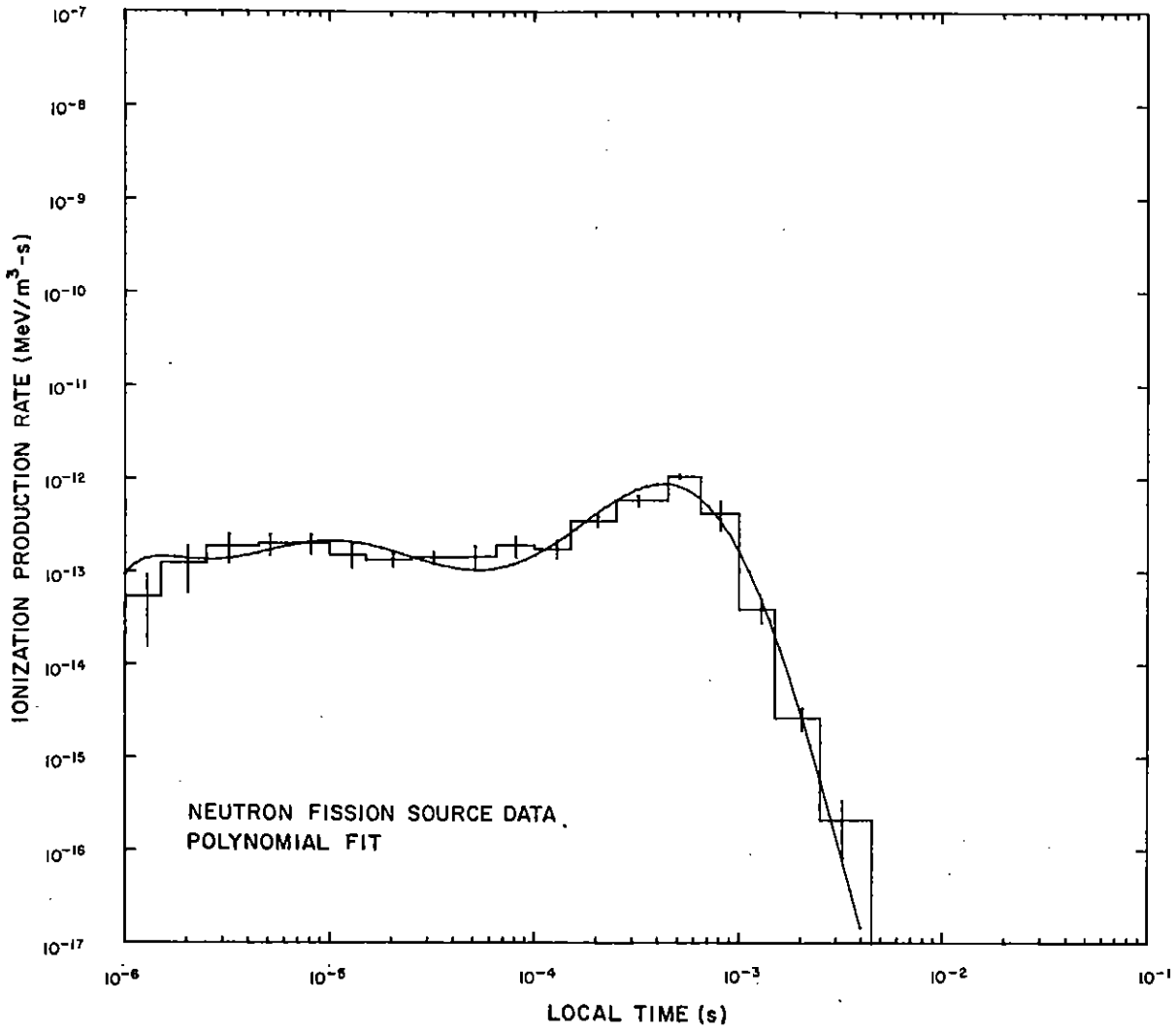

Figure 32. Ionization rate versus time for detector 11.

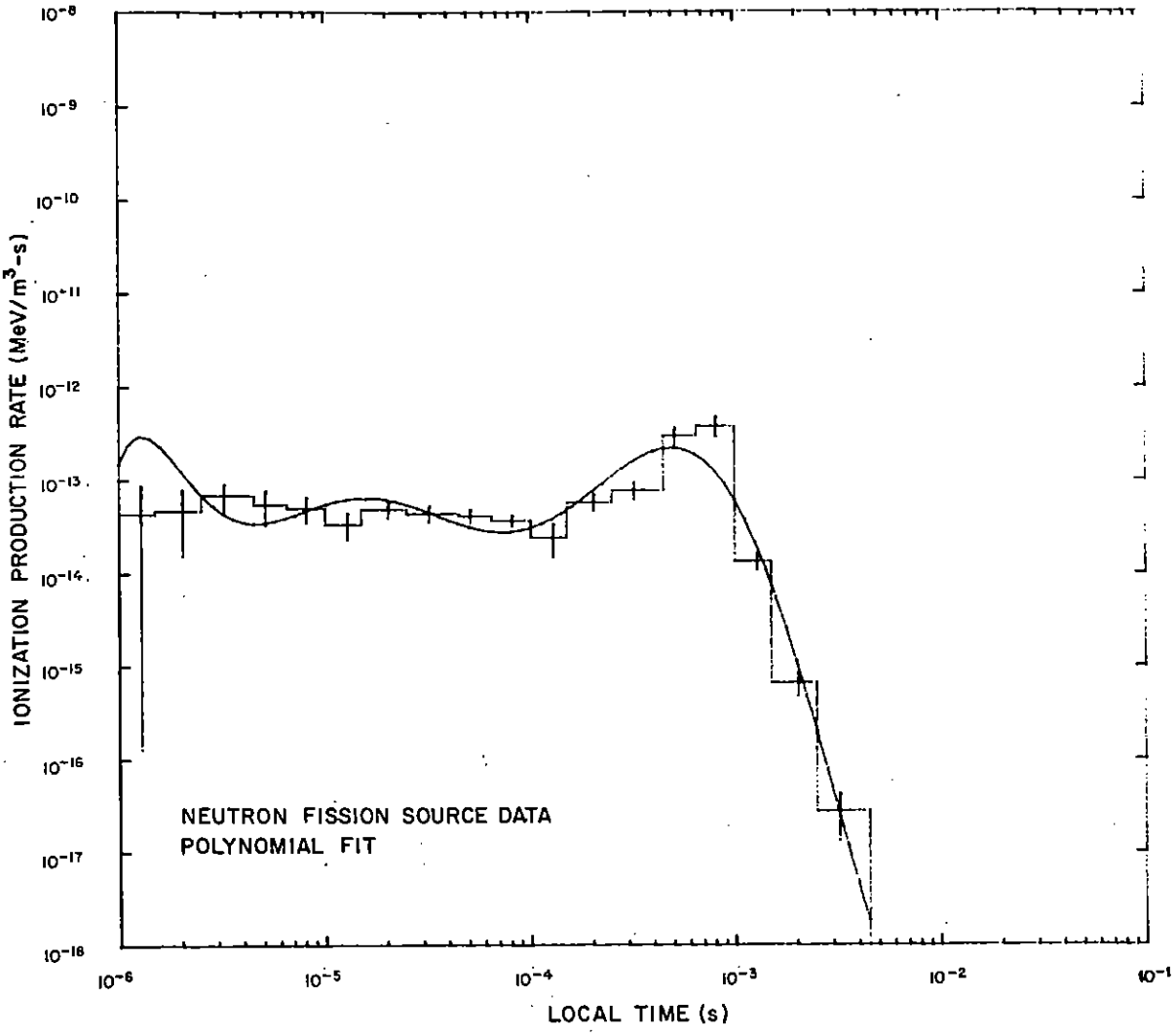

Figure 33. Ionization rate versus time for detector 12.

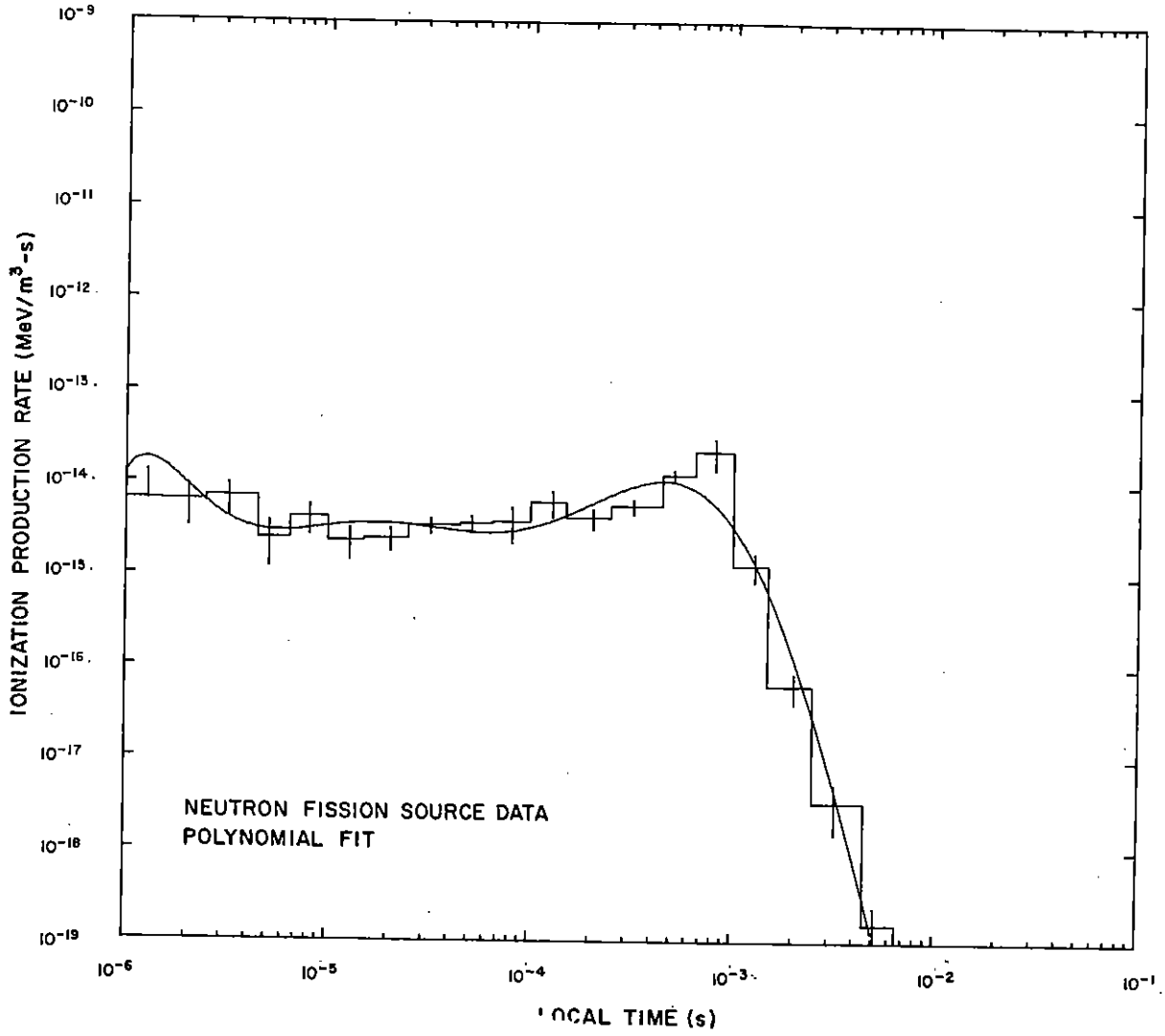

Figure 34. Ionization rate versus time for detector 13.

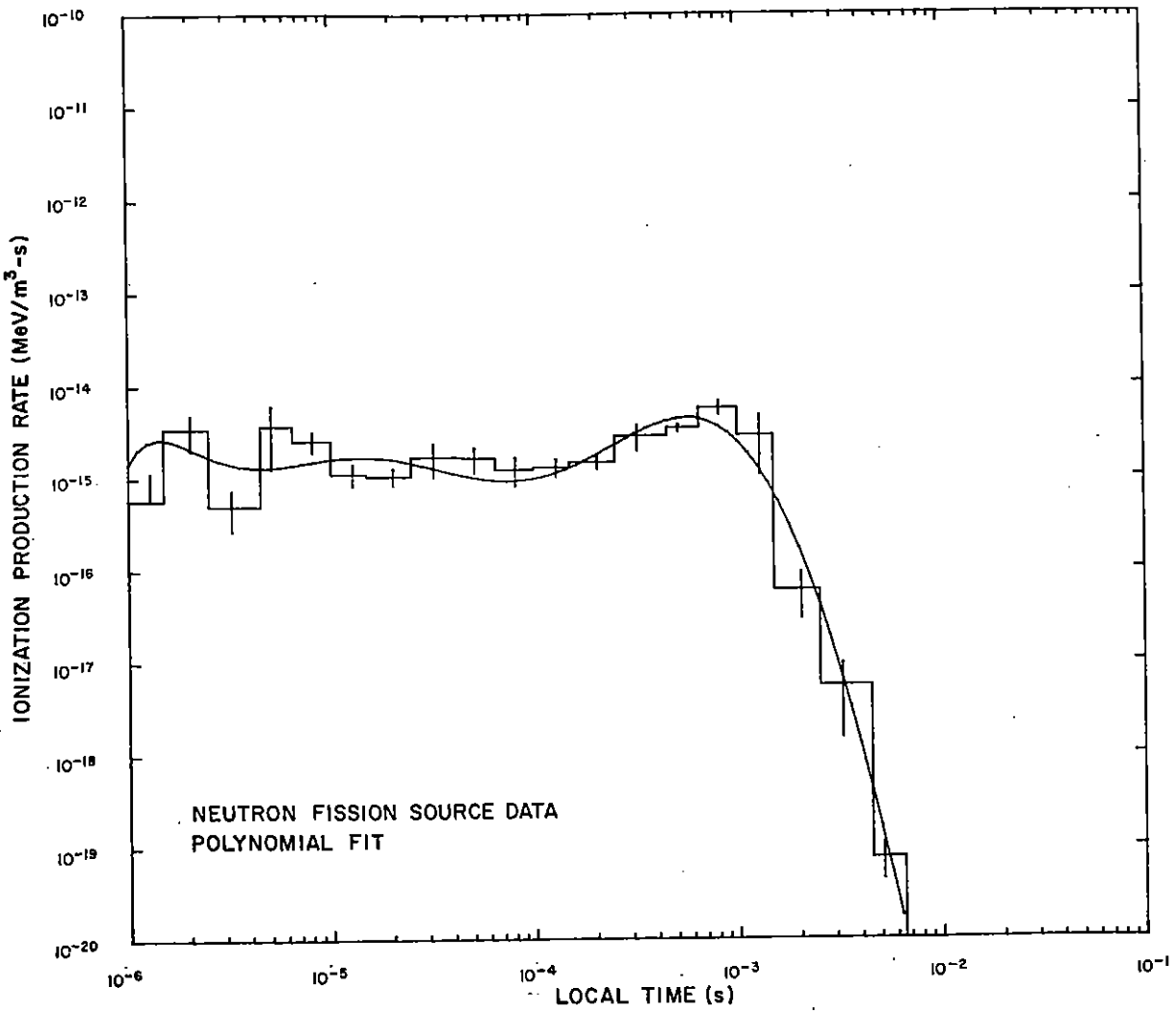

Figure 35. Ionization rate versus time for detector 14.

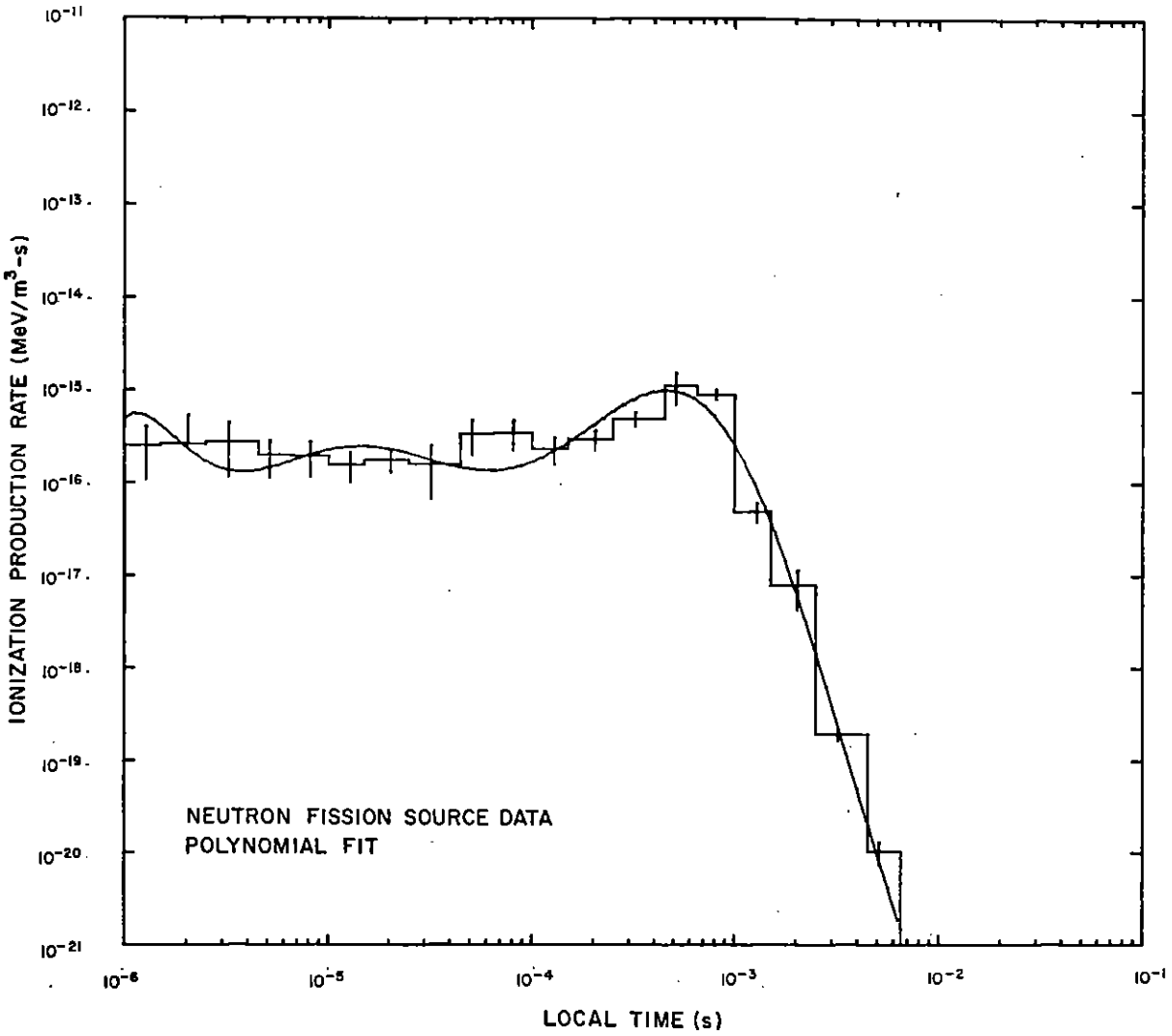

Figure 36. Ionization rate versus time for detector 15.

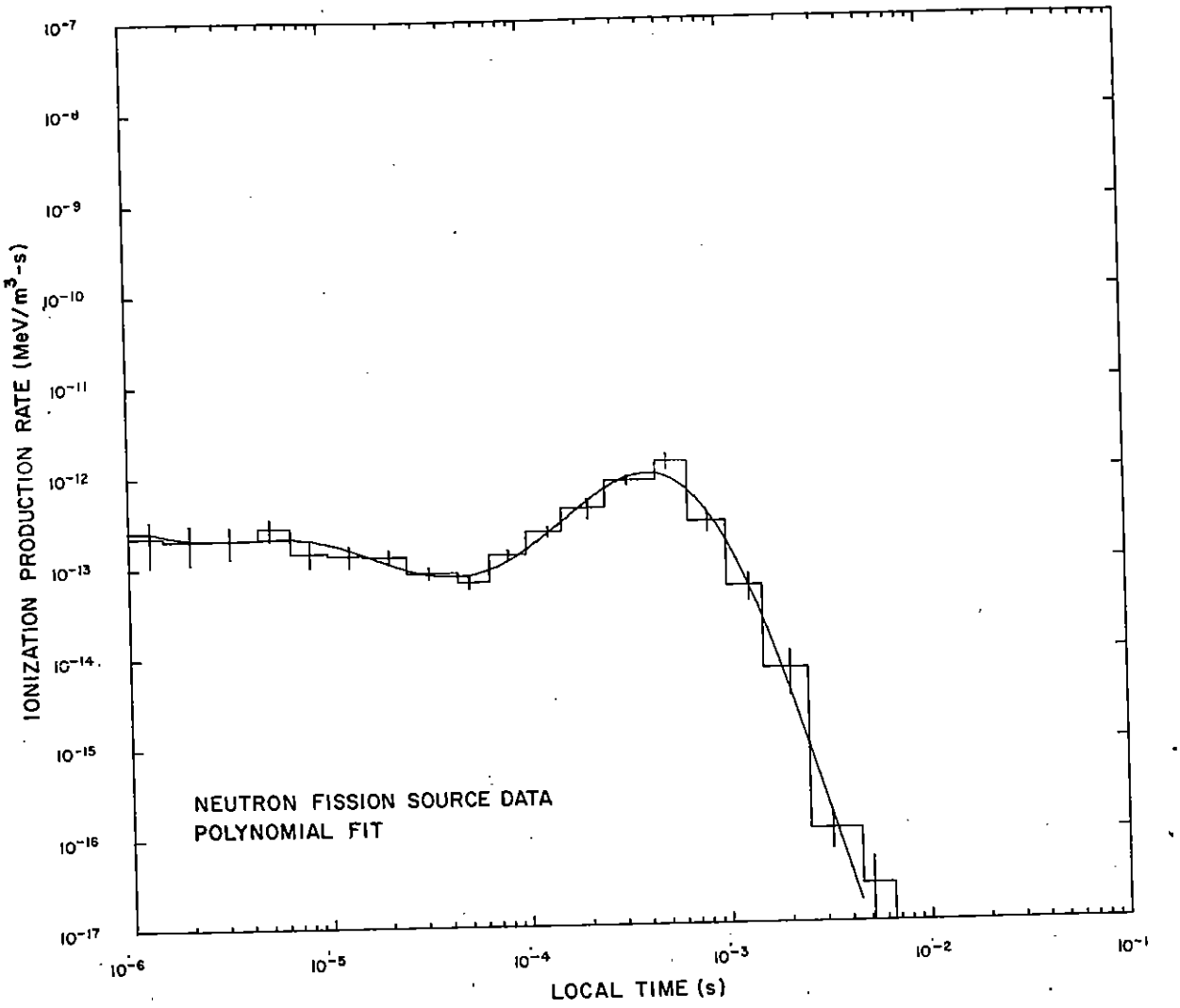

Figure 37. Ionization rate versus time for detector 16.

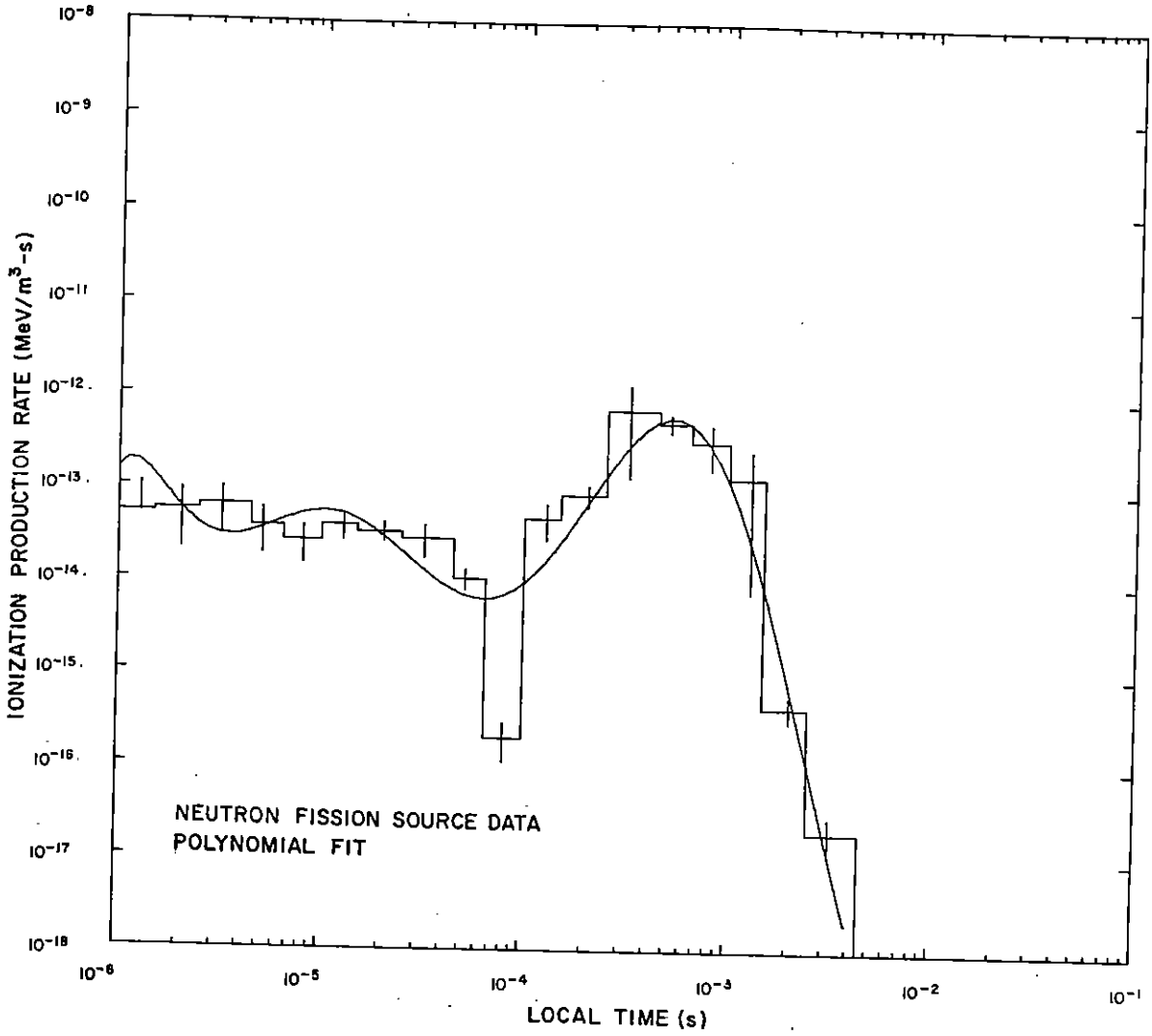

Figure 38. Ionization rate versus time for detector 17.

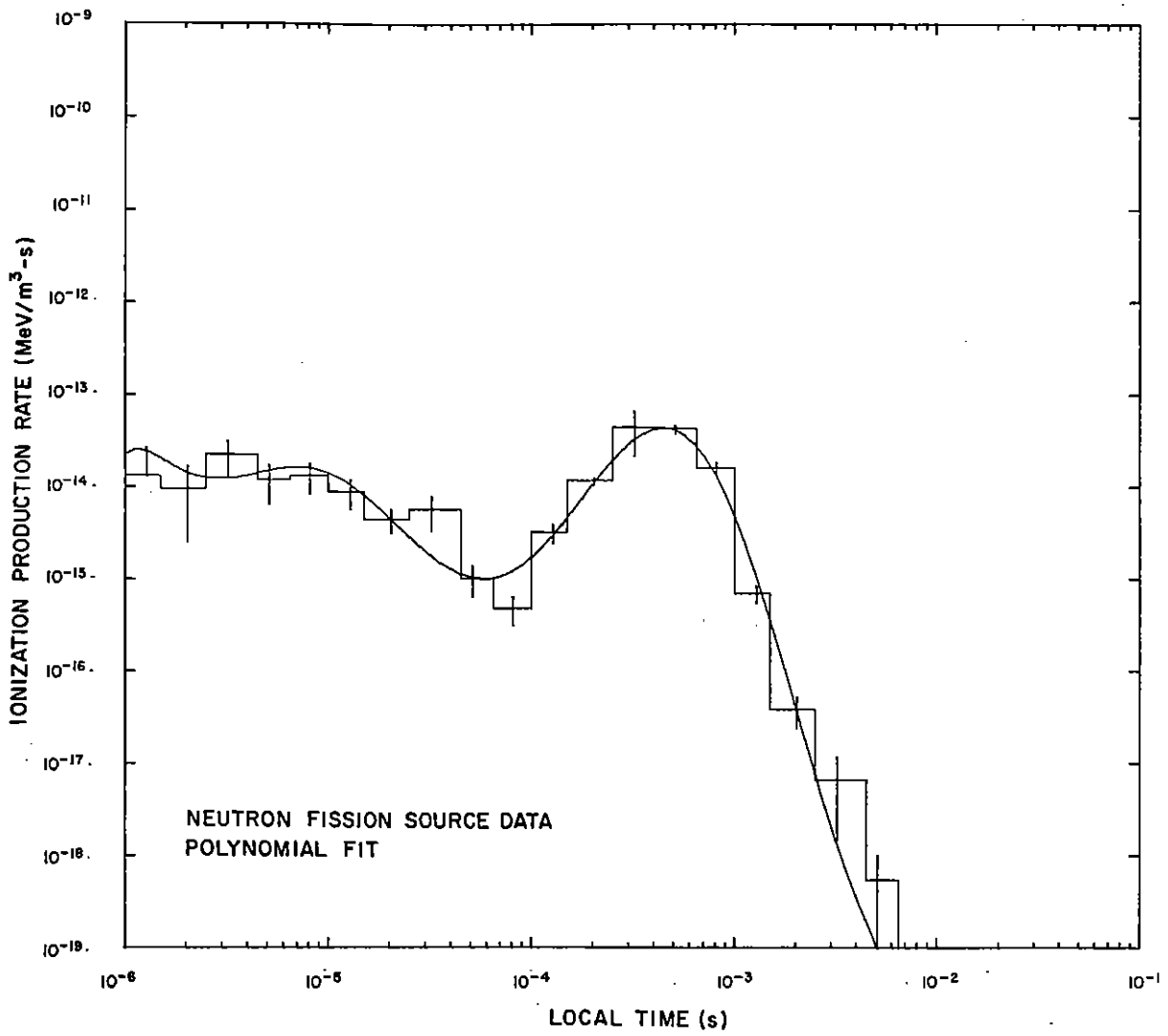

Figure 39. Ionization rate versus time for detector 18.

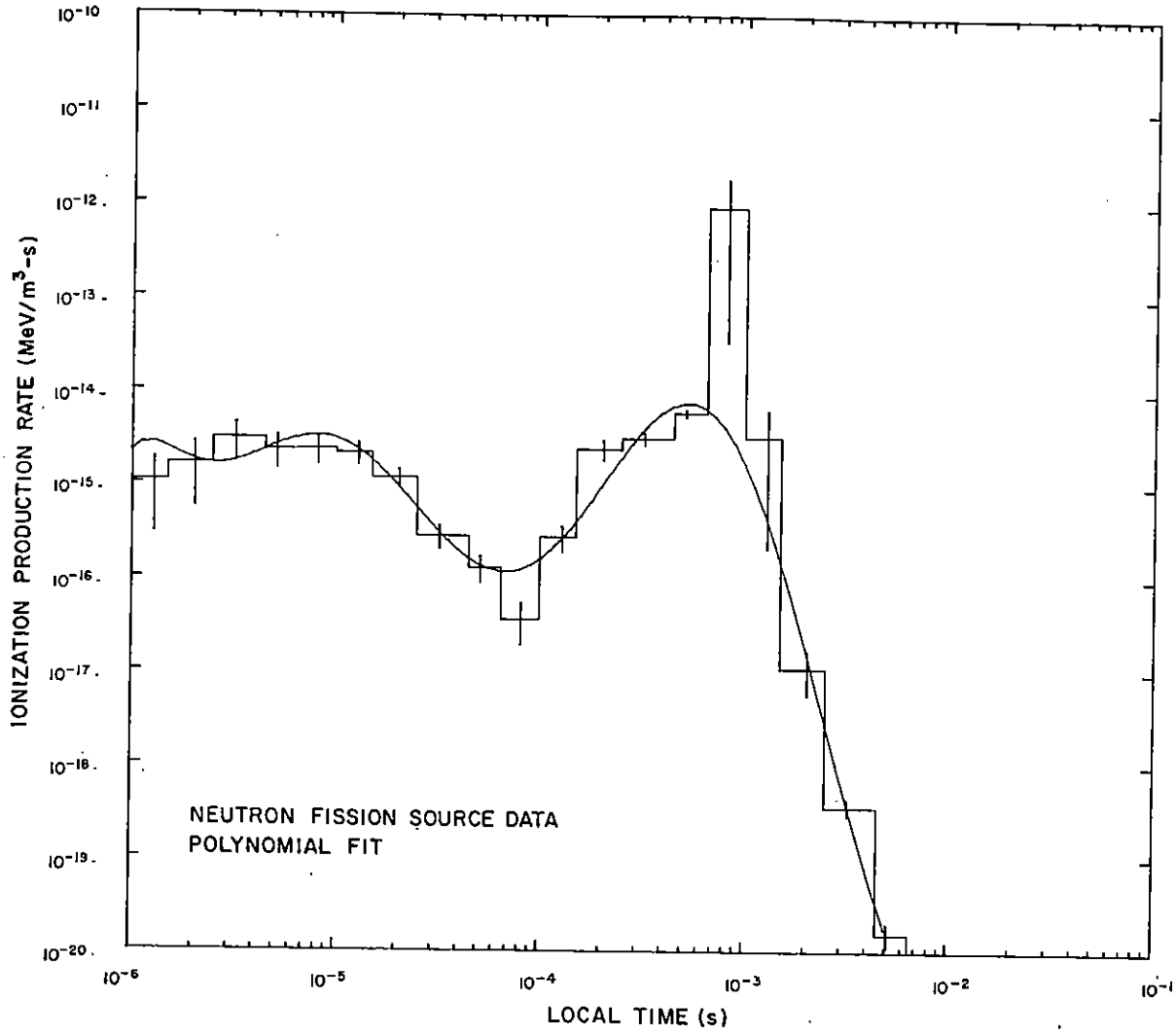

Figure 40. Ionization rate versus time for detector 19.

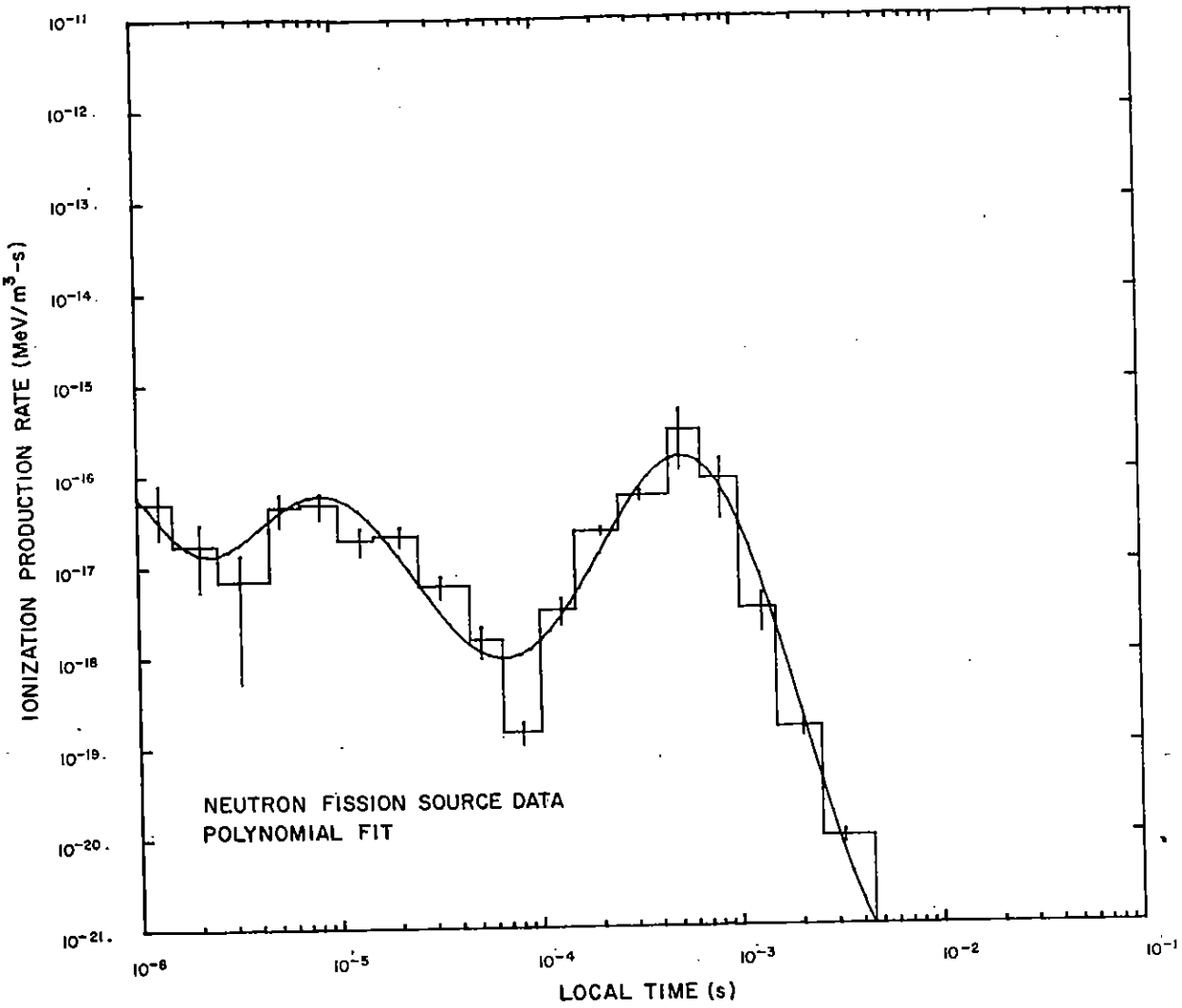

Figure 41. Ionization rate versus time for detector 20.

TABLE II. POLYNOMIAL COEFFICIENTS FOR THE 14-MeV NEUTRON SOURCE CALCULATIONS

Detector	a_0	a_1	a_2	a_3	a_4	a_5	a_6	a_7	a_8	t_{max}
1	-12.9330	-0.678826	3.53393	-8.04557	9.03330	-5.52394	1.87235	-0.327308	2.27358-2	7.01522-4
2	-13.8094	-0.595220	-0.689687	2.15765	-2.62040	1.94508	-0.834711	0.183202	-1.57623-2	2.88469-3
3	-15.0867	-1.07923	7.34023	-12.5737	8.74808	-2.36255	-5.59977-2	0.133492	-1.66356-2	3.71431-3
4	-15.6394	1.28210	-11.1028	28.4229	-33.2992	20.5286	-6.88429	1.18711	-8.23548-2	4.88057-3
5	-17.0627	4.18283	-16.0423	31.8902	-33.3659	19.2593	-6.17099	1.02827	-6.94594-2	4.91928-3
6	-11.5488	3.59478	-26.8622	58.6224	-60.5257	33.5764	-10.2486	1.62099	-1.04013-1	4.33098-4
7	-12.4745	0.549768	0.168298	-5.50734	10.6290	-8.72307	3.55446	-0.702775	5.34699-2	9.30468-4
8	-13.5223	1.25052	-0.647244	-3.90792	8.54136	-7.46099	3.20979	-0.666064	5.28630-2	7.96097-4
9	-14.4537	1.74387	-0.781115	-9.30783	14.1348	-9.86512	3.59269	-0.656069	4.70361-2	8.95255-4
10	-14.7805	7.49164-3	9.05508	-28.7519	36.1682	-23.0260	7.83596	-1.35342	9.28401-2	1.28997-3
11	-11.3996	-0.578562	1.35448	-0.279001	-0.942565	0.541295	1.29780-2	-5.43874-2	7.82732-2	4.21671-4
12	-11.8336	1.40946	-17.0620	43.1856	-47.2544	26.4878	-7.91066	1.19485	-7.18419-2	5.31823-4
13	-12.6055	0.283306	-7.89790	16.8928	-15.3132	6.92724	-1.55162	0.147980	-3.23229-3	5.91350-4
14	-13.2122	1.00740	-8.46783	17.5533	-16.1177	7.42577	-1.70842	0.172103	-4.61962-3	6.06973-4
15	-14.0960	1.88443	-6.61440	8.98516	-4.99333	0.287682	0.768072	-0.271029	2.72849-2	5.74807-4
16	-11.1931	-0.778750	2.83869	-3.23976	-2.37773-2	1.72993	-0.936700	0.193446	1.44173-2	3.70576-4
17	-11.6511	-0.483608	5.26097	5.26097	-10.7225	8.22898	-2.95374	0.501031	-3.25978-2	4.99431-4
18	-12.3890	0.349965	8.46983	8.46983	-1.36253	9.81913	-3.42331	0.567310	-3.59662-2	4.52088-4
19	-13.1104	-1.56264	-9.61296	-9.61296	3.69195	0.426903	-0.519800	9.25039-2	-4.18882-3	4.84852-4
20	-13.7460	-0.489365	27.0892	27.0892	-38.5689	25.7796	-8.77836	1.47613	-9.75117-2	4.29932-4

TABLE III. POLYNOMIAL COEFFICIENTS FOR THE NEUTRON FISSION SOURCE CALCULATIONS

Detector	a_0	a_1	a_2	a_3	a_4	a_5	a_6	a_7	a_8	t_{max}
1	-14.4163	0.289462	1.03900	-4.56943	6.02368	-3.92748	1.37665	-0.246037	1.74118-2	6.93713-4
2	-16.0562	0.390673	4.26475	-9.75943	8.39906	-3.48203	0.691290	-5.03218-2	-6.04539-4	2.11299-3
3	-16.3332	-1.68439	4.70947	-4.24056	0.159972	1.83464	-1.08998	0.251942	-2.10984-2	3.83085-3
4	-17.4627	0.772352	-8.51406	24.1406	-29.5349	18.5967	-6.29134	1.08549	-7.49222-2	5.71900-3
5	-17.3235	-0.346911	-13.3946	36.6087	-41.1512	24.0944	-7.69577	1.26929	-8.45379-2	6.04470-3
6	-12.8674	1.20071	-14.7286	32.6483	-32.2948	16.7810	-4.72671	0.681150	-3.93979-2	5.54010-4
7	-13.6912	2.10236	-12.6169	23.3136	-20.2789	9.26799	-2.24788	0.267869	-1.19890-2	7.47061-4
8	-14.7346	1.53150	-7.14661	11.4739	-8.58592	3.19096	-0.533424	1.98589-2	2.40943-3	7.51648-4
9	-15.3280	2.46479	-13.9429	24.9622	-21.0239	9.18134	-2.07251	0.217729	-7.45098-3	9.11380-4
10	-16.6441	3.32343	-15.6369	28.9079	-24.9679	11.0074	-2.47946	0.256819	-8.39590-3	1.01697-3
11	-13.0318	2.89287	-15.0961	34.1077	-37.5255	21.7649	-6.78132	1.07139	-6.74141-2	4.27070-4
12	-12.8304	6.33317	-40.2743	82.1288	-80.6423	42.7004	-12.4345	1.87102	-0.113662	4.90387-4
13	-13.8985	3.50683	-23.7684	47.1679	-45.1320	23.4151	-6.69738	0.989882	-5.90399-2	4.51871-4
14	-14.8474	4.25434	-21.6564	41.9002	-40.1738	20.8541	-5.93983	0.871510	-5.15545-2	5.64347-4
15	-15.3081	2.12662	-21.3942	50.1101	-53.1184	29.5689	-8.91614	1.37584	-8.51712-2	4.62820-4
16	-12.5919	0.338998	-5.38929	16.5815	-21.8974	14.2945	-4.82483	0.806982	-5.30091-2	4.09897-4
17	-12.8252	3.40676	-33.1637	80.7578	-89.2266	51.3146	-15.8639	2.49742	-0.157209	5.28577-4
18	-13.6472	1.78637	-18.9551	52.0273	-63.5217	39.3568	-12.8777	2.12115	-0.138651	4.46578-4
19	-14.6590	2.58062	-21.8058	58.1977	-69.4124	41.9739	-13.4095	2.15887	-0.138101	5.25945-4
20	-16.2284	-1.78453	-10.5863	49.1089	-59.1668	45.1408	-15.0711	2.50034	-0.163655	5.23254-4

Results are presented for the same 20 detector positions and two source spectra in figures 42 to 81. A fit to an analytical expression is used in this instance to yield a clearer physical insight into the process occurring during transport. Ionization production rate is shown as a function of local time. However, these results are now fitted to the function

$$y = \left(a + bt^{n}\right)e^{-ct} \quad .$$

Coefficients (a, b, n, c) for the above function are given for all detectors in table IV for the 14-MeV source and table V for the fission source. The parameters and the method of fitting of this equation to the data are explained in appendix A. Scaling methods are given in appendix B.

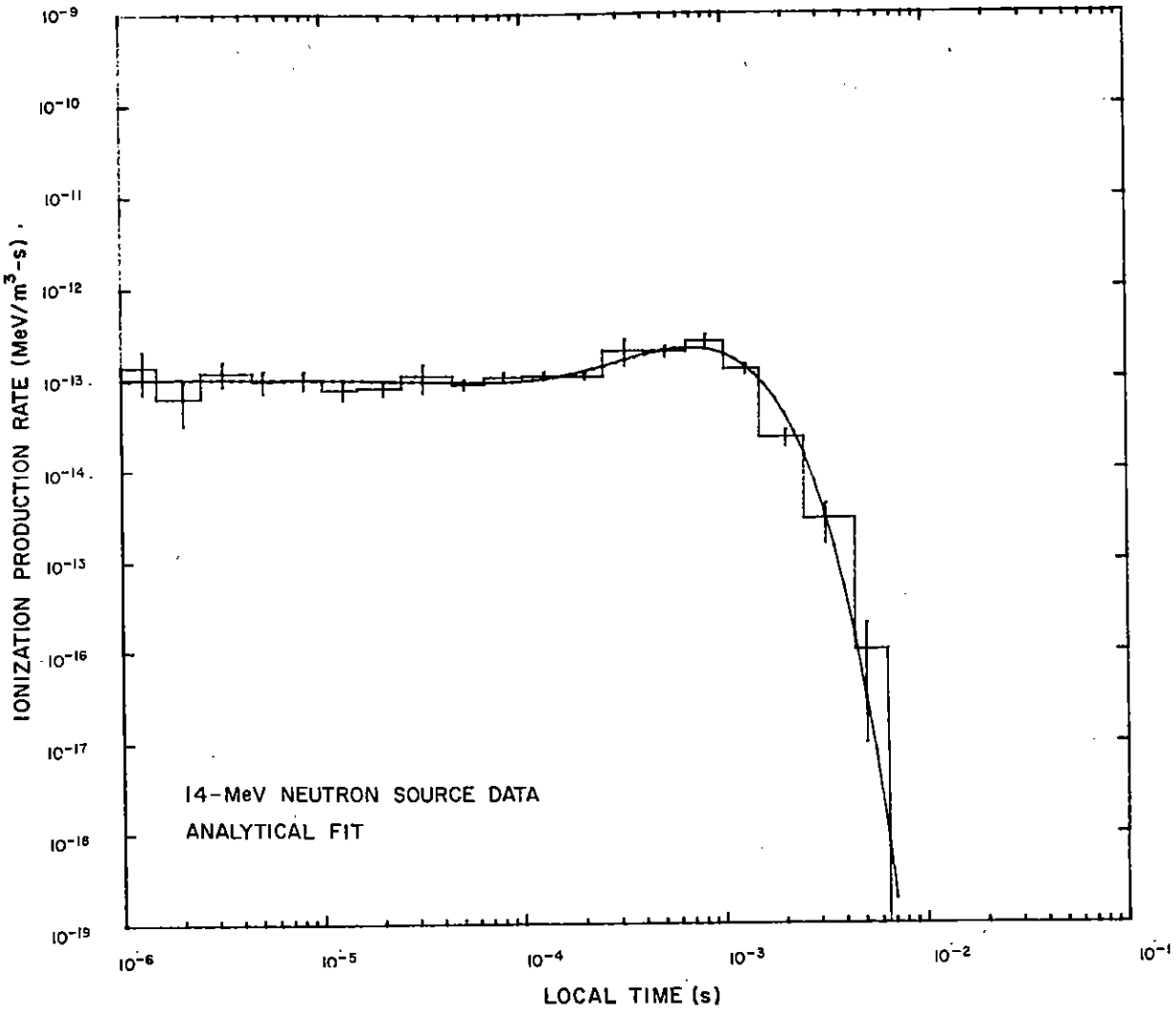

Figure 42. Ionization rate versus time for detector 1.

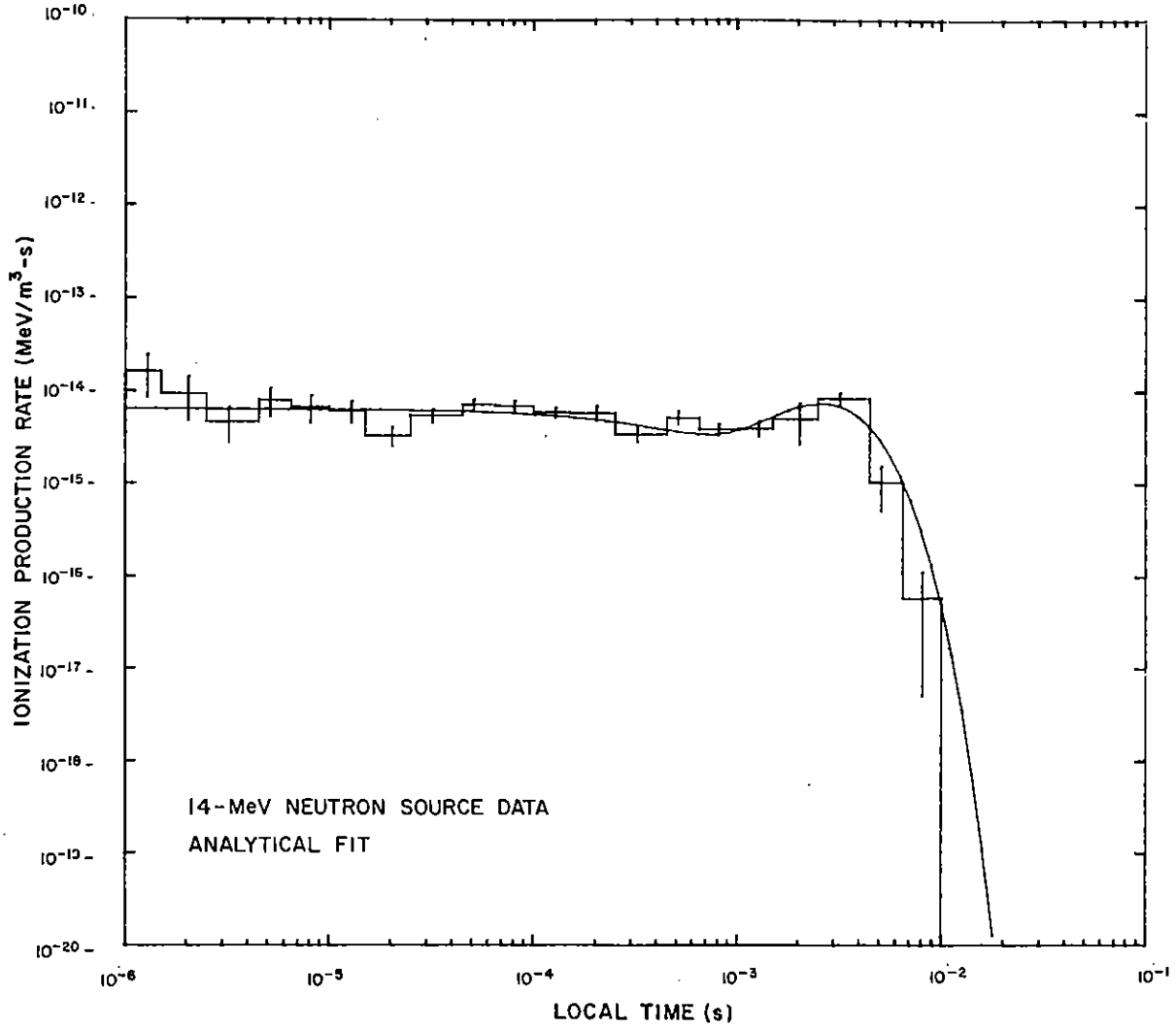

Figure 43. Ionization rate versus time for detector 2.

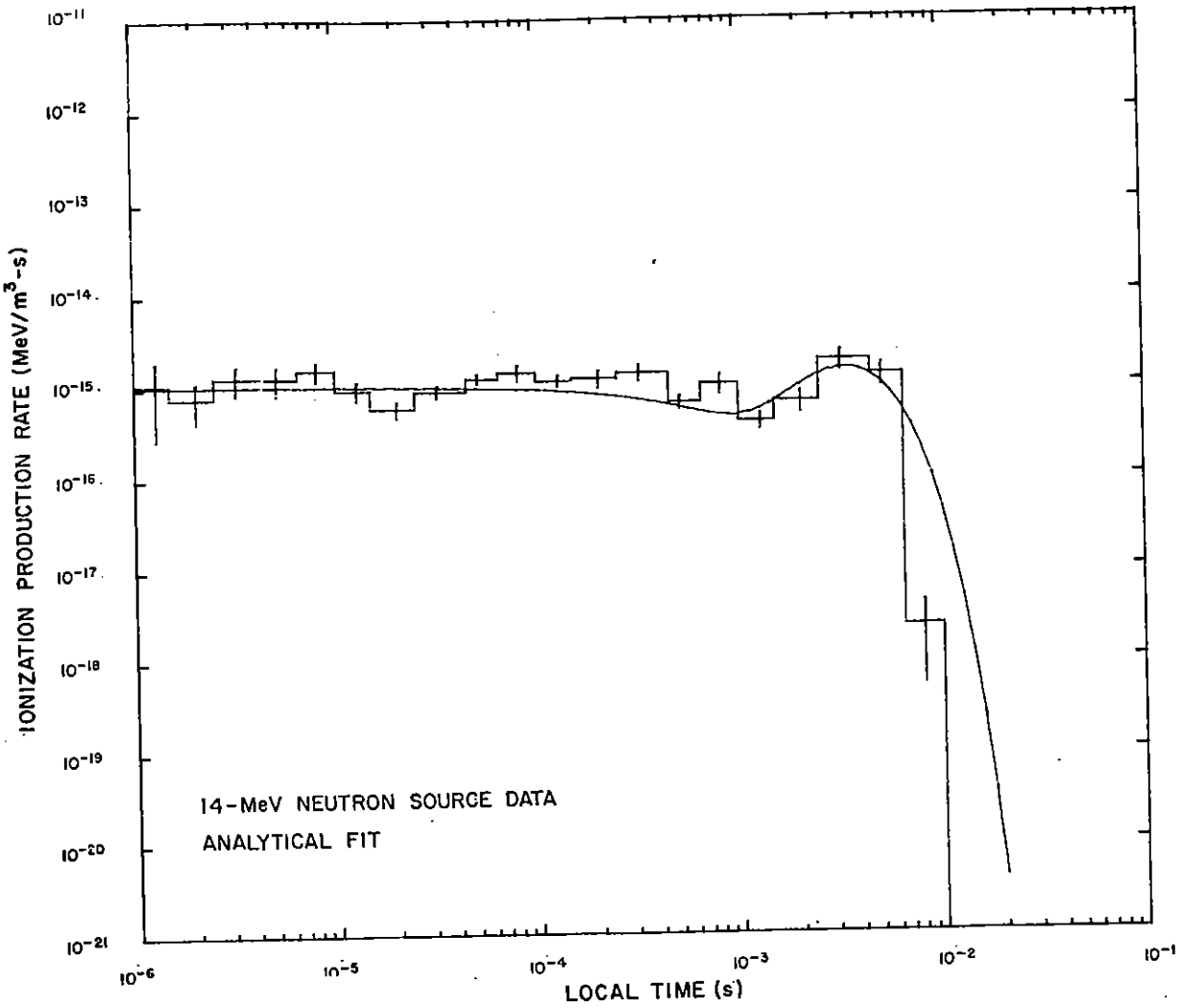

Figure 44. Ionization rate versus time for detector 3.

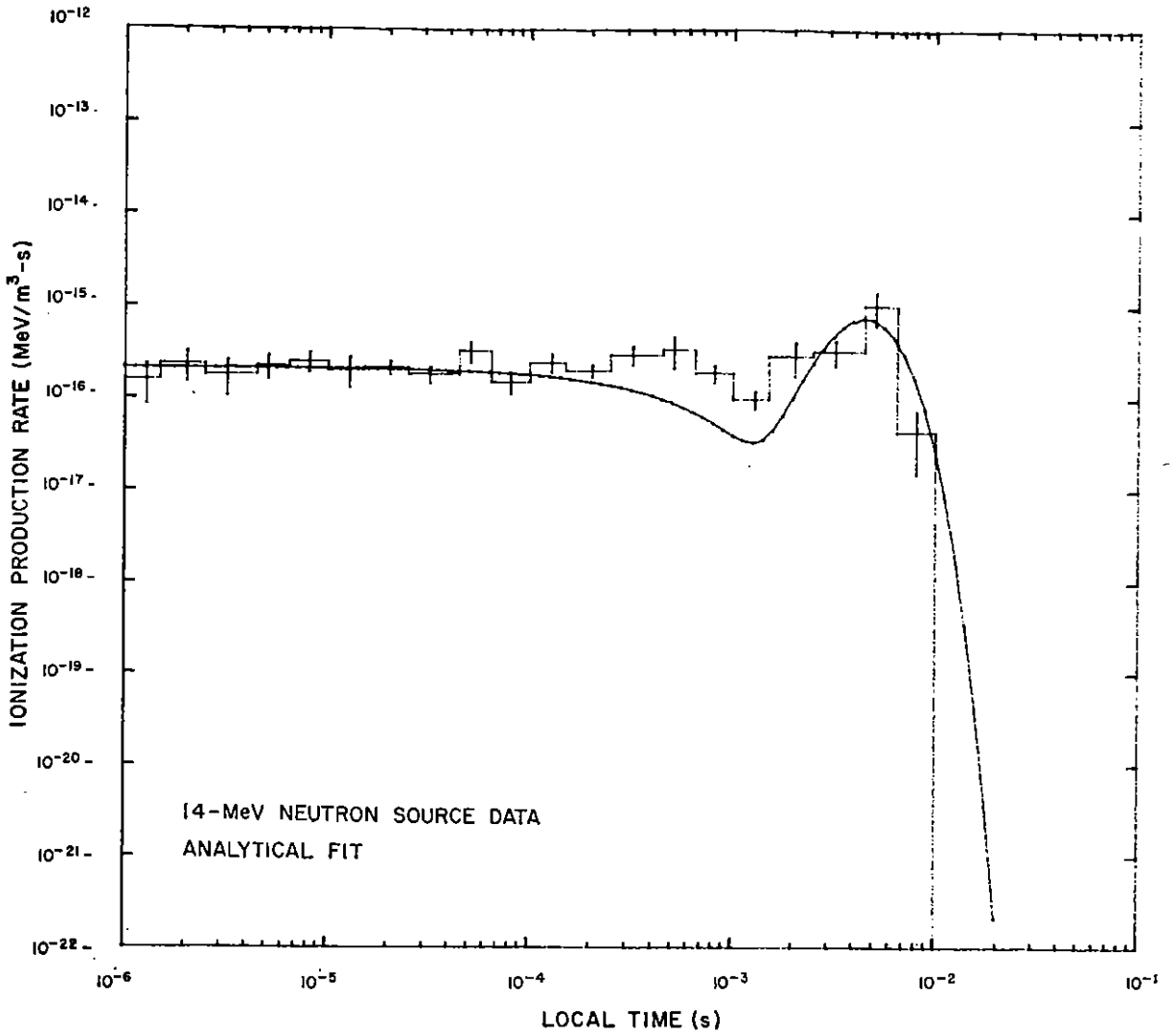

Figure 45. Ionization rate versus time for detector 4.

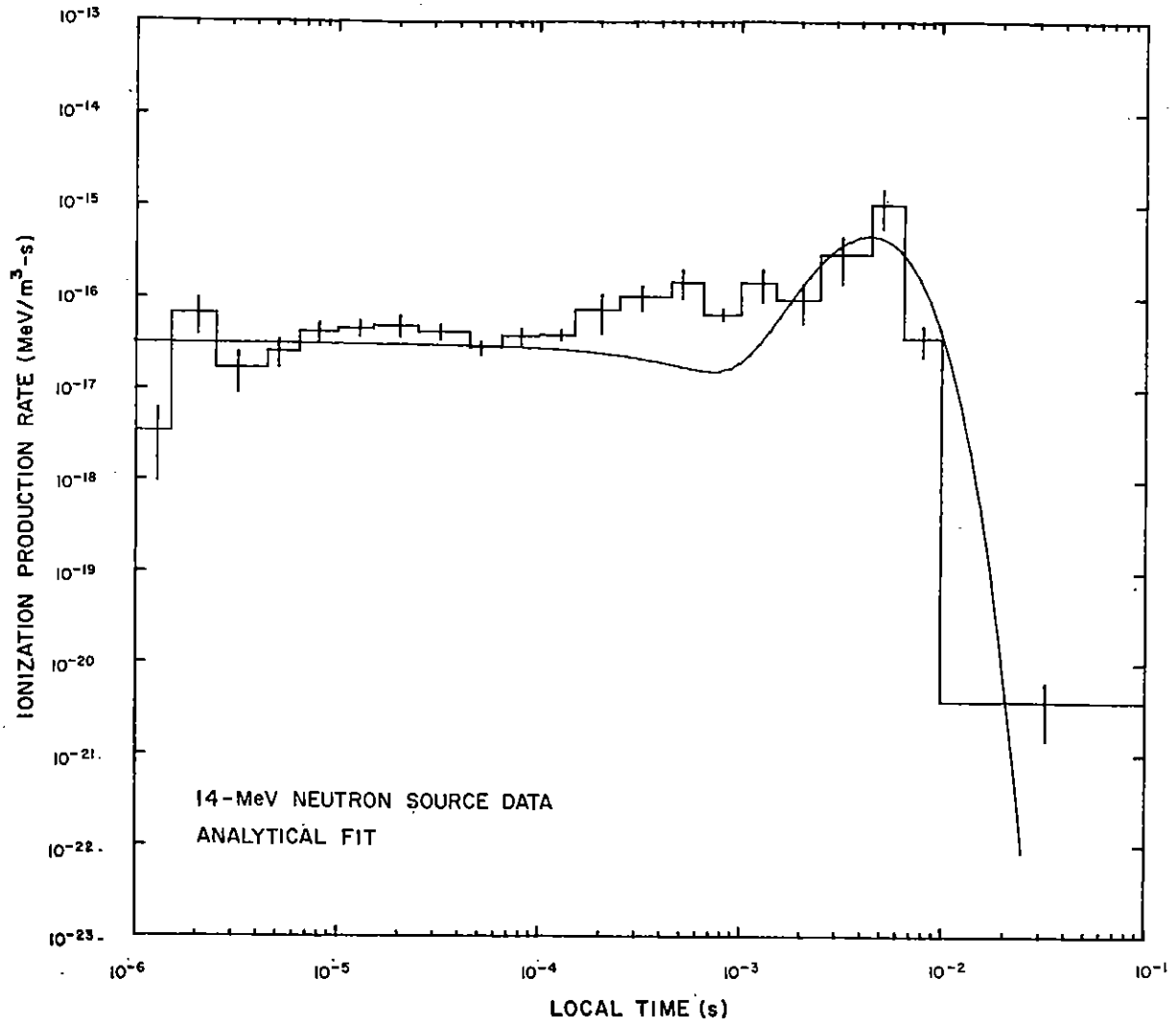

Figure 46. Ionization rate versus time for detector 5.

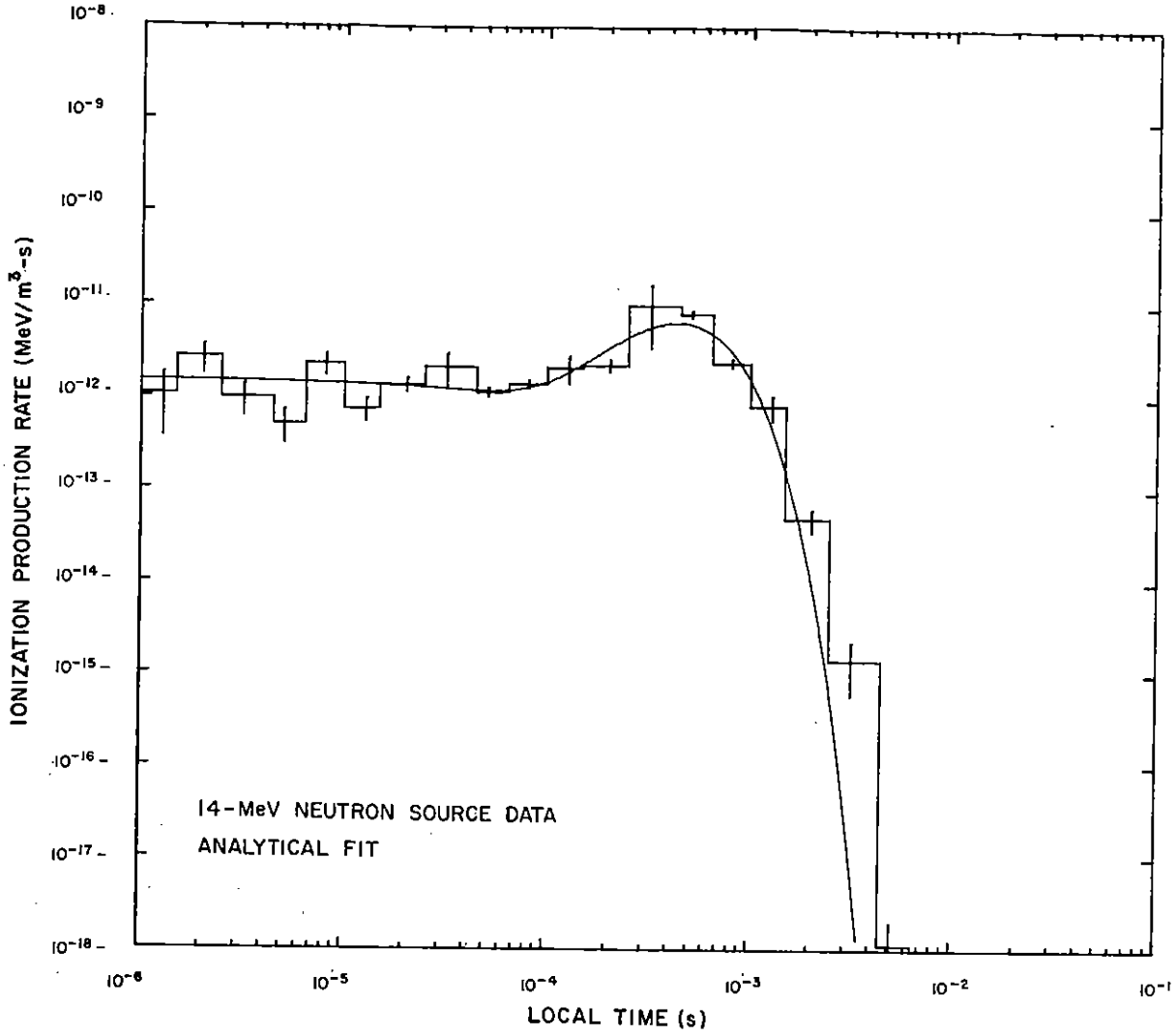

Figure 47. Ionization rate versus time for detector 6.

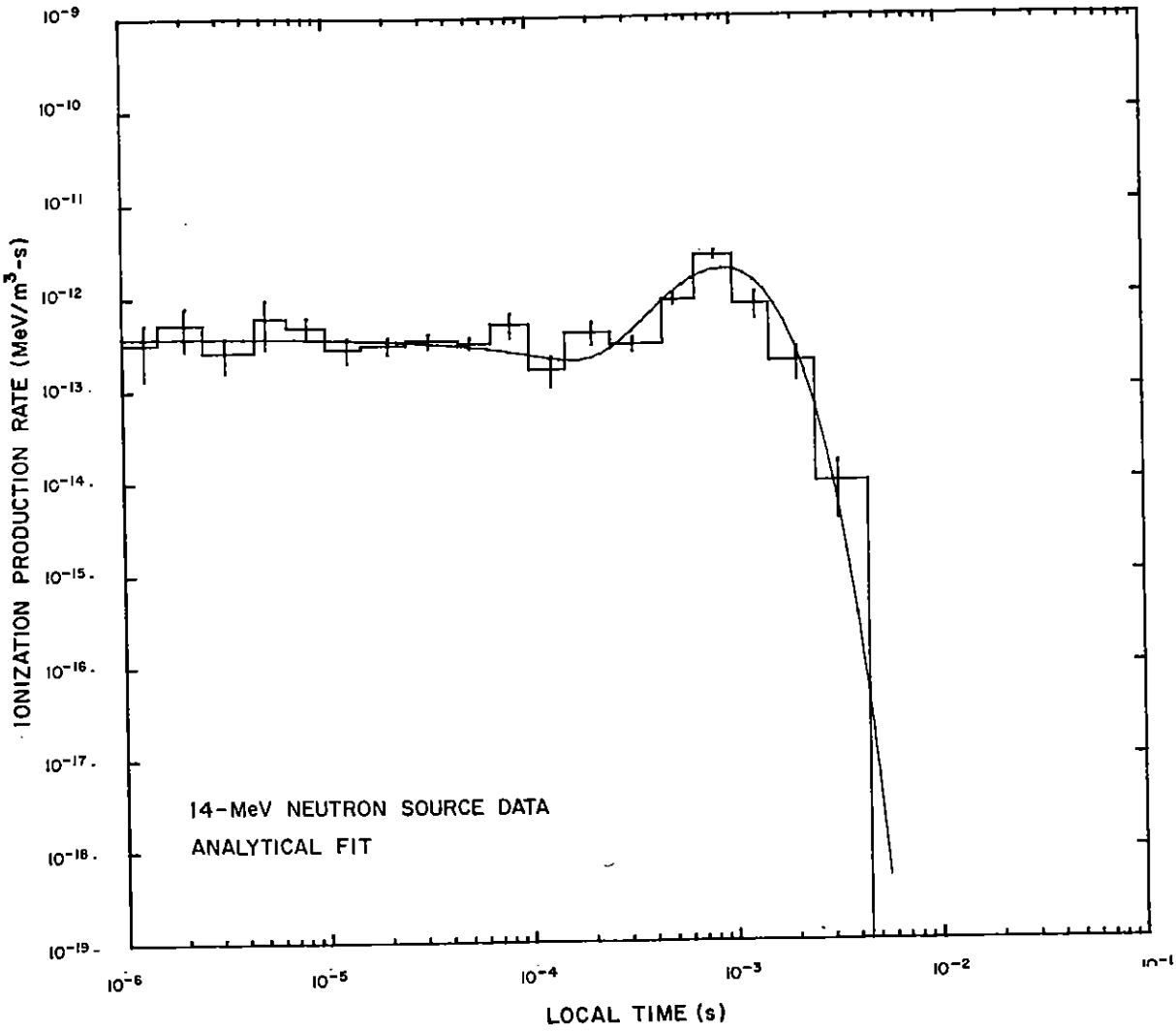

Figure 48. Ionization rate versus time for detector 7.

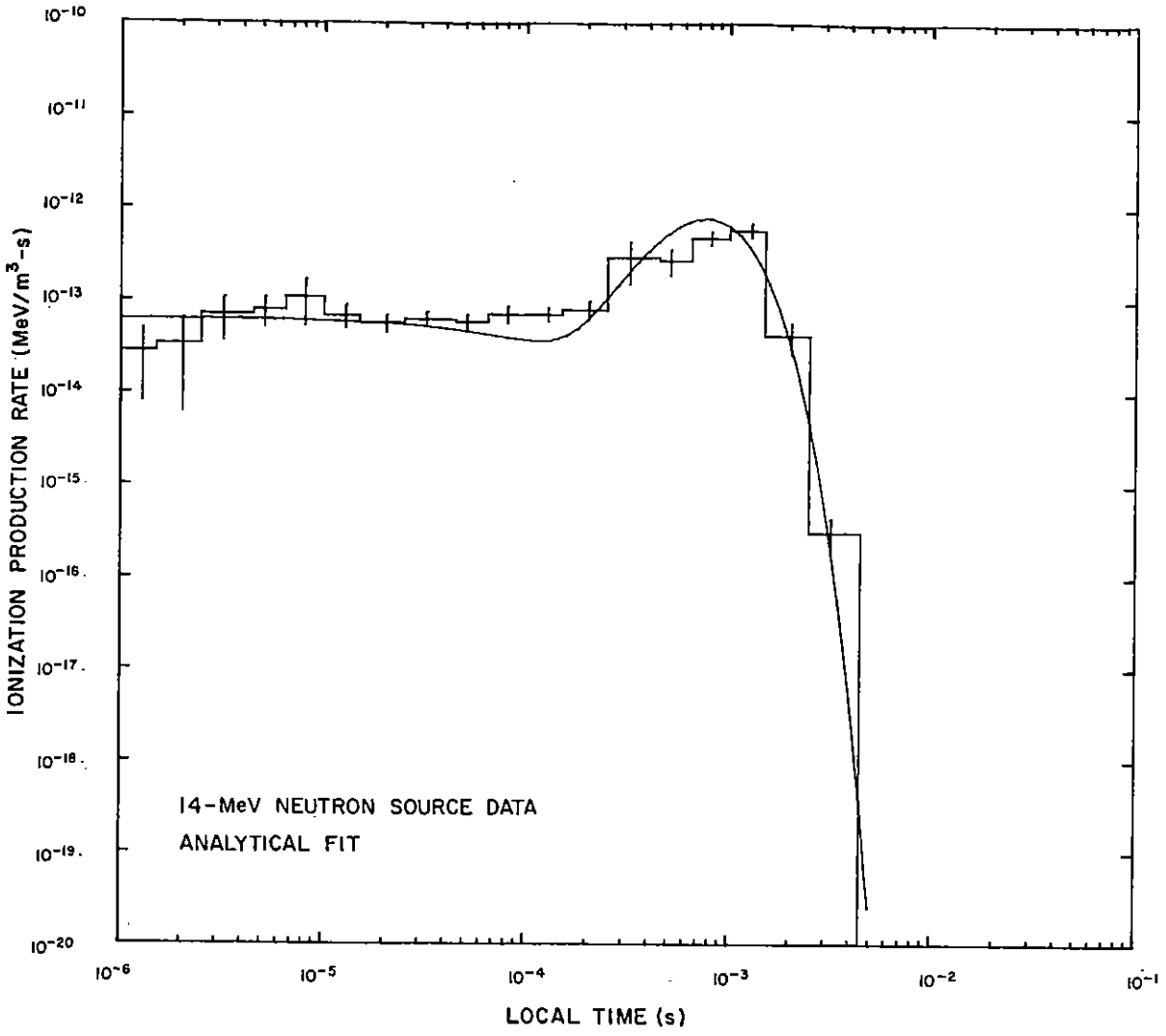

Figure 49. Ionization rate versus time for detector 8.

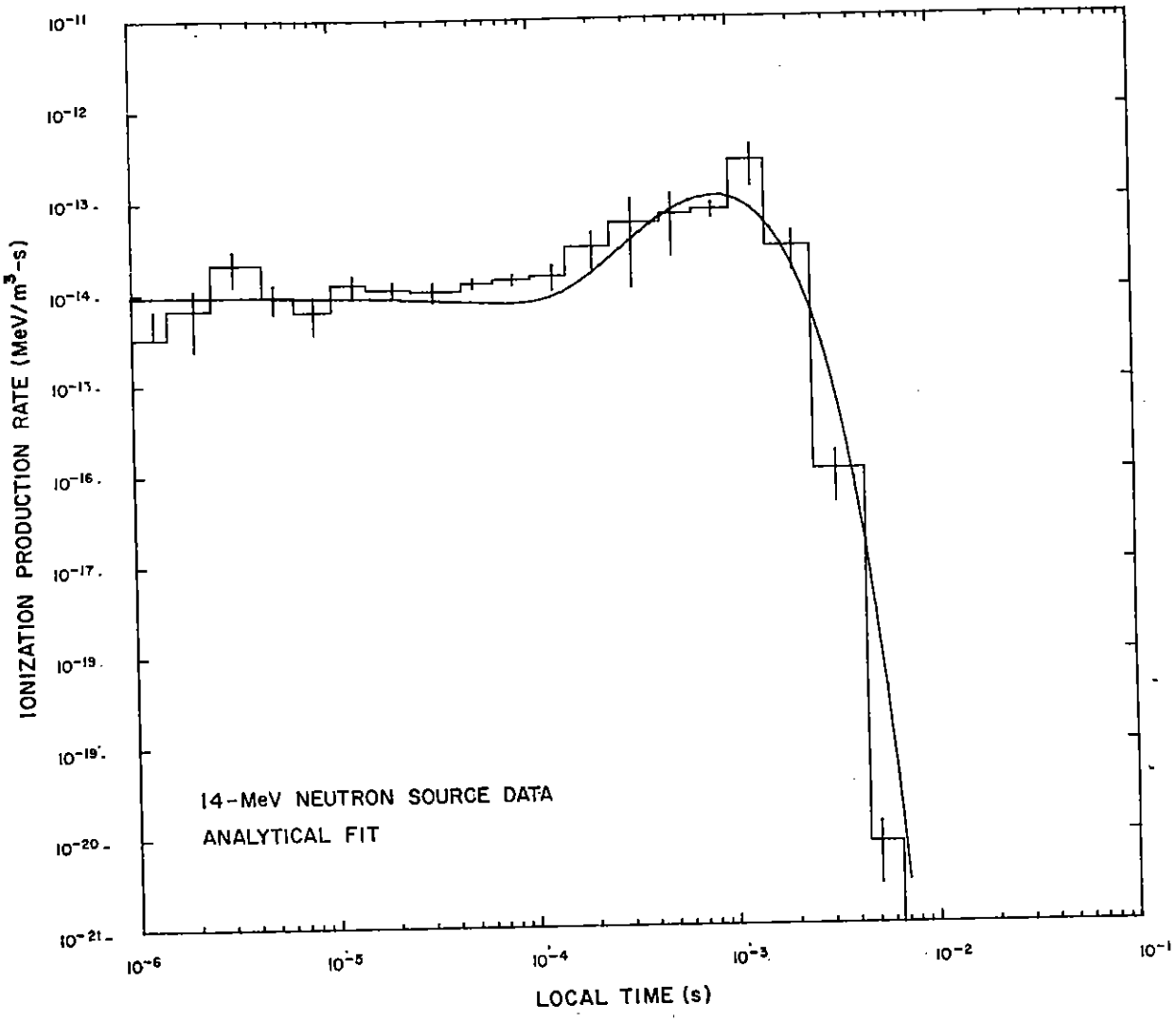

Figure 50. Ionization rate versus time for detector 9.

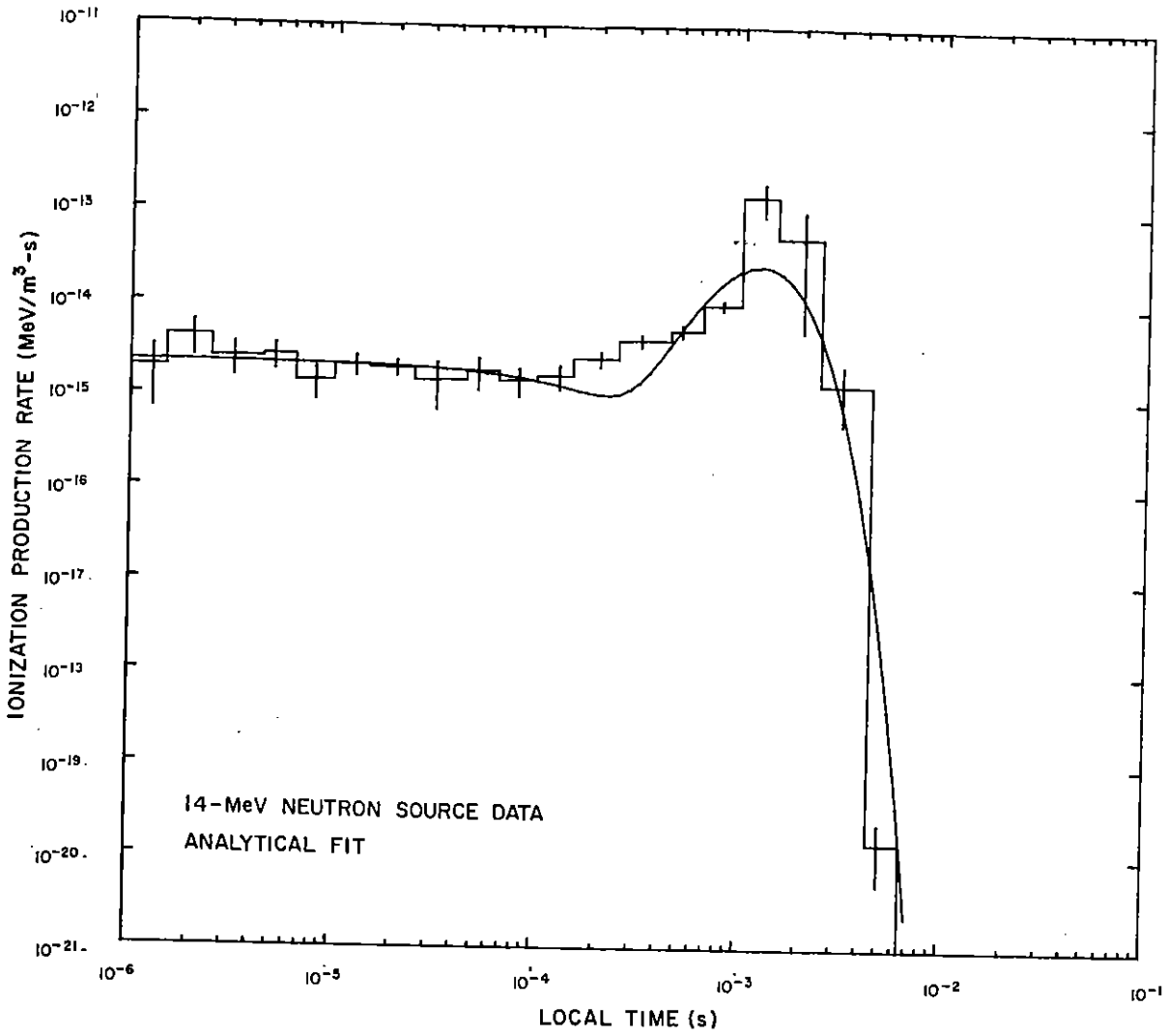

Figure 51. Ionization rate versus time for detector 10.

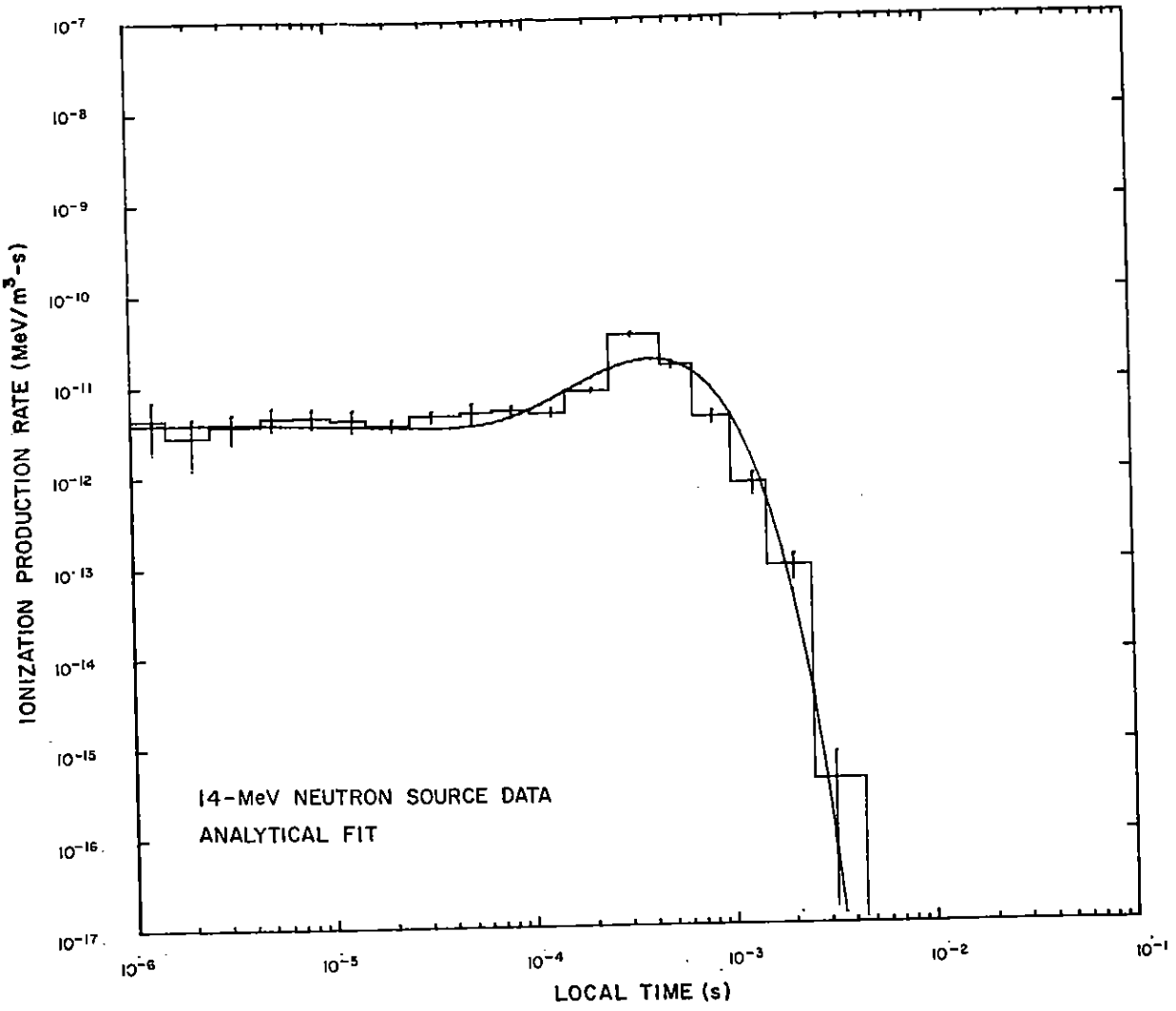

Figure 52. Ionization rate versus time for detector 11.

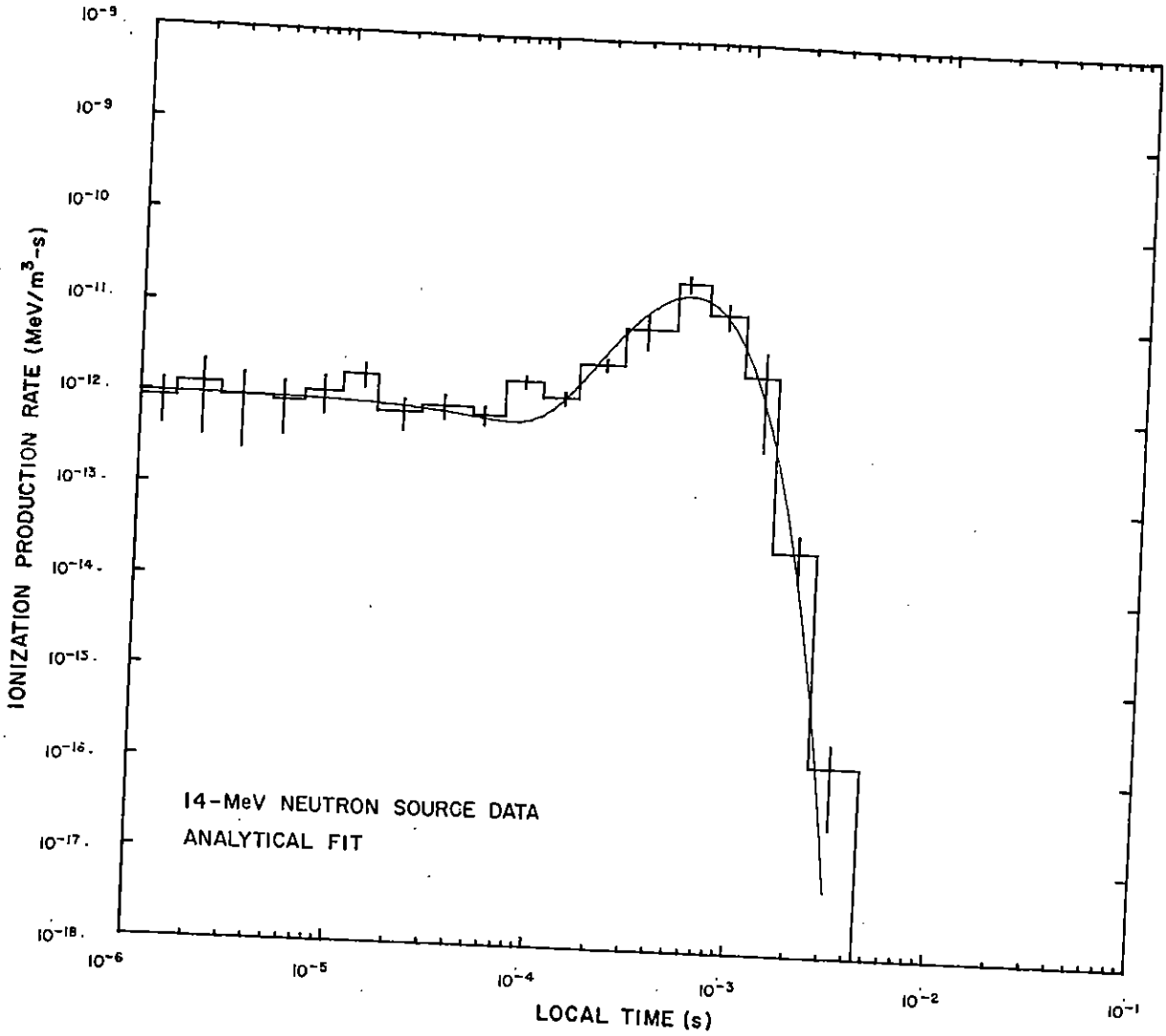

Figure 53. Ionization rate versus time for detector 12.

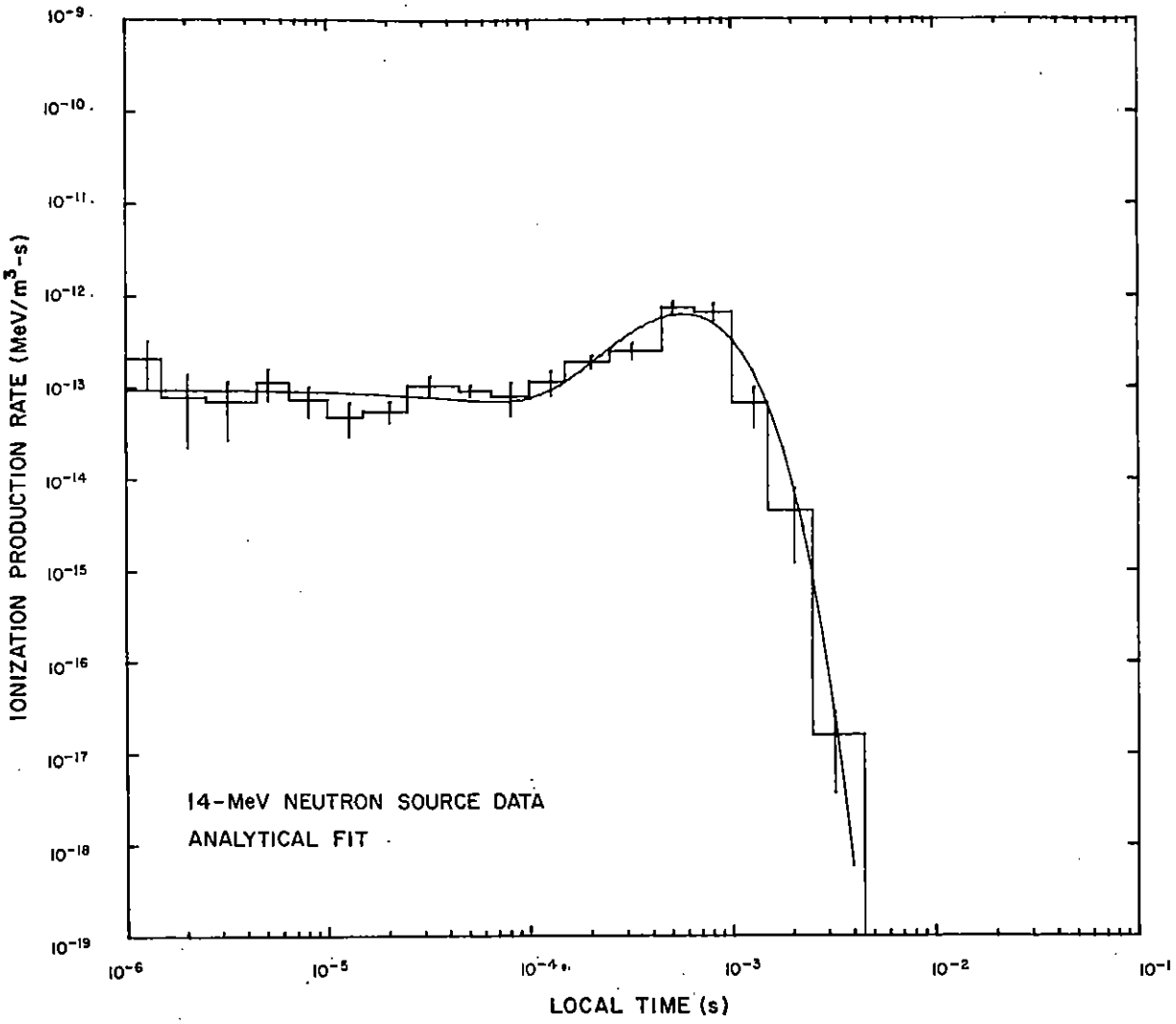

Figure 54. Ionization rate versus time for detector 13.

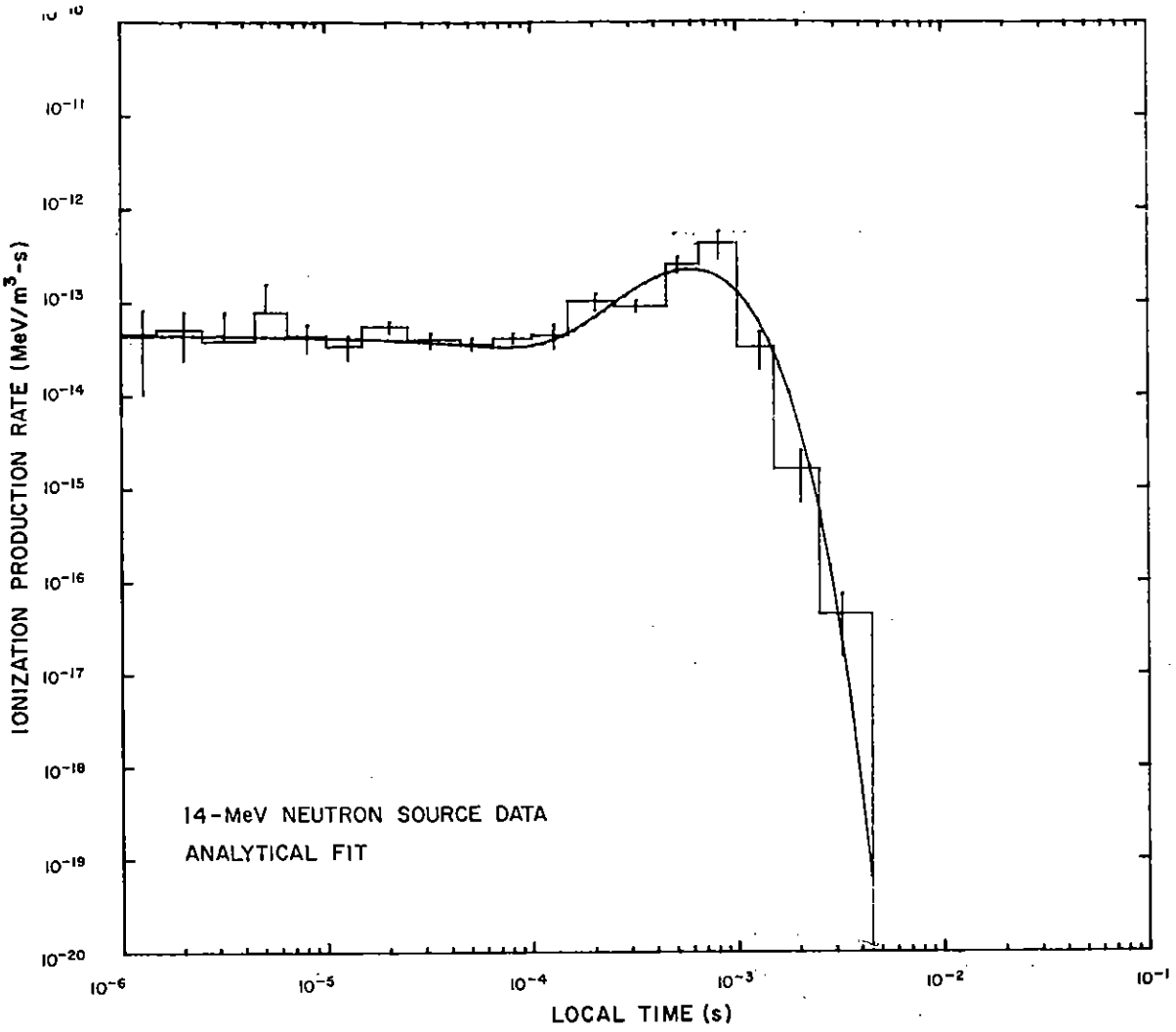

Figure 55. Ionization rate versus time for detector 14.

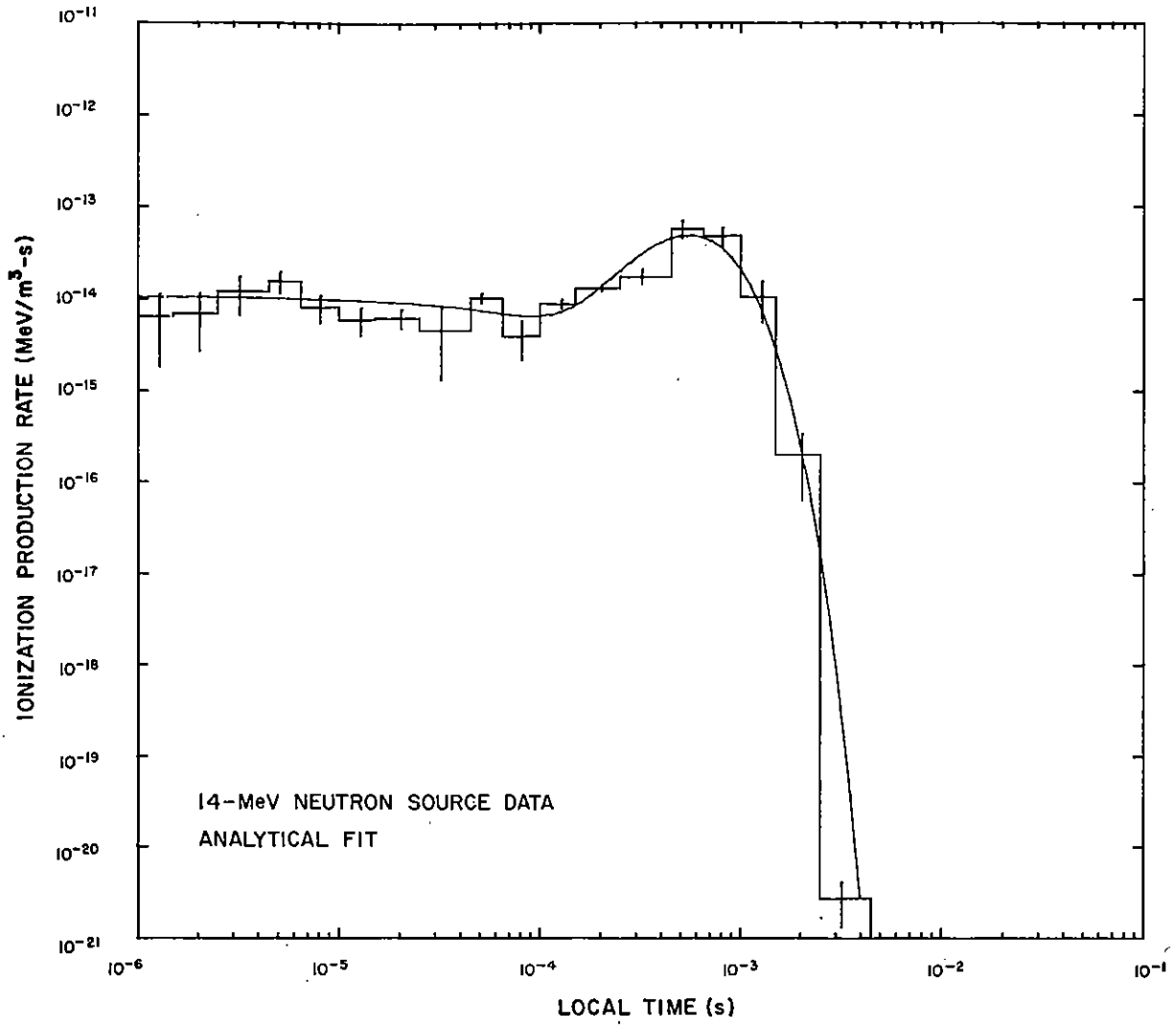

Figure 56. Ionization rate versus time for detector 15.

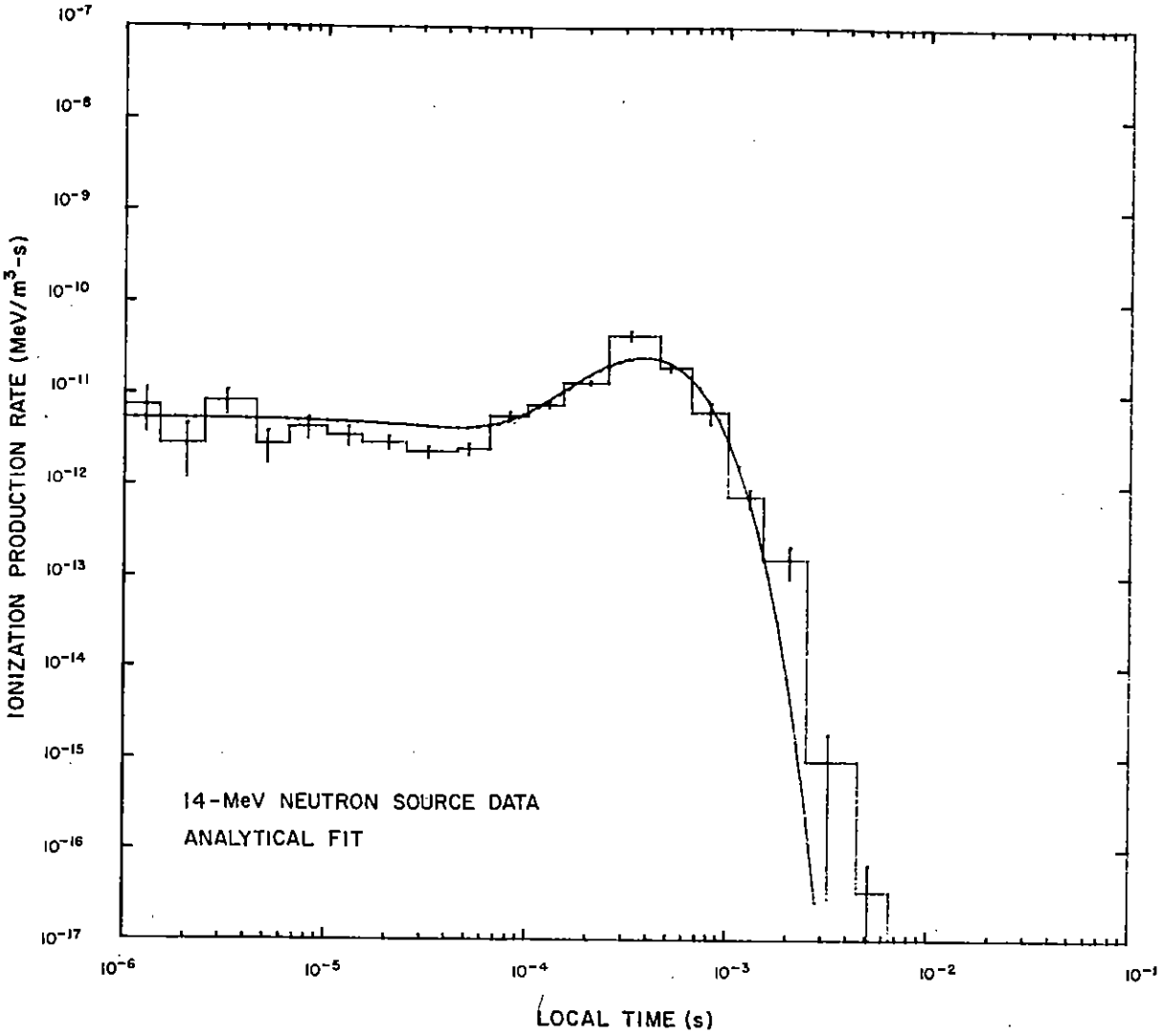

Figure 57. Ionization rate versus time for detector 16.

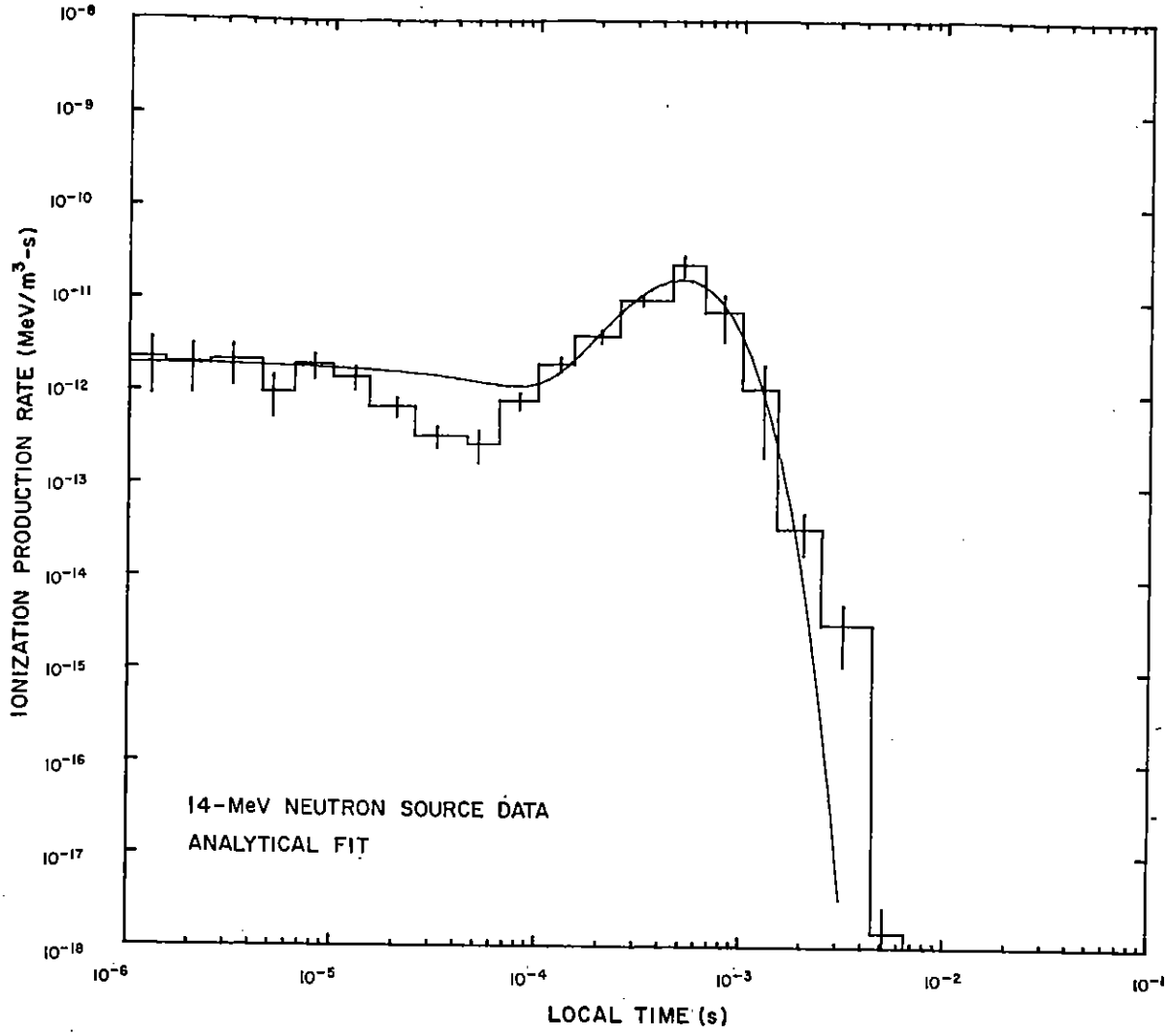

Figure 58. Ionization rate versus time for detector 17.

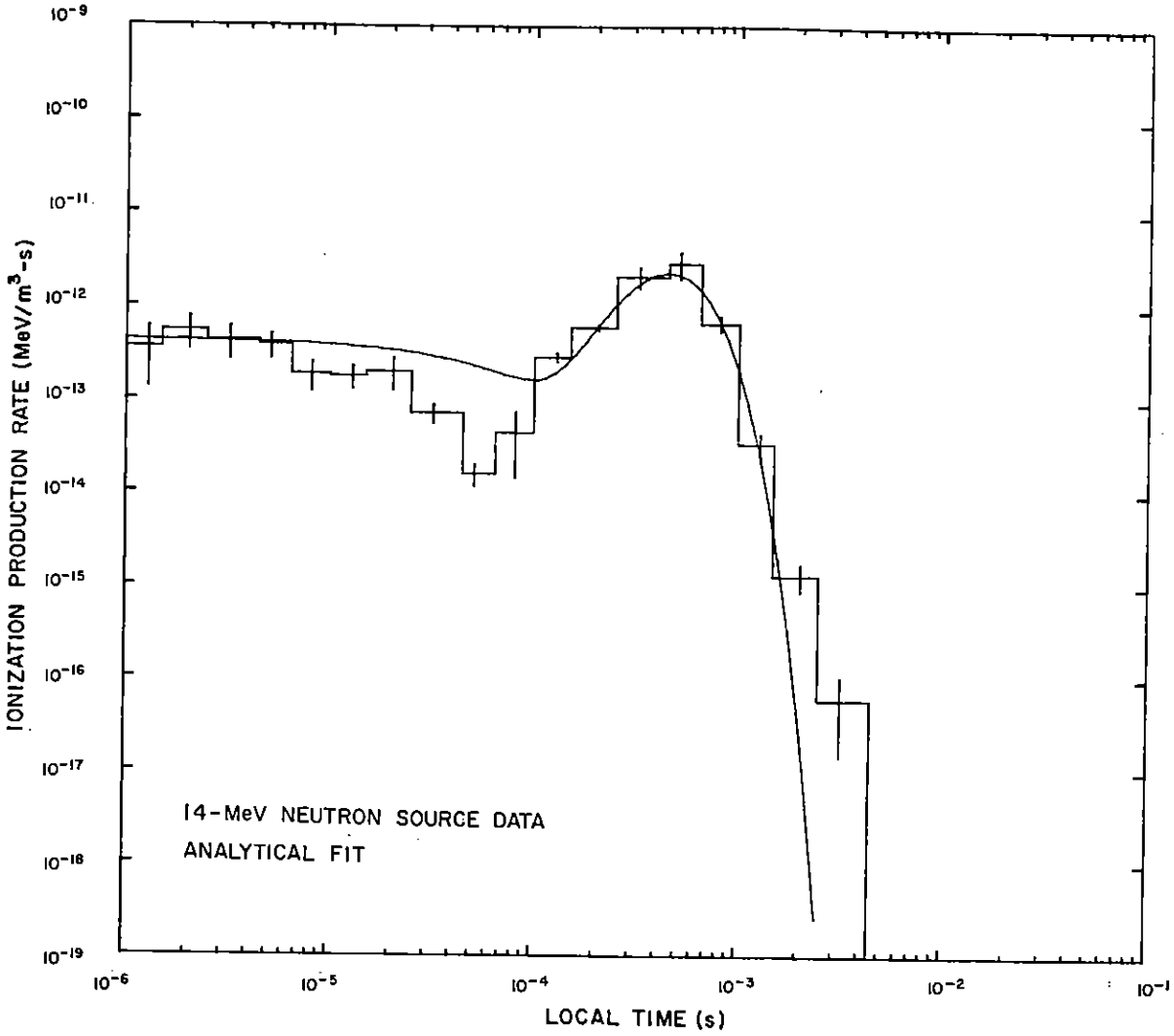

Figure 59. Ionization rate versus time for detector 18.

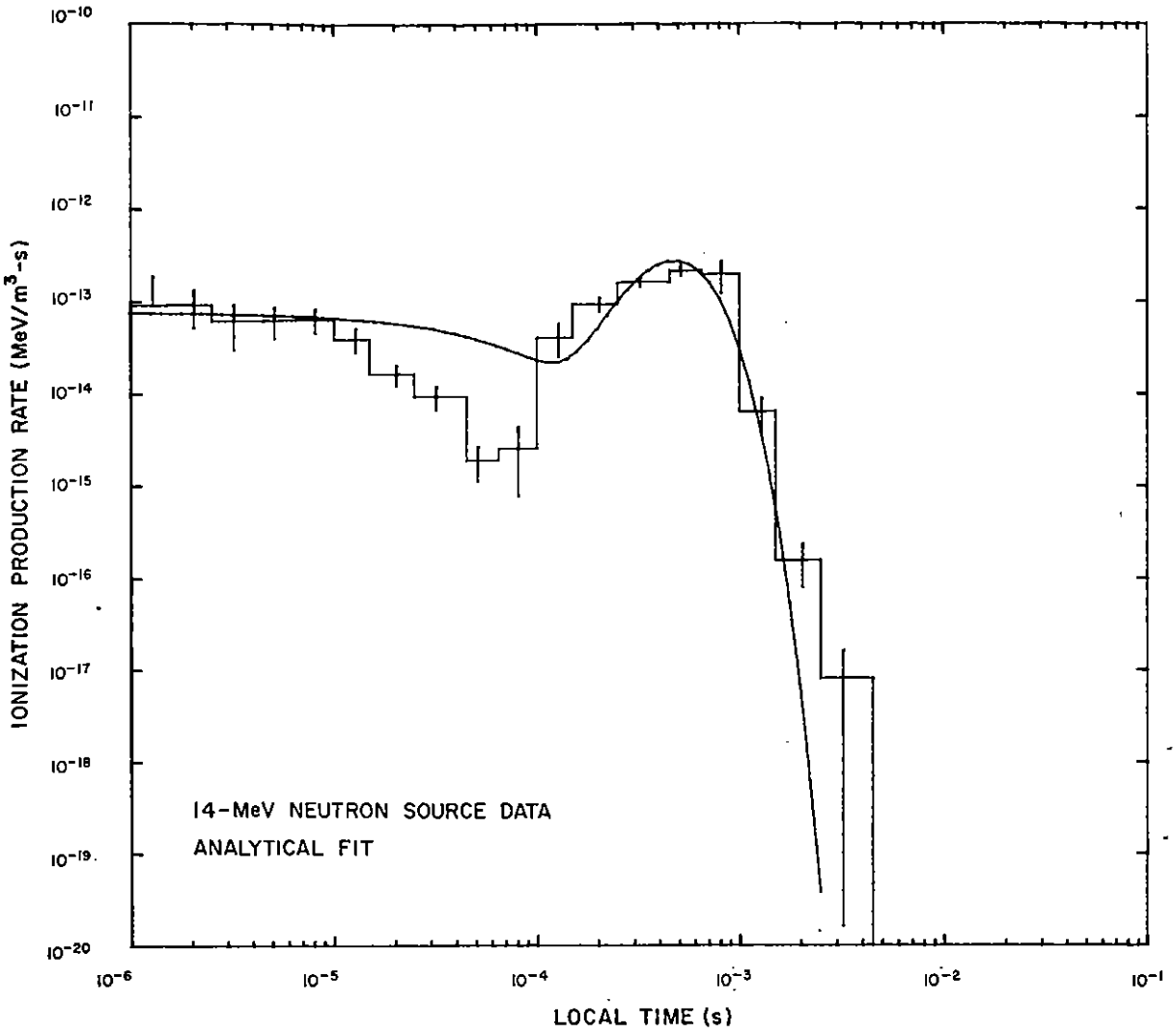

Figure 60. Ionization rate versus time for detector 19.

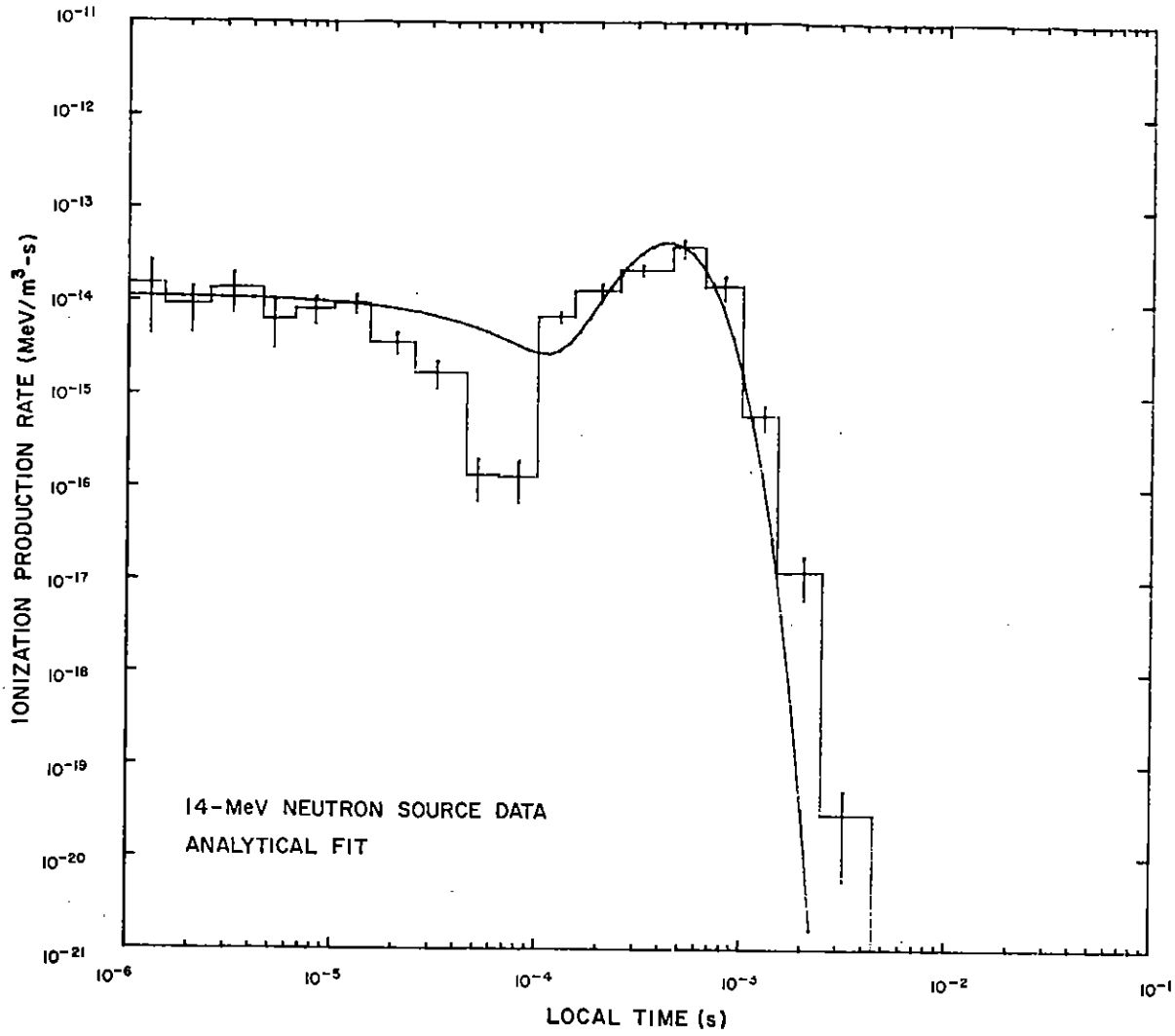

Figure 61. Ionization rate versus time for detector 20.

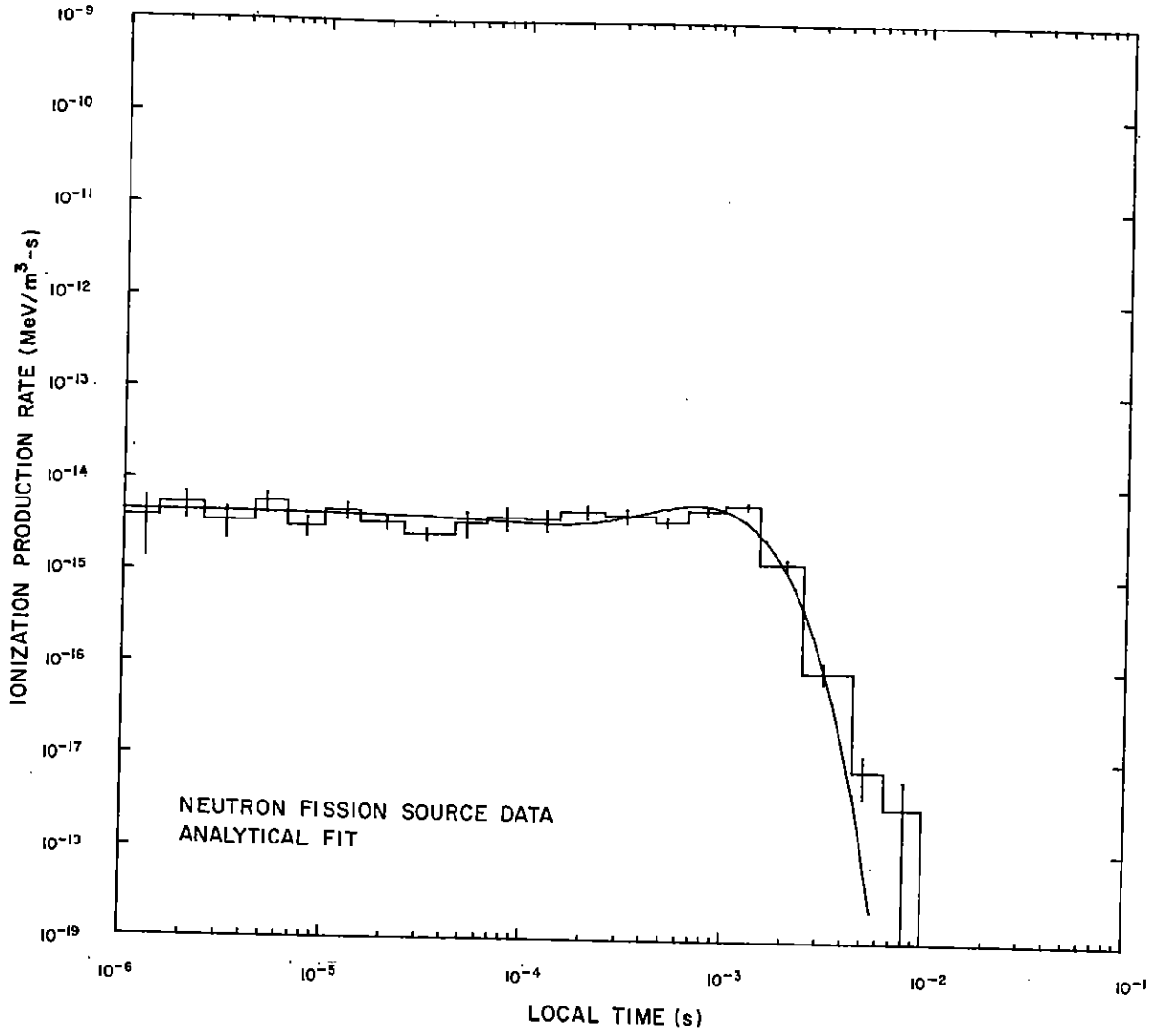

Figure 62. Ionization rate versus time for detector 1.

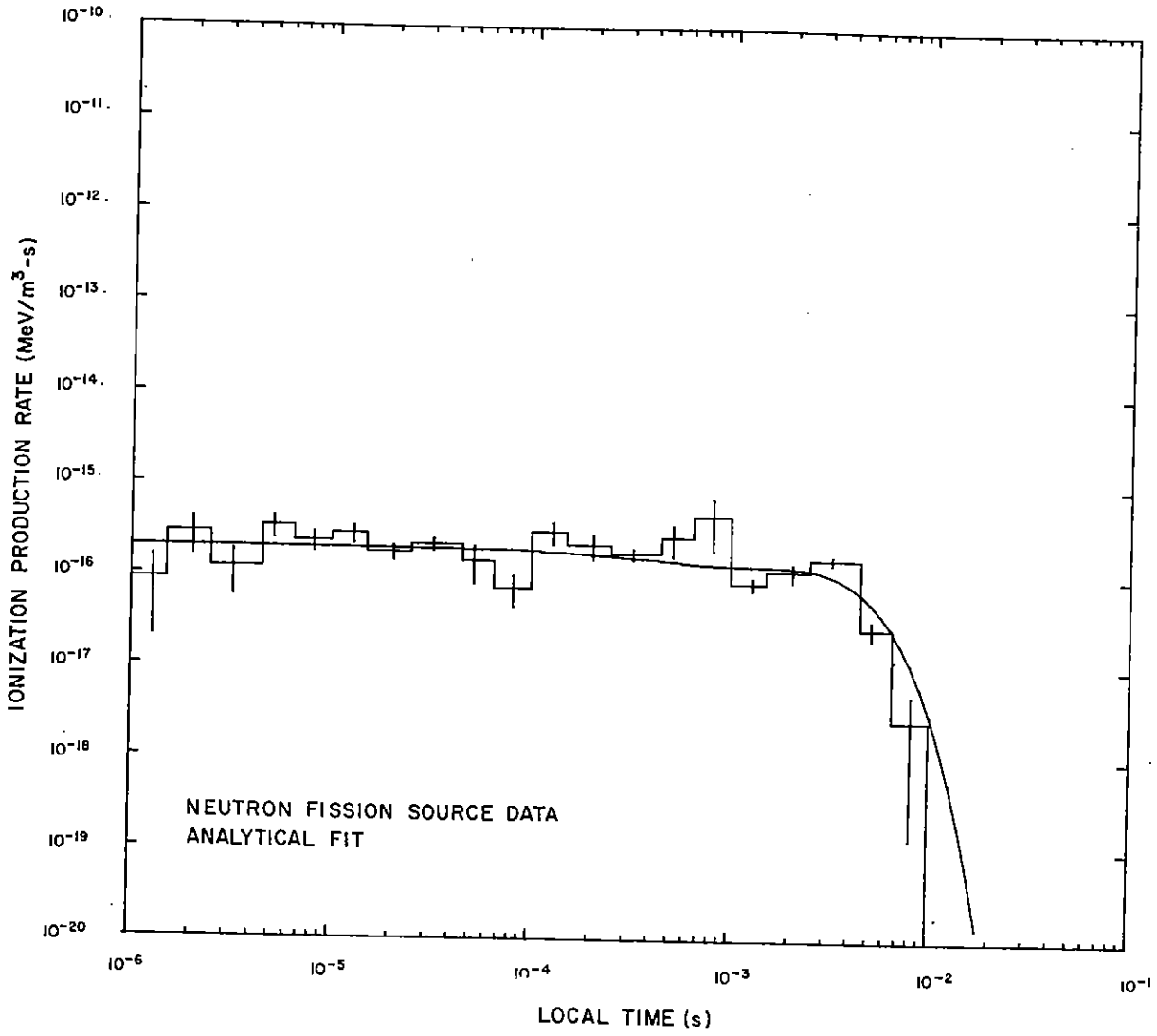

Figure 63. Ionization rate versus time for detector 2.

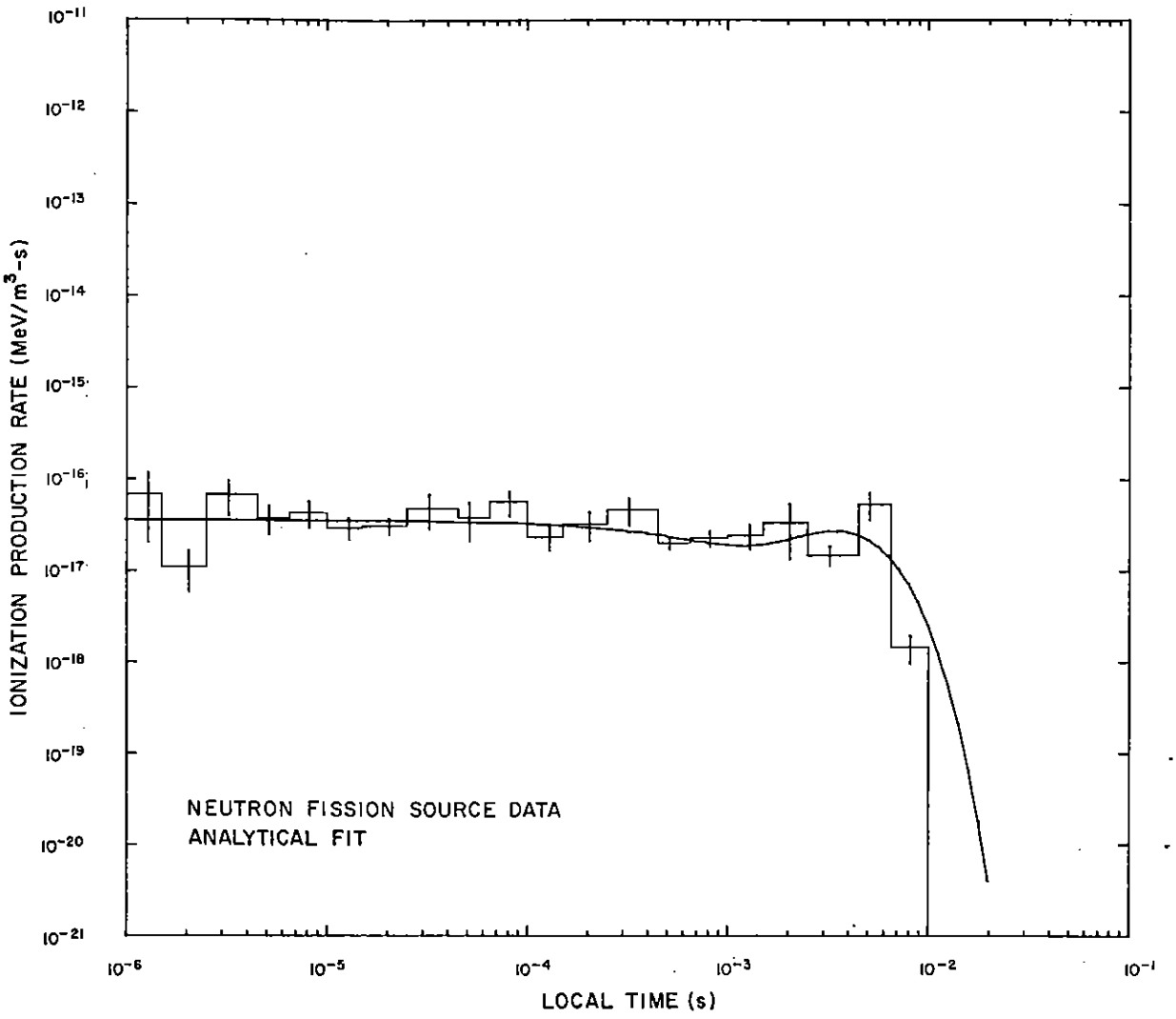

Figure 64. Ionization rate versus time for detector 3.

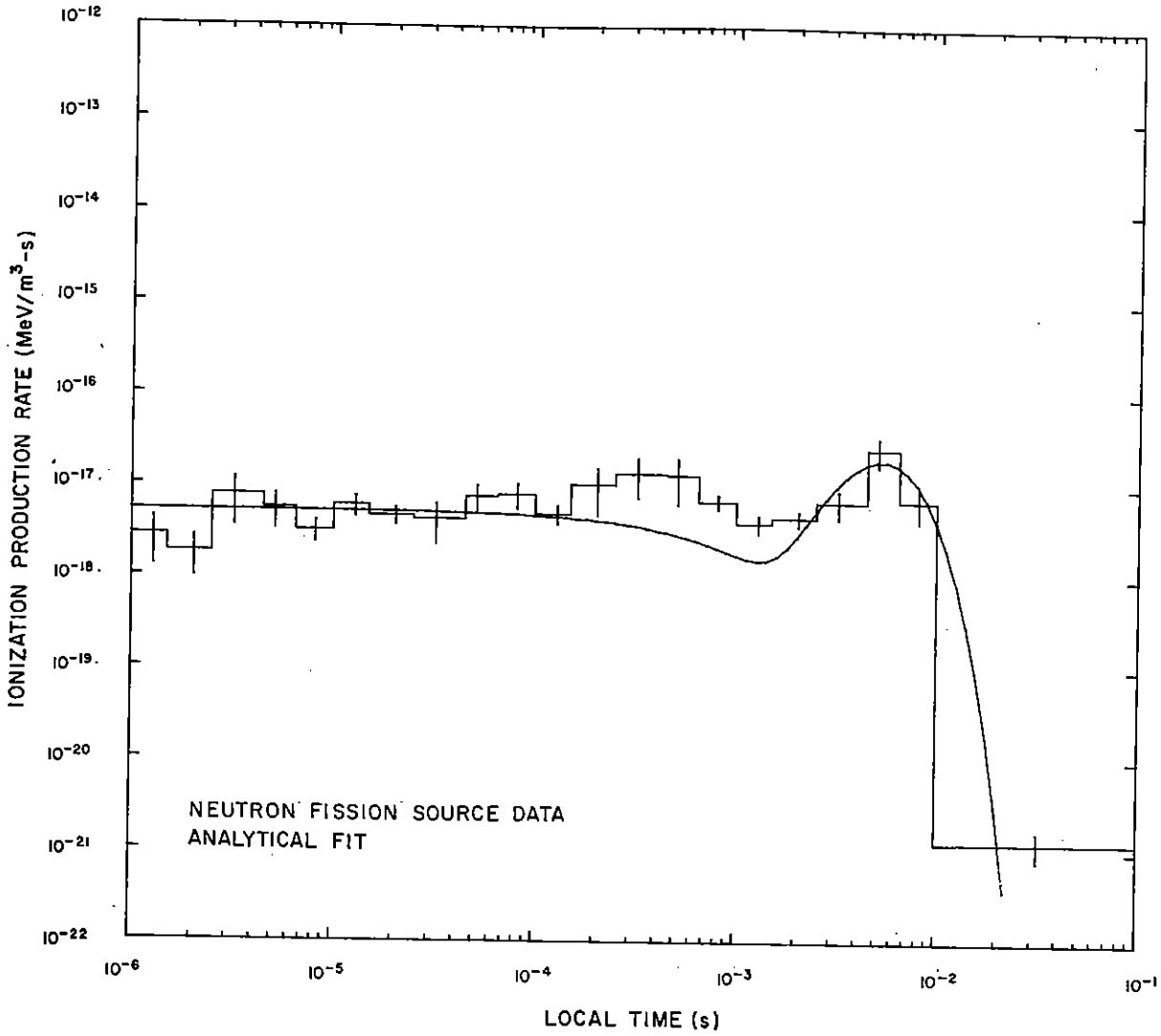

Figure 65. Ionization rate versus time for detector 4.

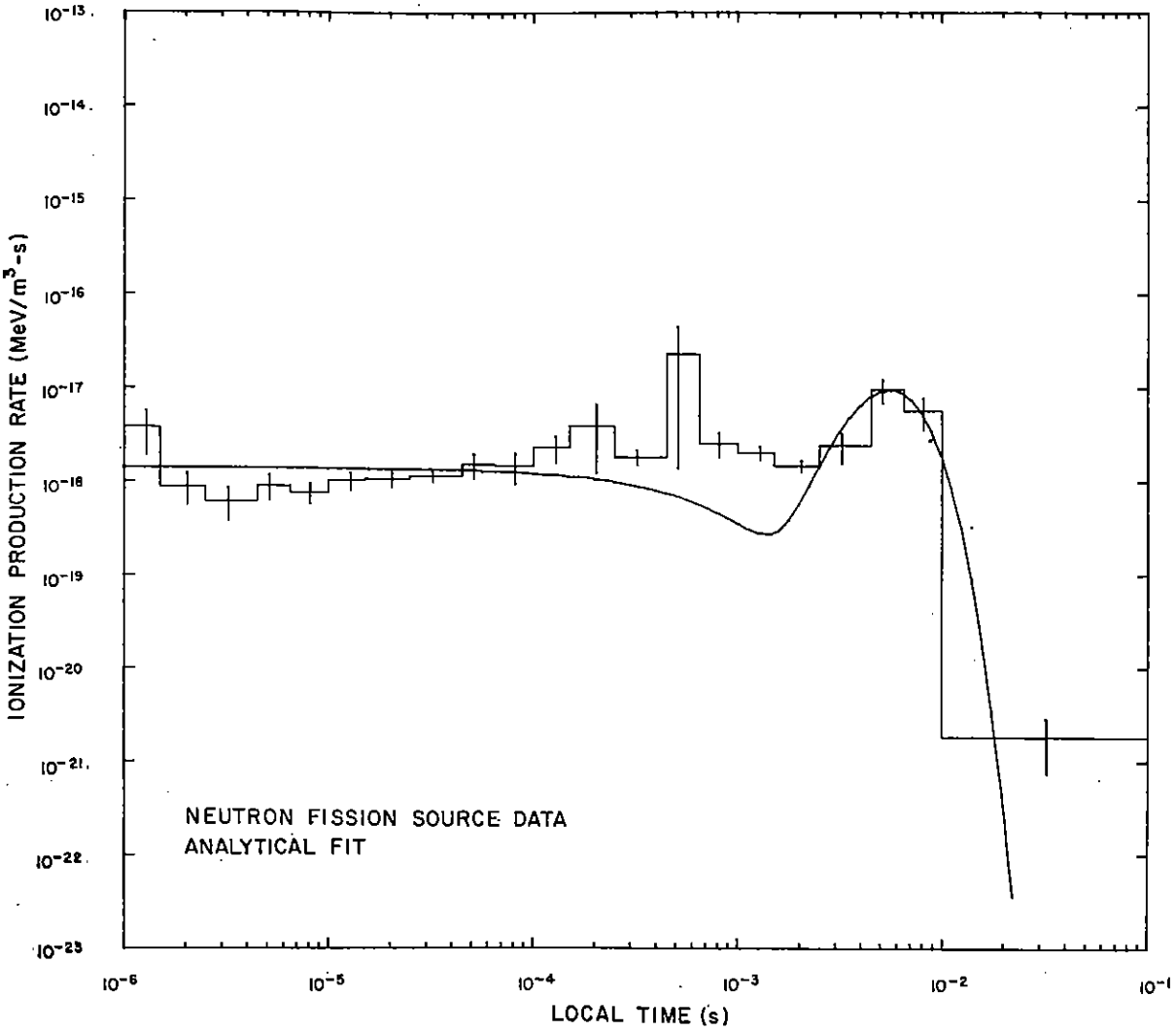

Figure 66. Ionization rate versus time for detector 5.

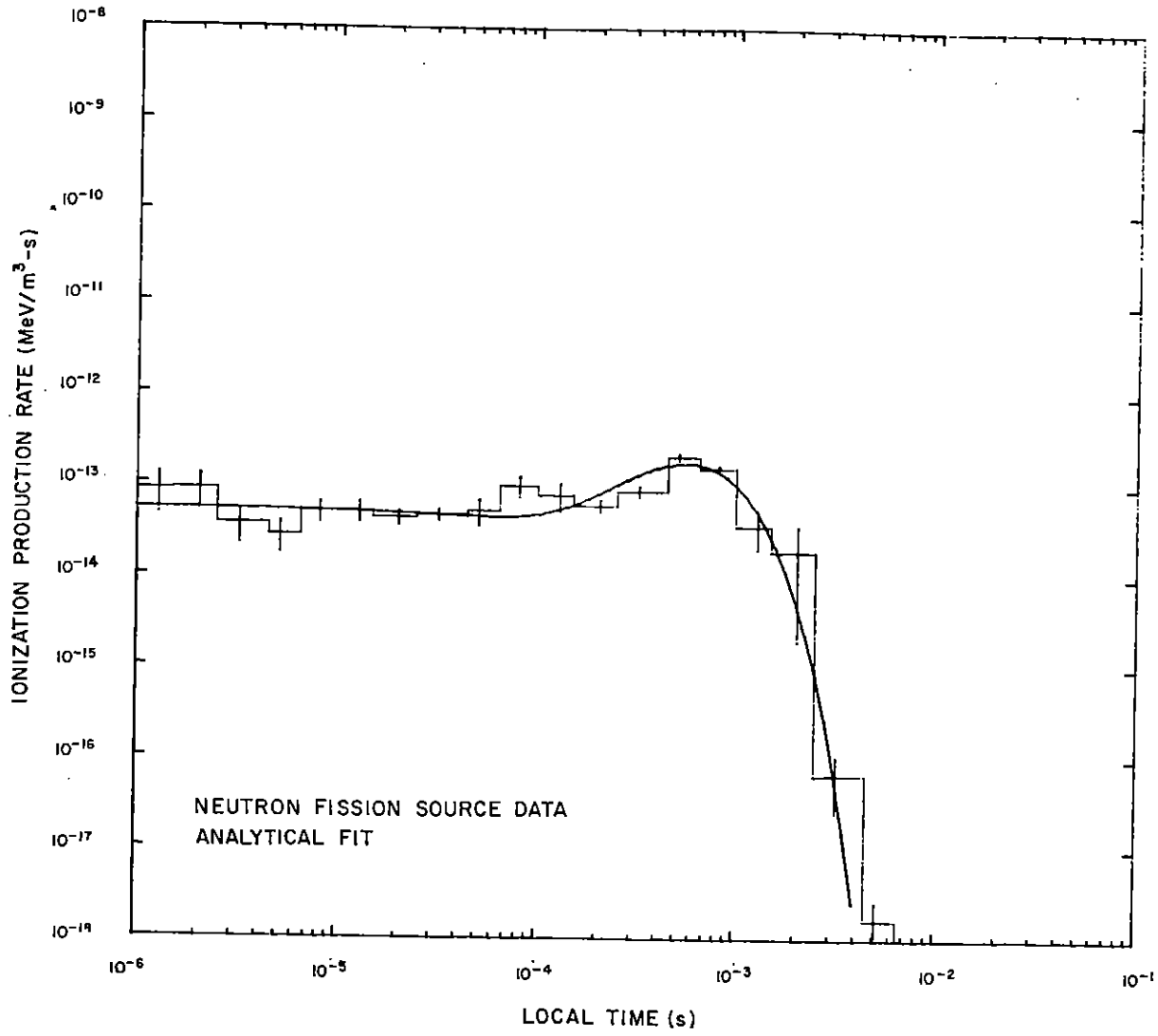

Figure 67. Ionization rate versus time for detector 6.

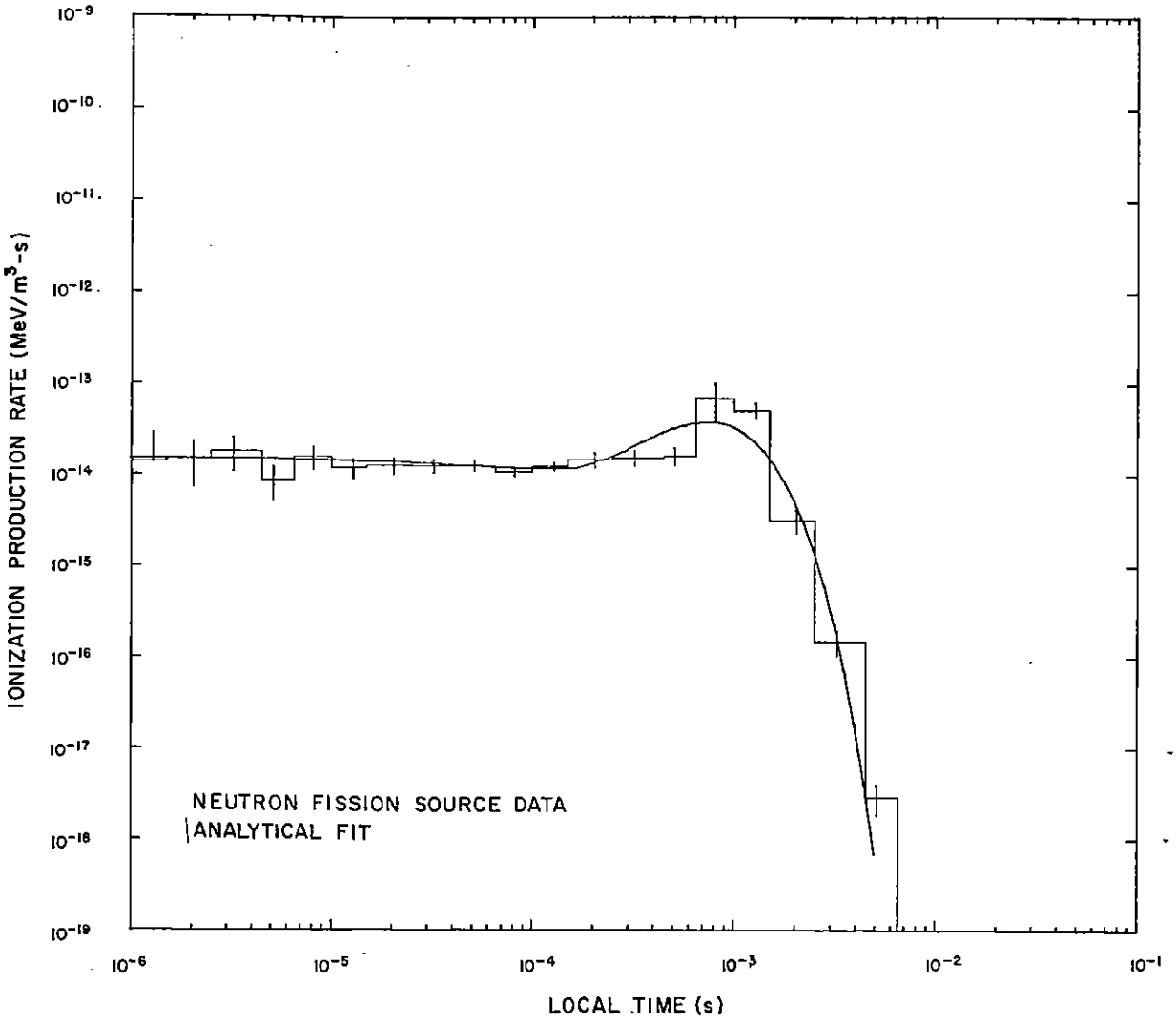

Figure 68. Ionization rate versus time for detector 7.

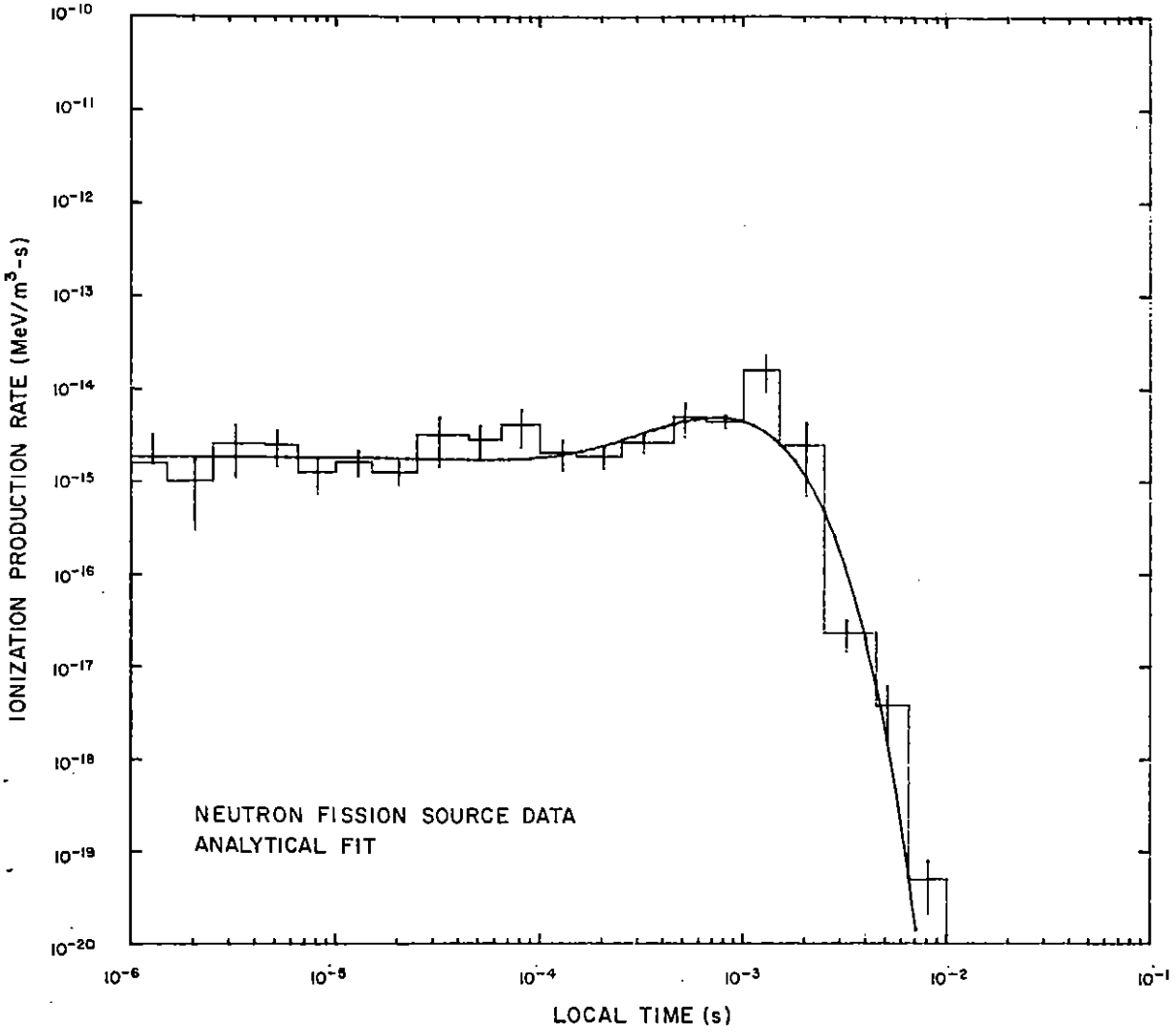

Figure 69. Ionization rate versus time for detector 8.

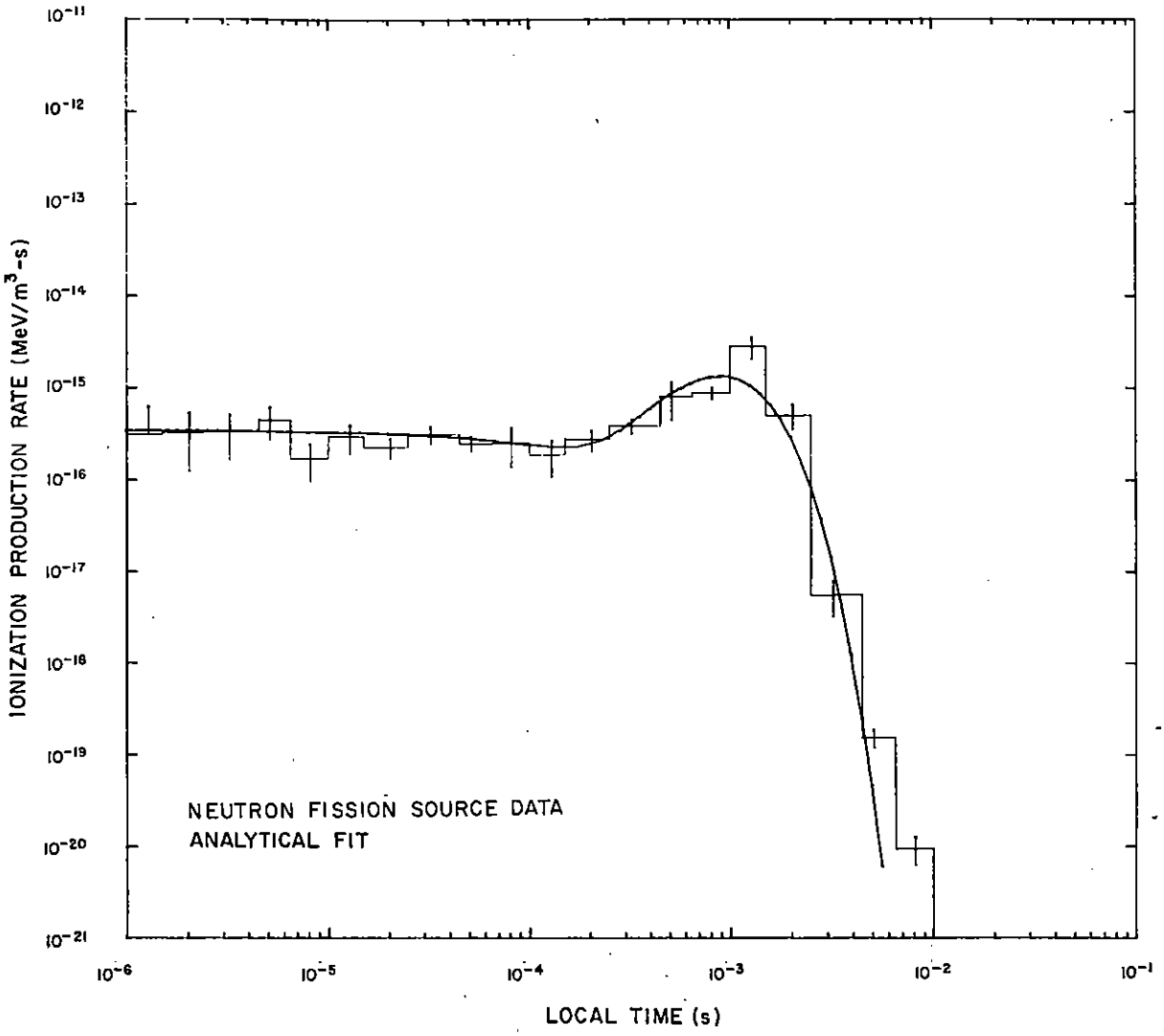

Figure 70. Ionization rate versus time for detector 9.

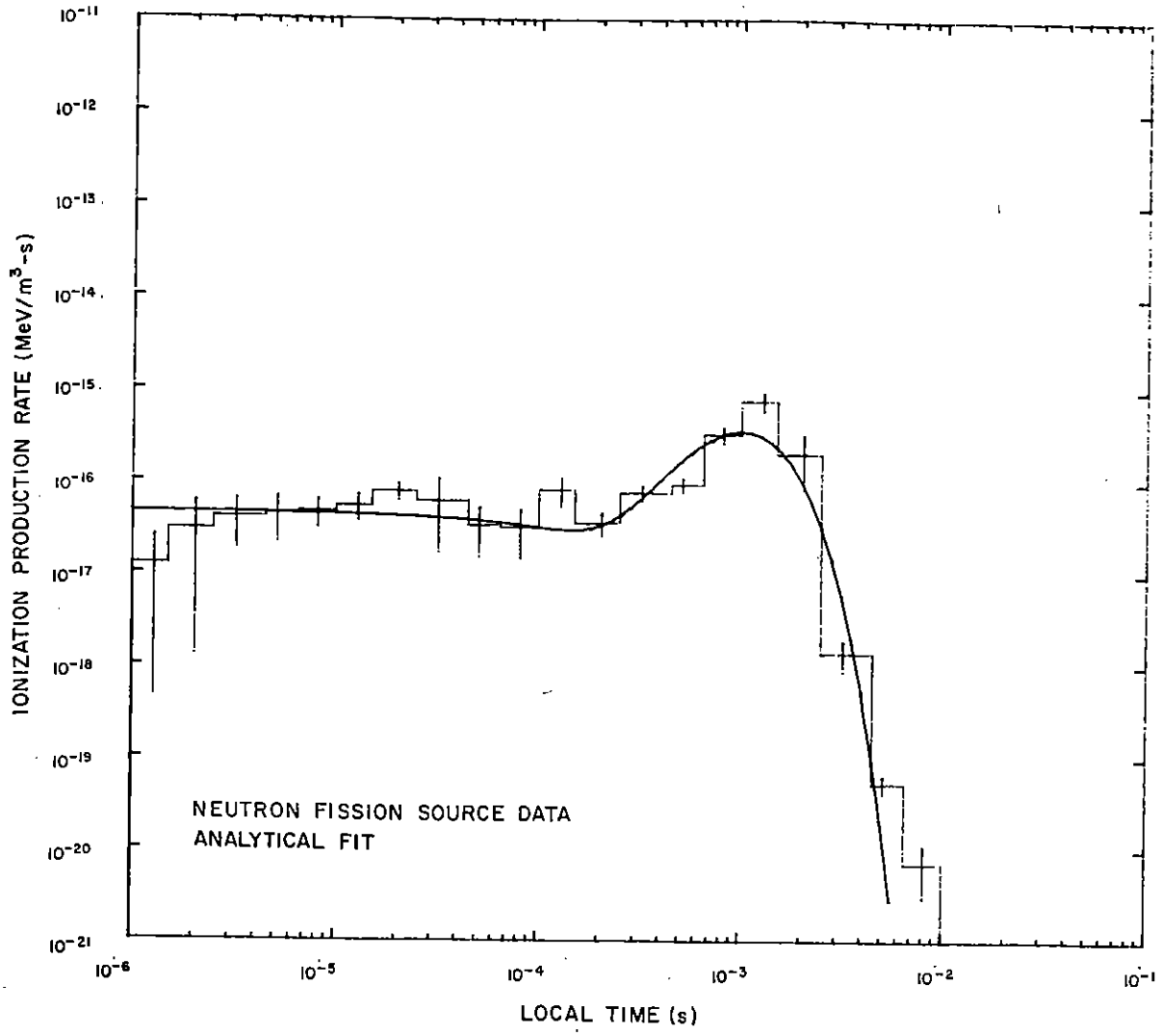

Figure 71. Ionization rate versus time for detector 10.

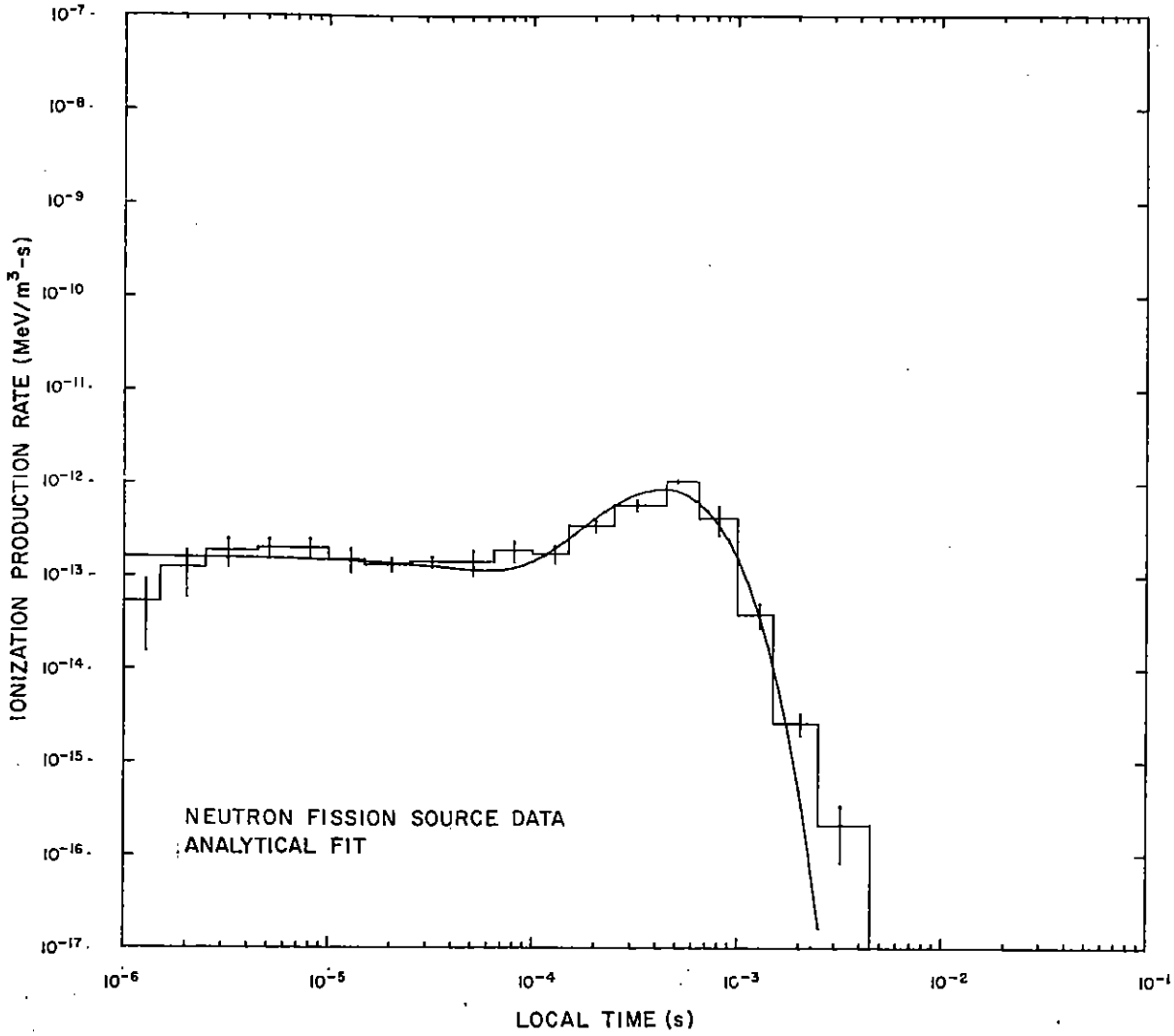

Figure 72. Ionization rate versus time for detector 11.

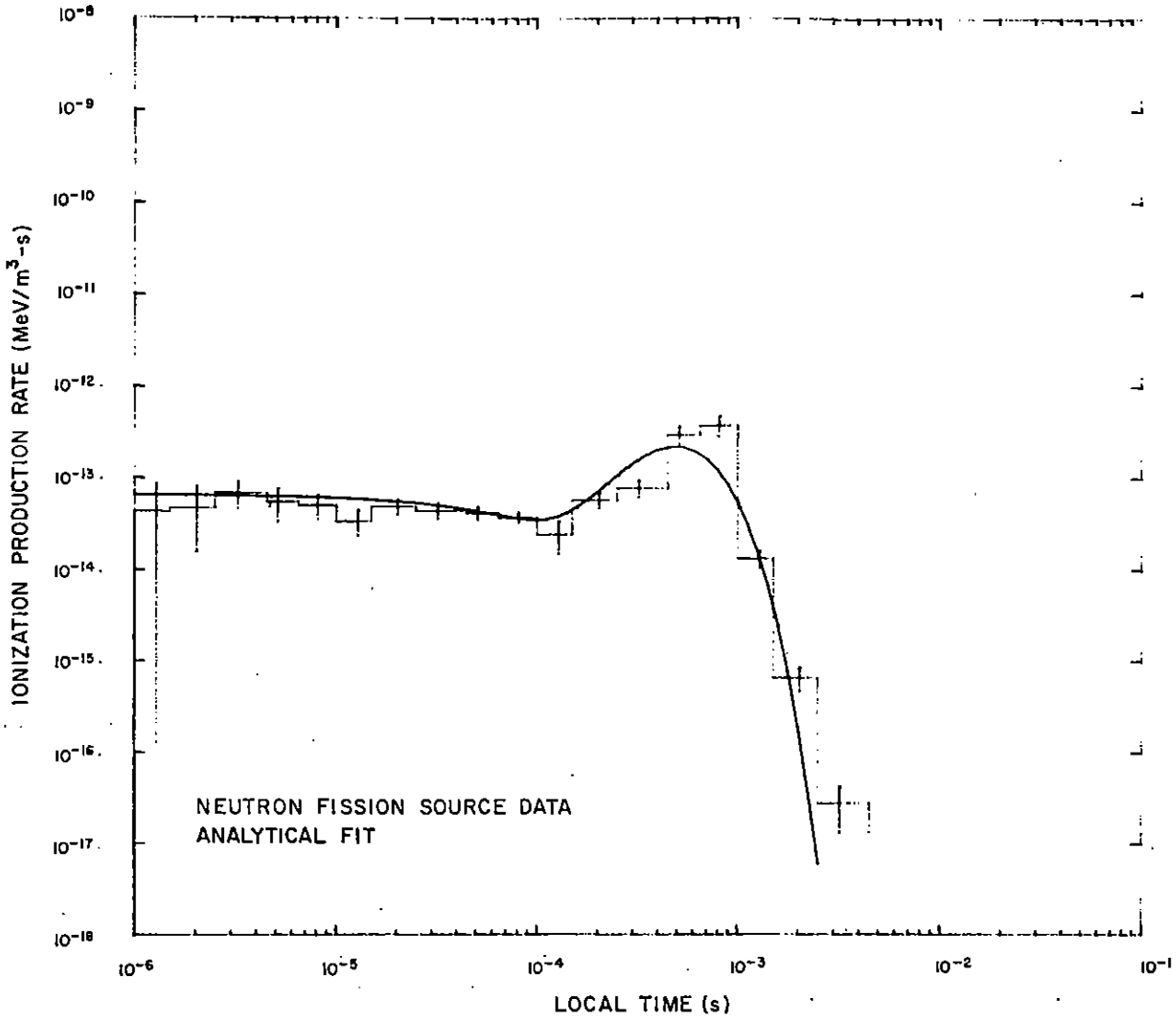

Figure 73. Ionization rate versus time for detector 12.

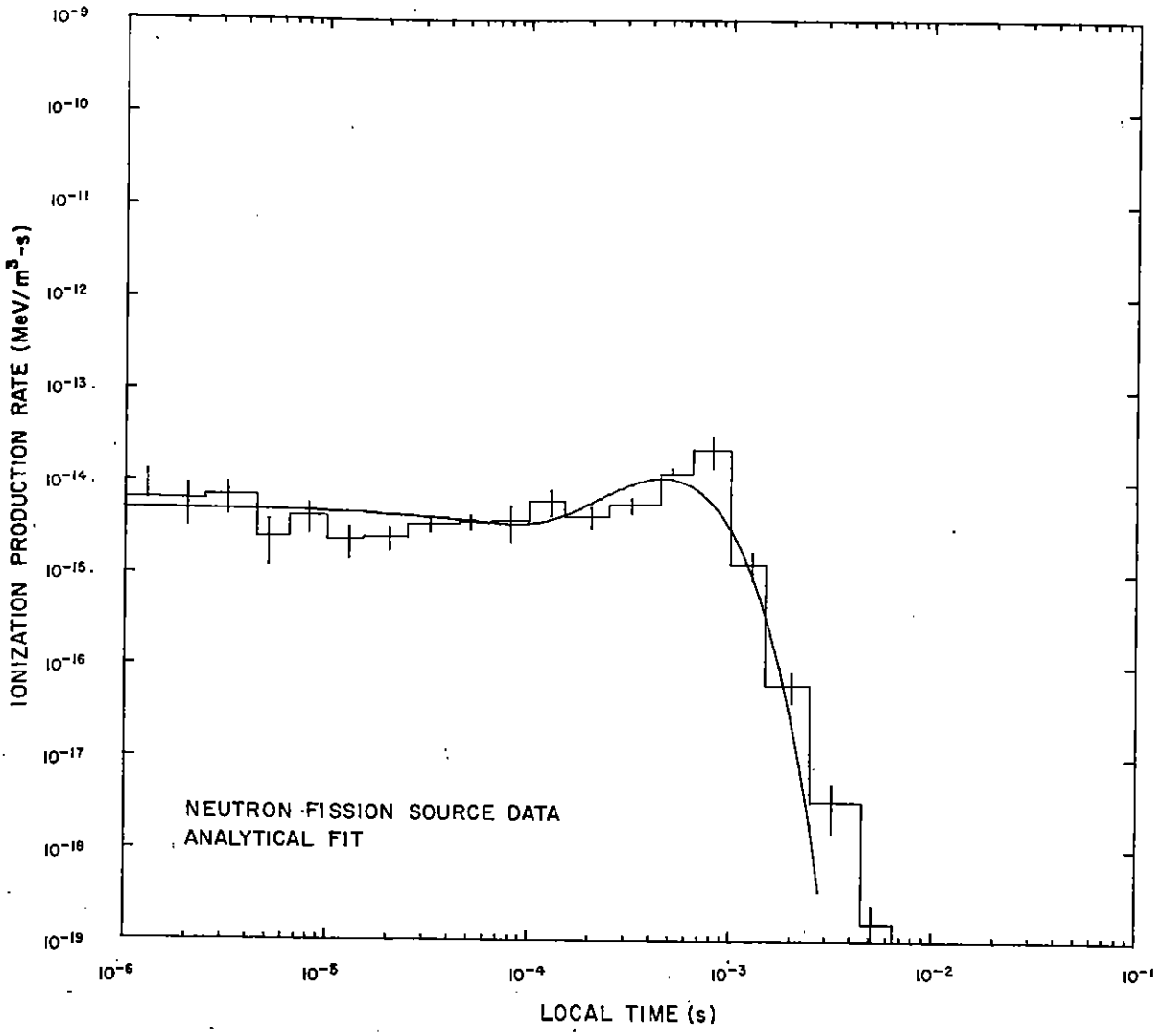

Figure 74. Ionization rate versus time for detector 13.

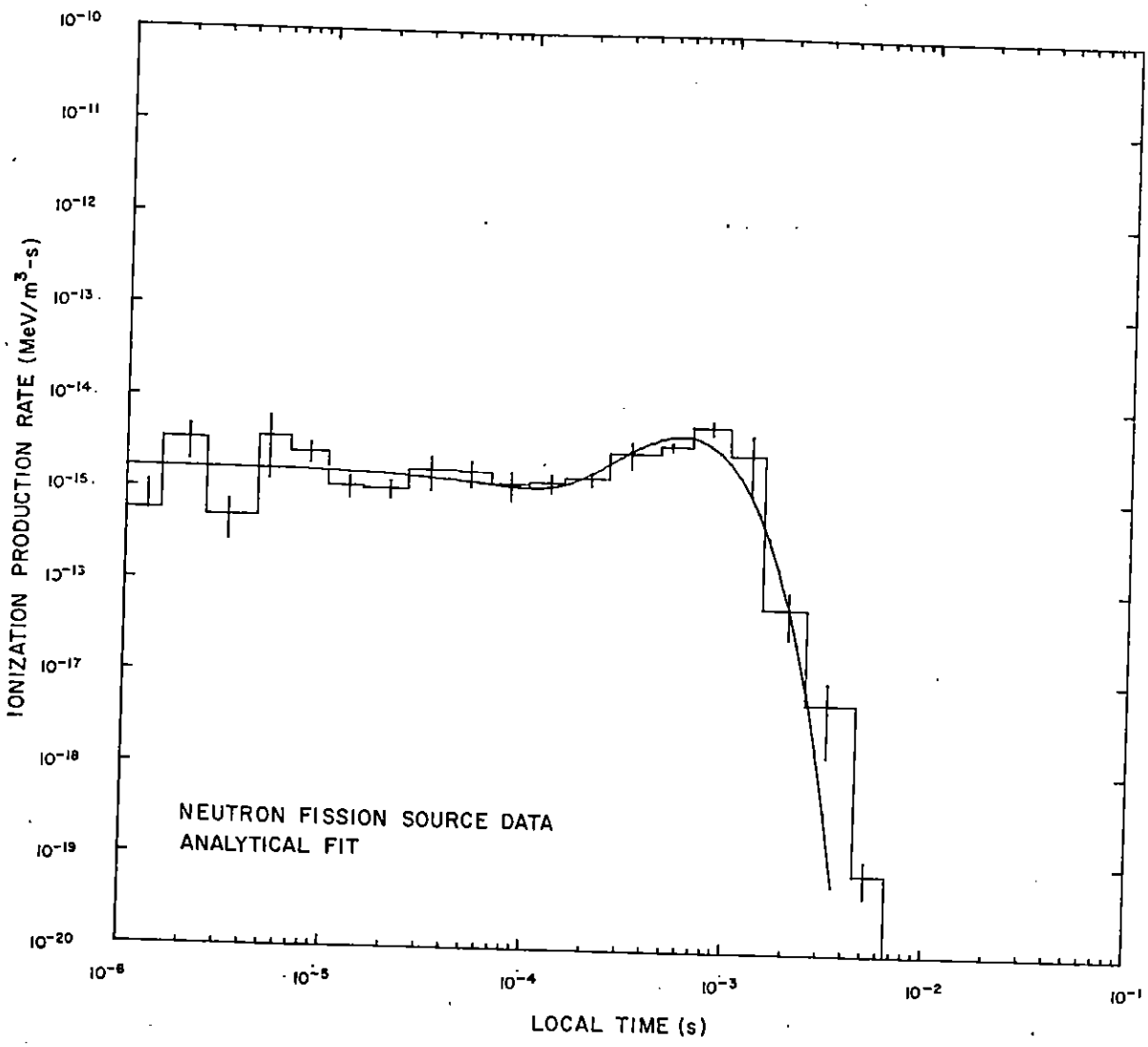

Figure 75. Ionization rate versus time for detector 14.

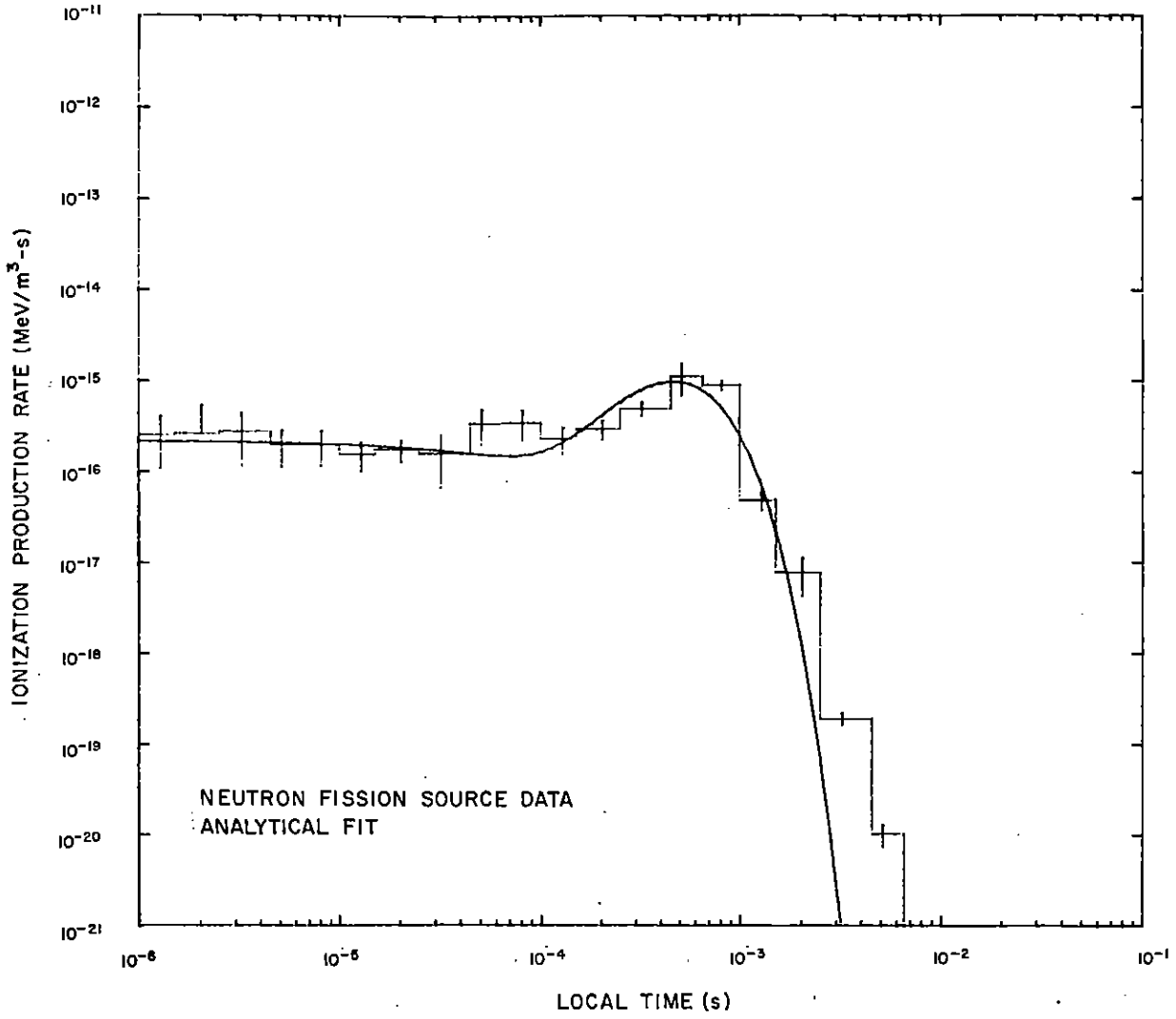

Figure 76. Ionization rate versus time for detector 15.

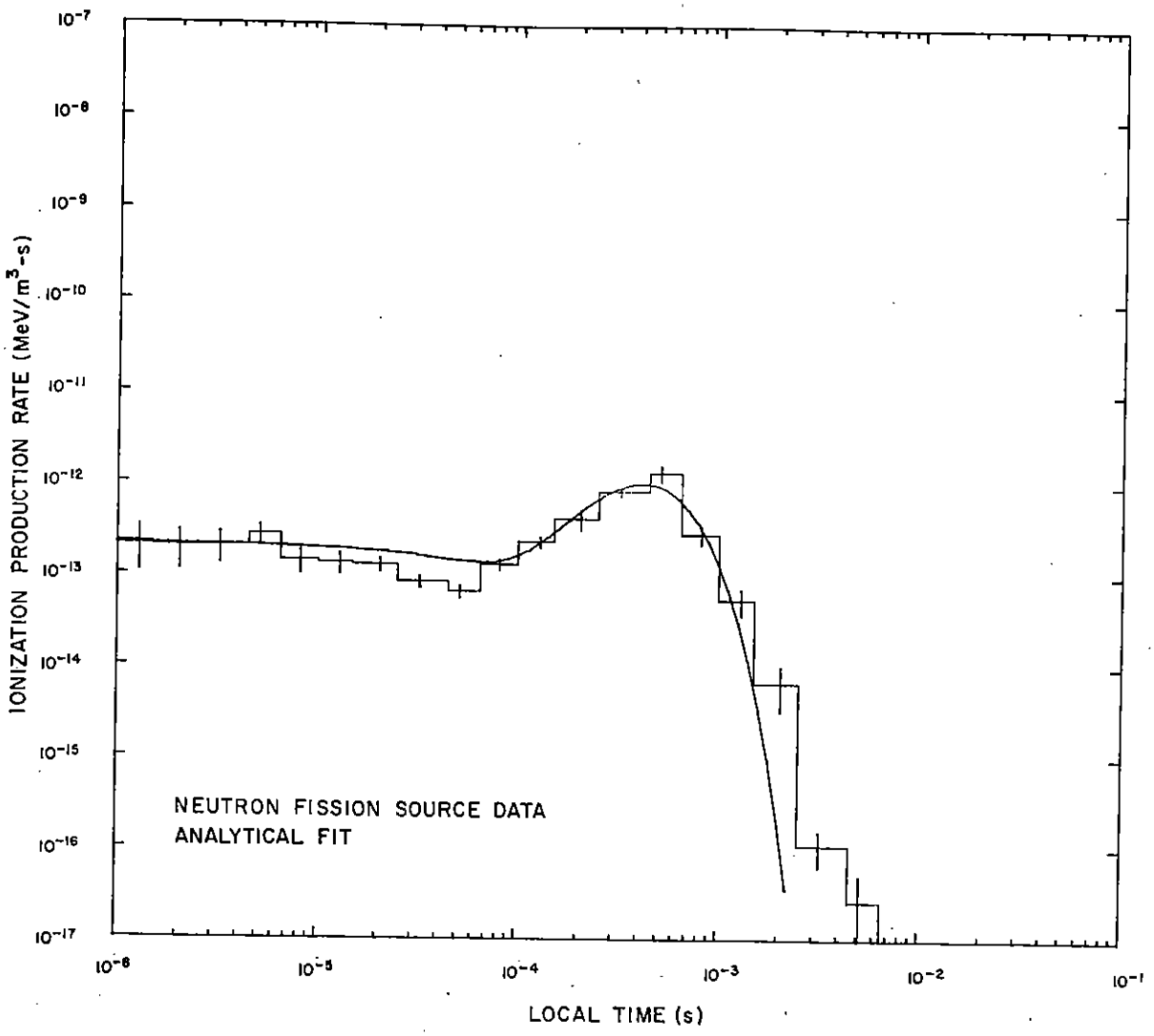

Figure 77. Ionization rate versus time for detector 16.

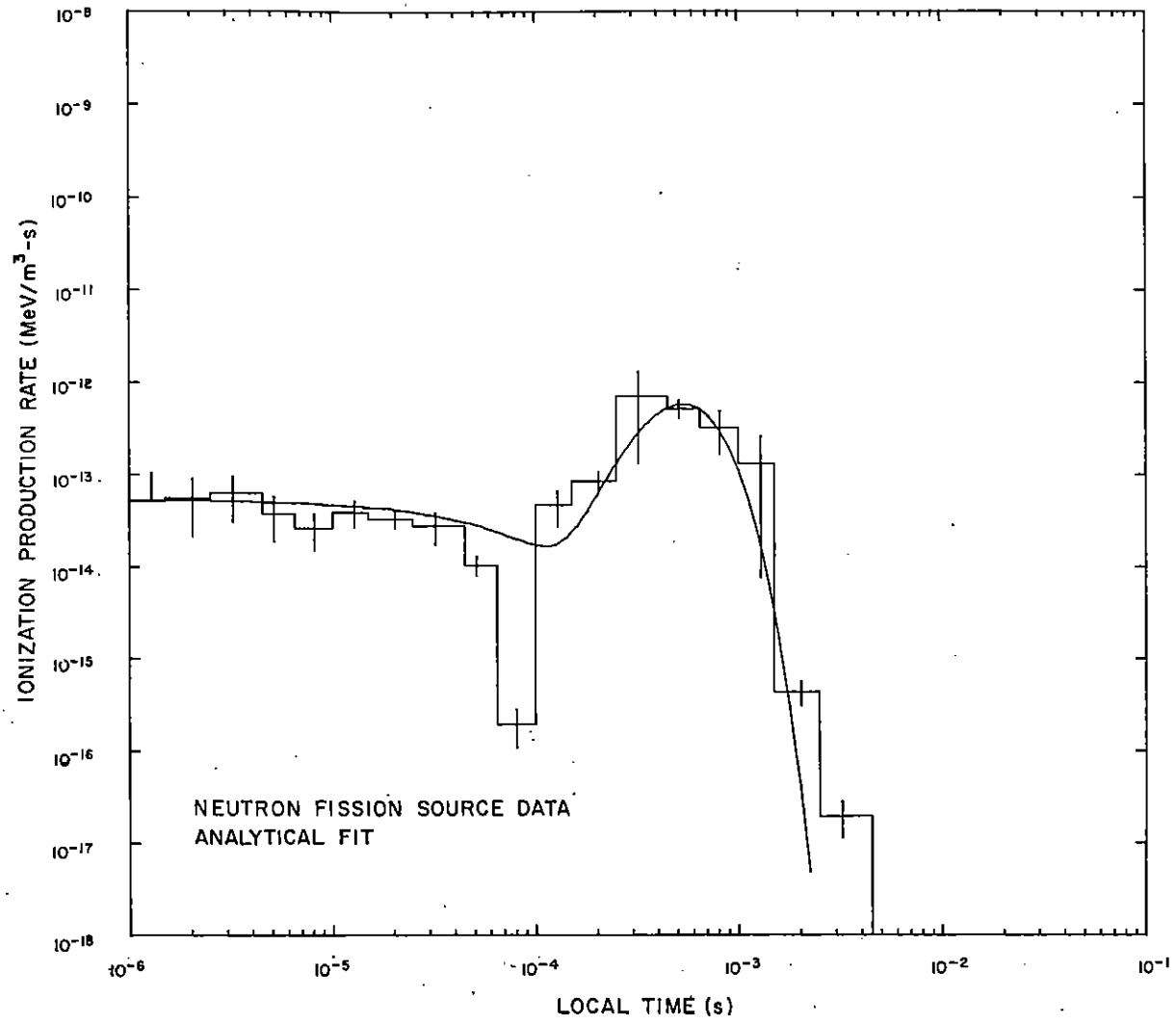

Figure 78. Ionization rate versus time for detector 17.

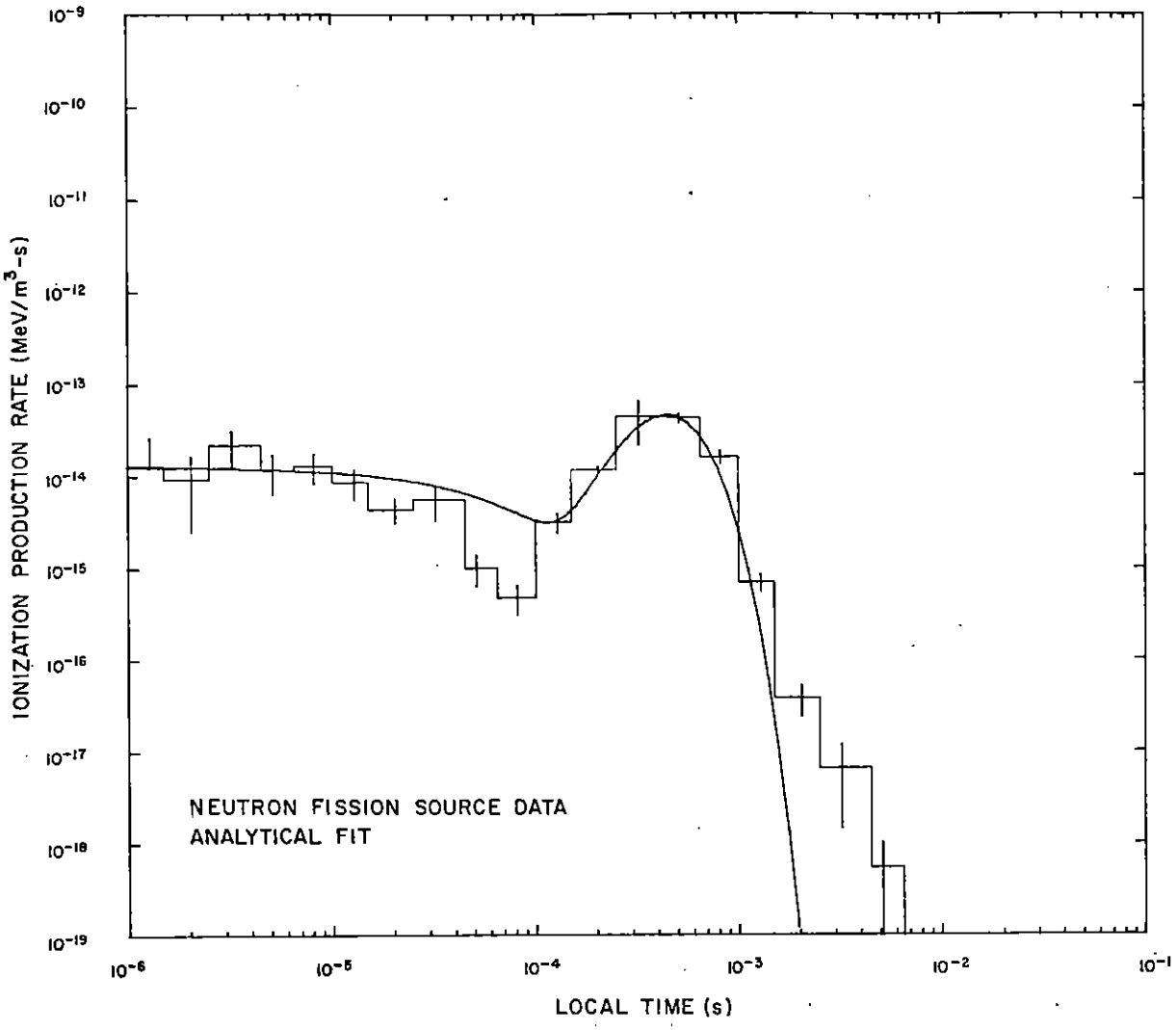

Figure 79. Ionization rate versus time for detector 18.

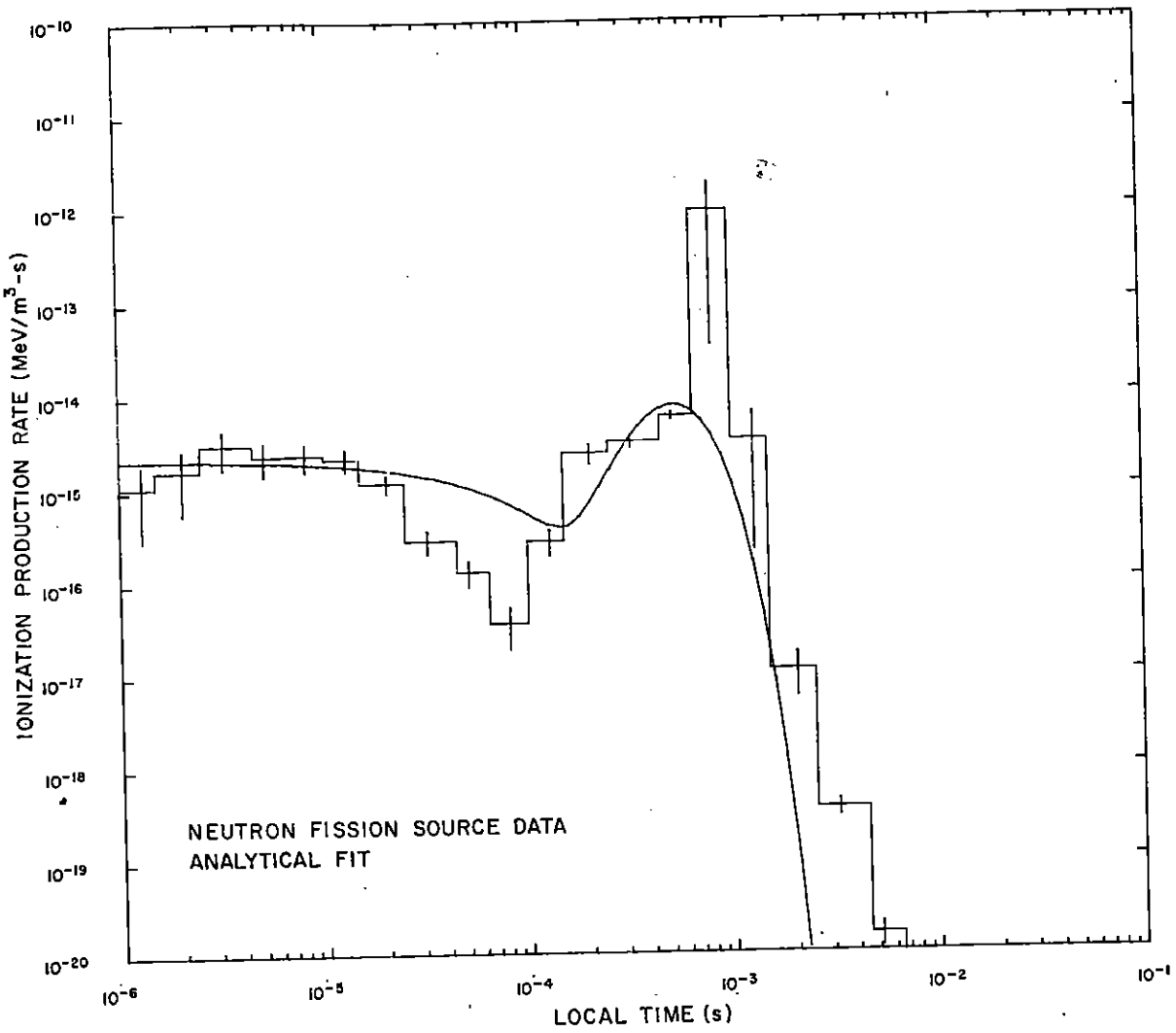

Figure 80. Ionization rate versus time for detector 19.

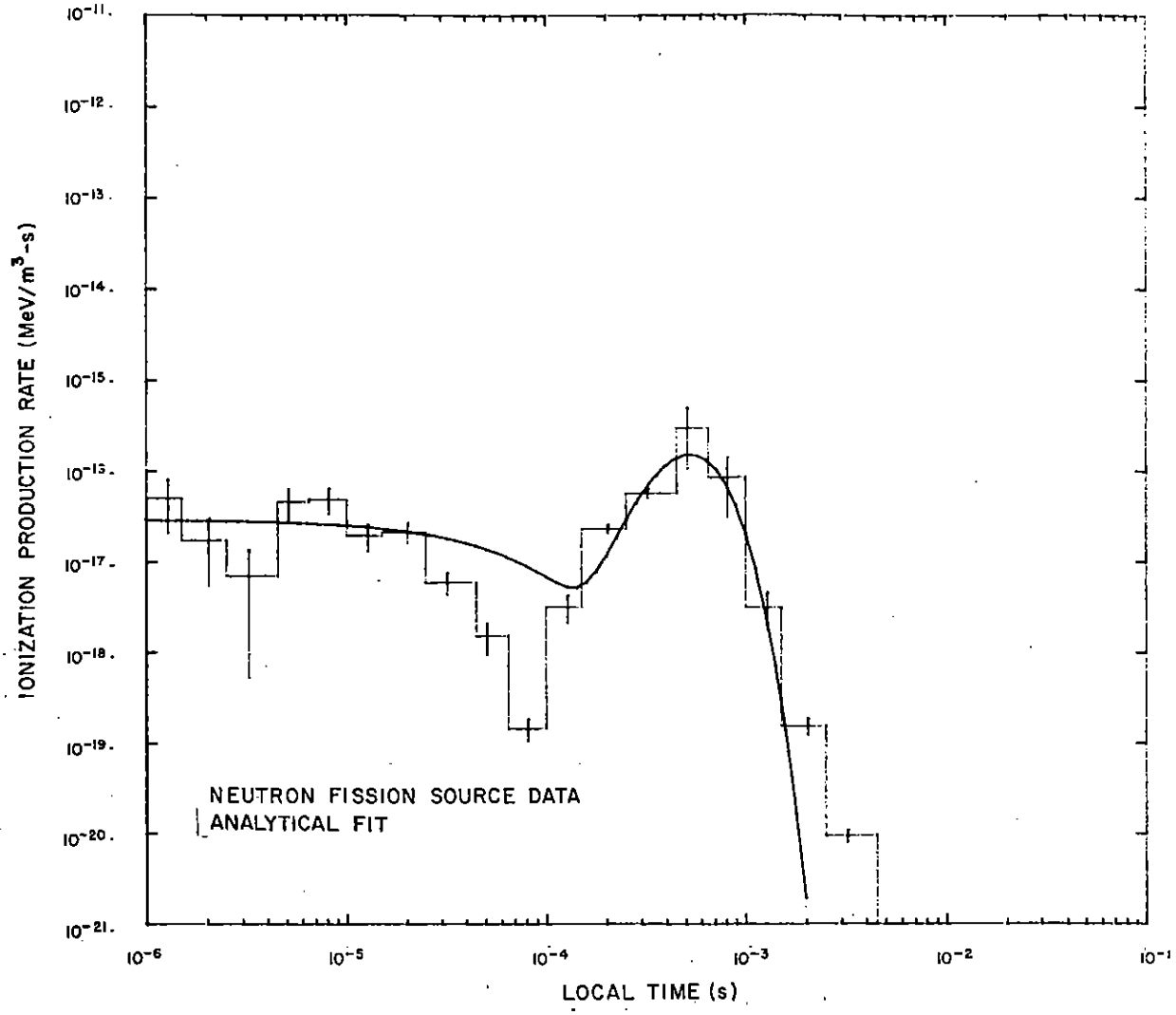

Figure 81. Ionization rate versus time for detector 20.

TABLE IV. COEFFICIENTS FOR THE 14-MeV NEUTRON SOURCE CALCULATIONS[1]

a	b	n	c	t_{max}
1.02156-13	6.38263-6	2.09289	2.93996+3	6.64339-4
6.46418-15	3.05204-4	3.53420	1.31821+3	2.60619-3
1.04216-15	2.24192-3	4.20265	1.22564+3	3.39121-3
2.14339-16	6.61323+6	7.90291	1.73797+3	4.54673-3
3.25304-17	0.424936	5.36964	1.20032+3	4.47208-3
1.47201-12	3.51146	3.09891	7.03806+3	4.35560-4
3.68858-13	4.71068+3	4.42293	4.92619+3	8.95720-4
6.10472-14	4.58288+4	4.73377	6.14901+3	7.69279-4
9.35175-15	4.88120-3	3.43517	3.92346+3	8.70113-4
2.25305-15	6.40522+4	5.50599	4.42671+3	1.24338-3
3.89485-12	0.157521	2.60633	6.30340+3	4.06561-4
1.00060-12	3.83852+6	4.67379	8.84687+3	5.28013-4
9.68190-14	3.76713	3.47443	6.05129+3	5.71443-4
4.53482-14	0.333006	3.32353	5.61237+3	5.87805-4
1.00161-14	19.3825	3.96147	7.14029+3	5.52510-4
5.32287-12	30.2351	3.13744	8.22614+3	3.77754-4
2.00345-12	9.61799+5	4.49171	8.90351+3	5.03806-4
4.36638-13	4.44924+9	5.63094	1.24585+4	4.51672-4
7.44779-14	2.85117+10	6.13597	1.27660+4	4.80361-4
1.14321-14	1.13074+12	6.68528	1.55573+4	4.29580-4

[1]*These are fitted to* $y = (a + bt^n)e^{-ct}$.

TABLE V. COEFFICIENTS FOR THE NEUTRON FISSION SOURCE CALCULATIONS[1]

a	b	n	c	t_{max}
4.47071-15	1.42009-6	2.37688	3.05086+3	7.11072-4
2.02826-16	3.67608-10	2.16568	8.55300+2	2.53207-3
3.52801-17	3.50367-8	3.18388	8.69016+2	3.66378-3
5.24215-18	0.651554	6.09485	1.14848+3	5.30691-3
1.39081-18	5.60459+3	7.73288	1.38077+3	5.60039-3
5.30850-14	1.94065-3	2.73044	4.81897+3	5.66602-4
1.48320-14	8.84696-4	2.91859	3.85738+3	7.56624-4
1.84360-15	1.28861-7	2.09497	2.75209+3	7.61230-4
3.39710-16	5.85762-3	3.63674	4.01420+3	8.99738-4
4.64725-17	3.69369-2	4.08419	4.06445+3	1.00486-3
1.63919-13	26.0878	3.54594	8.22860+3	4.30928-4
6.71219-14	1.83340+3	4.25407	8.62759+3	4.93077-4
4.92458-15	1.01442-2	3.18136	6.82374+3	4.66219-4
1.69744-15	1.02105-2	3.36542	5.84072+3	5.76200-4
2.24365-16	2.83517-2	3.57362	7.61957+3	4.69005-4
2.11928-13	4.31310+2	3.83699	9.16696+3	4.18567-4
5.33495-14	1.90743+12	6.61092	1.24052+4	5.32916-4
1.25617-14	3.92831+11	6.59457	1.46693+4	4.49550-4
2.21600-15	5.09463+13	7.49170	1.42009+4	5.27552-4
2.92490-17	1.03657+13	7.76650	1.47257+4	5.27410-4

[1]*These are fitted to* $y = (a + bt^n)e^{-ct}$.

3. DISCUSSION

The data obtained from neutron transport and subsequent gamma production and transport differ markedly from those of previous prompt gamma transport calculations.[5] Because of the difference in shape and time history, the use of different Monte Carlo techniques has been necessary.

Local time at a detector begins with the arrival of the first gamma ray, so the start of the local time is associated with neutron interactions near the source. The main body of the pulse, however, is associated with the arrival of neutrons near the detector. Since neutron speeds are small compared with the velocity of light, the pulse broadens considerably (fig. 2 to 21). The figures are drawn to the same vertical scale for the same detector positions as those in the previous study[5] for direct comparison. However, the horizontal scale is shifted by an order of magnitude.

The Monte Carlo procedure was very different from that for the gamma ray transport because of the different nature of the calculation. Each neutron was followed for 200 collisions, and each gamma produced was followed for 21 scatters. Cutoffs were set at the appropriate number of scatters and a sufficiently great altitude (700 km above the surface of the earth). A thermal energy cutoff was placed on the neutrons, but for energies below 0.1 MeV, a diffusion method replaced the Monte Carlo method.[1]

Because of the large number of separate events, machine time proved to be a problem: 600 neutron histories took about as much machine time as 25,000 histories for the gamma ray transport. In general, statistics for this number of histories were satisfactory for late times (> ~ 30 μs), although 1800 histories were necessary at the farthest detectors, and a few others required 900 or 1200 histories. Early times were more problematical, however, because large standard deviations accompanied the data in the early time regime due to the limited amount of data available from 600 histories. Indeed, some early time bins contained no events at all.

---

[1] *T. M. Jordan, FASTER III, A Generalized Monte Carlo Computer Program for the Transport of Neutrons and Gamma Rays, Vol. II, Users Manual, ART Research Corporation, ART-45 (November 1970).*

[5] *J. P. Roberts and J. S. Wicklund, Transient Ionization Effects from Primary Gamma Fission Radiation in the Upper Atmosphere, Harry Diamond Laboratories TR-1725 (October 1975).*

To solve this problem, it was noted that multiple events probably should not contribute significantly to the early time bins. Hence, second runs were made with cutoffs radically reduced to two scatters for each neutron and five scatters for each gamma ray. In this way, 6000 histories could be traced in about the same time as 600 histories with the full complement of scatters. Statistics at early times improved to the point of usability; naturally, behavior at late times was worthless. In the region of overlap of good statistics for both cases (~ 30 μs), the agreement was excellent, so quite a bit of confidence can be placed in this procedure of using separate calculations for early and late times. (Actually, the selection of the reduced number of scatters was not fortuitous: trial runs were made with different numbers of scatters until the point was reached where further reduction of scatters would harm the agreement in the overlap range. This point turned out to be two neutron scatters and five gamma ray scatters.)

Detector positions 18 and 8 are compared as examples of the important results of this study (fig. 9, 19, 29, 39). Detector 18 is directly below the source at a distance corresponding to 10 mean free path lengths for a 14-MeV neutron (30.9 km). Detector 8 is at the same mass distance from the source, but along a line 30 deg below the horizontal. Consequently, detector 8 is at a greater geometric distance from the source (53.2 km). (Results for these detectors are compared also for a primary fission gamma spectrum.[5]) For both sources, the ionization production rate at detectors 18 and 8 peaks at late local times (based on the speed of light) of about 0.5 and 0.8 ms, respectively. These times correspond roughly to the time of arrival of the most energetic (fastest) neutrons at the detectors.

Other factors complicate peak times and magnitudes as detector positions change. These include the effect of an atmospheric density that varies exponentially with altitude, source energy spectra, and the contribution to the ionization rate at late times by multiply scattered secondary gamma photons (from early neutron interactions). The atmosphere causes both a loss of neutrons and photons upward and scatterings from denser altitude regions below the source and detectors. The smaller magnitudes of the results for the fission source, relative to those of the 14-MeV source, are due to smaller fractions of energetic neutrons. The contribution of multiply scattered photons to ionization rate pulses at late times is not as clear as it was in previous 45-km altitude primary gamma source calculations,[5] but minima occur at about 0.1 ms prior to the peaks, a result compatible with those of the primary gamma calculations. These minima are much more pronounced for detector

---

[5] *J. P. Roberts and J. S. Wicklund, Transient Ionization Effects from Primary Gamma Fission Radiation in the Upper Atmosphere, Harry Diamond Laboratories TR-1725 (October 1975).*

18 for both source spectra than for detector 8. For the remaining detectors, the late peak in the secondary gamma ionization rate due to the arrival of neutrons near a detector and the minimum preceding it in time differ pronouncedly only for those detectors directly below the source at 5 to 20 mfp lengths (fig. 18 to 21, 38 to 41). However, except for detectors 1 to 4, 6, 11, and 16, the late peak (occasioned by the arrival of the neutron pulse near a detector) generally exceeds the ionization rate in the early part of each pulse by a factor of 10 or more. Detectors 2 to 4 lie along the 5-deg radial. Geometric distance and multiple scattering of gamma photons are most effective in extending the ionization pulses in time and flattening peaks along this nearly coaltitude radial. Detectors 1, 6, 11, and 16 are only 1 mfp length from the source.

The time of arrival of the neutron pulse in the volume near the detector determines the approximate time at which the ionization rate peaks, and that time of arrival depends directly on the geometric distance of the source from the detector. Thus, pulse peaks range for all detectors from about 0.4 ms for detector 16 (geometrically closest to the source) to about 6 ms for detector 5 (geometrically farthest from the source) (tables II, III).

The neutron fission-source results for the remaining detectors shown in figures 22 to 28, 30 to 38, 40, and 41 are very similar to the 14-MeV source results for corresponding positions, as were results for detectors 8 and 18. For the same detector position, the pulses show peaks and minima at approximately the same times. However, the ratio of the peak value of the ionization rate at late times to the ionization rate at early times is generally somewhat less. Also, the pulses due to the fission source are much lower in magnitude than the pulses due to the 14-MeV source. Results for detectors closest to the source are between 10 and 100 times smaller in pulse height than for the 14-MeV source. At detector 20, this factor lies between 100 and 1000.

Examination finds that the magnitudes of the fission pulses decrease with distance from the source more rapidly than the 14-MeV ionization rate pulses for detectors from 5 to 20 mfp lengths along the 60- and 90-deg radials (detectors 12 to 15 and 17 to 20). This finding is not unexpected, since the mfp length of fission neutrons is less than that from 14-MeV neutrons. For example, "for sea level air density ($\rho = 1.29 \times 10^{-3}$ gm/cm^3), the mean-free-path of fission neutrons in air is approximately 265 ft, and for fission neutrons (~ 14 MeV), the mean-free-path is approximately 480 ft."[7] However, a nonhomogeneous

---

[7] *R. L. French and L. G. Mooney, Prediction of Nuclear Weapon Neutron Radiation Environments, RRA-M, Radiation Research Associates (26 November 1969).*

medium is implicit in these calculations. The atmospheric density depends exponentially on altitude. The altitude above the zone where mass equivalent scaling can be used with accuracy is approximately 2000 to 30,000 ft.[6] Consequently, for the detector positions at 1-mfp length and for those detectors along radials that penetrate less steeply downward into the atmosphere, no clear-cut relationships are discernable from comparing fission and 14-MeV results.

However, in terms of source-detector orientation in the nonhomogeneous atmosphere at very deep penetration distance (20-mfp lengths), a relationship is observed. For detectors 5, 10, 15, and 20, as the detector position ranges from 5 deg below the horizontal level of the source to directly below the source (90 deg), the ratio in magnitudes of the 14-MeV source-generated pulses to the fission source-generated pulses increases from about 10 to greater than 100. For the 15-mfp length, a similar increase is observed from 30 to 90 deg; but at shorter distances, no clear relationships are readily apparent.

4. CONCLUSIONS

From these studies, a general observation can be made. A large contribution to ionization production rates occurs at late (~ 1 to 10 ms) local times, primarily due to the neutrons with their attendant secondary gamma production in a volume near the detector. This contribution exceeds that of earlier times by as much as an order of magnitude or more.

Examination finds that the gamma photon energy spectra associated with these ionization peak times are relatively energetic, as expected. Thus, we may expect that the Compton source currents and the saturated electric fields with the ionization rates will peak at very late times. Since the time scale of these results shown is logarithmic, these peaks are not only late, but also very broad. For circumvention designs, this result can be of singular importance.

---

[6] *E. A. Straker, Status of Neutron Transport in the Atmosphere, ORNL-TM-3065, Oak Ridge National Laboratory (29 July 1970).*

LITERATURE CITED

(1) T. M. Jordan, FASTER III, A Generalized Monte Carlo Computer Program for the Transport of Neutrons and Gamma Rays, Vol. II, Users Manual, ART Research Corporation, ART-45 (November 1970).

(2) R. W. Roussin and J. B. Wright, Defense Nuclear Agency Working Cross Section Library, ORNL-RSIC-34, Vol. 1, Oak Ridge National Laboratory (June 1974).

(3) W. J. Veigele et al, X-ray Cross Section Compilation from 0.1 keV to 1 MeV, Input Data and Supplemental Results, Vol. II, Revision 1, DNA2433FO (31 July 1971).

(4) E. A. Straker and M. L. Gritzner, Neutron and Secondary-Gamma Transport in Infinite Homogeneous Air, ORNL-4464, Oak Ridge National Laboratory (December 1969).

(5) J. P. Roberts and J. S. Wicklund, Transient Ionization Effects from Primary Gamma Fission Radiation in the Upper Atmosphere, Harry Diamond Laboratories TR-1725 (October 1975).

(6) E. A. Straker, Status of Neutron Transport in the Atmosphere, ORNL-TM-3065, Oak Ridge National Laboratory (29 July 1970).

(7) R. L. French and L. G. Mooney, Prediction of Nuclear Weapon Neutron Radiation Environments, RRA-M, Radiation Research Associates (26 November 1969).

APPENDIX A.--TREATMENT OF DATA

In some respects, the data are presented similarly to those in the previous paper.[1] The same vertical scale is used for each detector as has been used for the primary gamma-ray transport results, to facilitate direct comparison. However, the local time scale is shifted by one decade to better comprehend the expansion of time due to the lesser speeds of the neutrons. The data are plotted histogrammically (fig. 2 to 81 in the body of the report) with error bars: absence of the half of the error bar beneath the mean value indicates a standard deviation $\geq$ 100 percent.

An eighth-order log-log polynomial was least-squares fitted to the data at each detector, and each point was weighted with the inverse square of its probable error. The rationale and the method for doing this is given in appendix A of the previous paper.[1] Thus,

$$Y = \sum_{i=0}^{8} a_i X^i ,$$

where $Y = \log_{10} y$, y is the ionization production rate in MeV/m^3-s, $X = 6 + \log_{10} t$, and t is local time. The number 6 is used in the transformation to X in this paper: the number 7 was used in the equivalent formulation for the gamma-ray transport.

In the body of this report, the coefficients for the expansion are given in table II for the 14-MeV neutrons and table III for fission neutrons. In addition, t_{max}, the local time to the important maximum

---

[1] *J. P. Roberts and J. S. Wicklund, Transient Ionization Effects from Primary Gamma Fission Radiation in the Upper Atmosphere, Harry Diamond Laboratories TR-1725 (October 1975).*

near the end of the plot, is tabulated because it is necessary for the interpolation method given in appendix B. Similar to the gamma-ray case, the coefficients are not really working very hard, and the eighth-order polynomials could probably be economized down to the fourth order. This economizing was not done, however, because the shape suggests that an analytical expression might instead be fitted to the data for some further physical insight.

Accordingly, the form $y = (a + bt^n)e^{-ct}$ was selected for least-squares fitting to the data. This form describes the general details of the data: it is constant near the origin, rises to a maximum, and drops off sharply at large times. Since the form is nonlinear, special techniques are required. The method selected is an iterative Taylor expansion.[2]

However, the data used was generated at regular intervals of X using the eighth-order polynomial, so the analytical form is an approximation to the equation, rather than to the data itself. The fitting was done over the range from 10^{-6} s to a point where the value at times later than the principal maximum has dropped about an order of magnitude below the starting value. Secondly, the value of a was obtained simply by averaging values for early times. The slow decrease at early times validates this procedure. Thirdly, the process used did not always converge until the time scale had been normalized to units of t_{max}. This ameliorated the bitter conflicts between the t^n and the e^{-ct} terms, and then no troubles with convergence appeared. The transformations proceed as follows: Let

$$y' = \frac{Y}{a} = \left(1 + \frac{b}{a} t^n\right)e^{-ct} .$$

---

[2] *A. Hald, Statistical Theory with Engineering Applications, John Wiley & Sons, Inc., New York (1952).*

Define

$$\tau = t/t_{max} ,$$

$$c' = ct_{max} ,$$

and

$$b' = \frac{b}{a} t_{max}^{n} .$$

Then

$$y' = \left(1 + b'\tau^{n}\right)e^{-c'\tau} .$$

This equation was solved iteratively for b', n, and c': by use of t_{max}, b and c are then obtained.

In the body of the report, the coefficients a, b, n, and c are given in table IV for 14-MeV neutrons and table V for fission neutrons. The equation $y = \left(a + bt^{n}\right)e^{-ct}$ describes the ionization production rate as a function of the local time, in contradistinction to the eighth-order polynomial, which describes the common logarithm of the ionization production rate as a function of the common logarithm of the local time. Additionally, tables IV and V give values of t_{max} that correspond to the maxima of the analytic expressions. As might be expected, these are slightly different from the values of t_{max} for the corresponding polynomial.

APPENDIX A

In the body of the report, the values of t_{max} in tables IV and V were obtained quickly by another iterative procedure. Setting the derivative of the equation

$$y = (a + bt^n)e^{-ct}$$

to zero gives, after some manipulation,

$$t = \frac{a}{b} t^{1-n} + \frac{n}{c} .$$

This is the form used for iteration, so

$$t_{j+1} = \frac{a}{b} t_j^{1-n} + \frac{n}{c} ,$$

where t_j is the value after the jth iteration. A first guess (t_{max} from the polynomial expressions) gave almost immediate convergence.

APPENDIX B.--SCALING THE DATA

The presence of a prominent maximum complicates the simple interpolation scheme given in the previous report,[1] but not much. The interpolative scheme is described for the analytical expression; with suitable modification, it can be used for the polynomial formulation. The analytical expression terms are y (MeV/m^3-s) and t (seconds local time), whereas the polynomial is given in terms of $\log_{10} y$ and $X = 6 + \log_{10} t$.

The analytical expression describes the data fairly well, though the positions of the maxima do not show the regularity that might be desired--probably due to a combination of computational standard deviation and multiple-scattering effects at late times. The inability of the analytical expression to describe adequately (in some cases) the minimum that precedes the principal maximum cannot be considered a serious flaw: the figures are log-log plots. Were they on linear scales, they would show a very small precursor followed by an enormous pulse: the magnitude of any ripples in the precursor would be academic.

The first step in the interpolative scheme is to obtain the interpolation along a radial line of detectors. For any such line, the constant a varies nicely as an exponential function of the number of 14-MeV neutron mean free paths (mfp)--i.e., a least-squares fit of the values of a as functions of the numbers 1, 5, 10, 15, and 20 (14-MeV neutron mfp for the corresponding detectors) shows a strong correlation to the form $y = y_o e^{-sx}$. The coefficients and the correlation indices are not listed here; with two sets of neutrons, a proliferation of tables does not seem desirable in view of the large number of graphs in the body of the report. Besides, it is not particularly useful, because exponential interpolation can be used.

---

[1] *J. P. Roberts and J. S. Wicklund, Transient Ionization Effects from Primary Gamma Fission Radiation in the Upper Atmosphere, Harry Diamond Laboratories TR-1725 (October 1975).*

APPENDIX B

That is, if the known ionization production rates at two detectors are y_1 and y_2, and if f is the fraction of the distance between the two detectors to the desired interpolated position--i.e.,

$$f = \frac{x - x_1}{x_2 - x_1}, \quad x_1 < x < x_2,$$

then

$$y = y_1 \left(\frac{y_2}{y_1}\right)^f$$

is the exponentially-interpolated ionization production rate. For example, a position halfway between two detectors would have $y = \sqrt{y_1 y_2}$, i.e., the geometric mean, for its exponentially interpolated value.

If the pulses at all detectors along a radial line are normalized to a common intercept and a common position of the principal maximum, they are sufficiently close so that interpolation between any two of them is practical. The common intercept is achieved by dividing the ionization production rate at each detector by the corresponding value of a (if the polynomial formulation is used, a_o is subtracted from $Y = \log_{10} y$). The common position of maximum is obtained by dividing t by t_{max} (expressing t in units of t_{max}). Interestingly, this process has transformed the equation $y = (a + bt^n)e^{-ct}$ into the form $y' = (1 + b'\tau^n)e^{-c'\tau}$ used in appendix A.

Thus, to interpolate between two detectors on a radial line, a t_{max} for the intermediate point should be obtained: linear interpolation appears to be sufficient for this. The time of interest is then expressed in units of this t_{max}--that is, one finds $\tau = t/t_{max}$. The quantities y' for this value are then found for the two detectors by use of their normalized equations and the value of τ. Exponential interpolation between the two provides y' for the point in question, which is then multiplied by the interpolated value of a to obtain y.

This procedure gives the value of the ionization production rate for only one moment in time. To describe the entire pulse, a general rule can be stated: exponentially interpolate for a and the transformed coefficient, b'; linearly interpolate for t_{max}, n, and the transformed coefficient, c'. Exponential interpolation is known to be valid for a. If the natural logs of the transformed equations for each detector on a radial are plotted as functions of time, the graphs are sufficiently similar for c', which is linear in a logarithmic transformation, to be linearly interpolated. Similarly, if the logarithms of $y'e^{c'\tau} - 1$ for each detector on a radial line are plotted as functions of τ, sufficient similarity permits linear interpolation of n (which is linear in this transformation) and of ln b' (which is also linear in this transformation). Since a quantity that is linear in its logarithm should be interpolated exponentially, the general rule follows.

The above procedure for the analytical form is clumsy and involves exponentials and exponential interpolation, costly in machine time. If possible, then, the user should slightly modify the method given in the previous report: for the polynomial at each detector,

$$y - a_o = \sum_1^m a_i X^i = \sum_1^m a'_i T^i$$

where

$$T = X/X_{max}$$

and

$$a'_i = a_i X_{max}^i .$$

For a point between two detectors, the a'_i coefficients are then linearly interpolated. A value for X_{max} at the intermediate point is

also obtained by linear interpolation. The procedure works best if an economized series is obtained, since much less calculation is involved and the coefficients are more regular.

For points off radial lines, the procedure given in appendix B of the previous paper should be used for the polynomial form (modified as above, with X_{max} again obtained by interpolation), using the g interpolation factors given there. If the analytical form is used, interpolation as above can be employed (linear interpolation for t_{max}, n, and c'; exponential interpolation for a and b'), again by use of the g interpolation factors. The same general statements about applicability of the interpolation that were made in the previous report also apply here.